JSCSEN 79(11)1337–1460(2014)

ISSN 1820-7421(Online)

Journal of the Serbian Chemical Society

eVersion
electronic

VOLUME 79

No 11

BELGRADE 2014

Journal of the Serbian Chemical Society
JSCS-info@shd.org.rs • www.shd.org.rs/JSCS

J. Serb. Chem. Soc. Vol. 79, No. 11 (2014)

CONTENTS

Published by the Serbian Chemical Society
Karnegijeva 4/III, P. O. Box 36, 11120 Belgrade 35, Serbia
Printed by the Faculty of Technology and Metallurgy
Karnegijeva 4, P. O. Box 35-03, 11120 Belgrade, Serbia

Journal of the Serbian Chemical Society

JSCS-info@shd.org.rs • www.shd.org.rs/JSCS

J. Serb. Chem. Soc. *79* (11) 1337–1346 (2014)
JSCS–4668

UDC 547.537.3+547.37+547.563.13'023+
544.275–128
Original scientific paper

An efficient and highly selective ortho-*tert*-butylation of *p*-cresol with *tert*-butyl methyl ether catalyzed by sulfonated ionic liquids

REZA FAREGHI ALAMDARI*, FAEZEH GHORBANI ZAMANI and NEGAR ZEKRI

Department of Chemistry and Chemical Engineering, Malek Ashtar University of Technology, Tehran, Iran

(Received 17 July 2013, revised 4 July 2014, accepted 9 July 2014)

Abstract: A novel series of sulfonic acid-functionalized ionic liquids (SFILs) was found to act as efficient catalysts for ortho-*tert*-butylation of *p*-cresol with *tert*-butyl methyl ether (MTBE) as the *tert*-butylating agent without an added solvent. The mono *o*-*tert*-butylated product was obtained in up to 85.8 % isolated yield and 95.2 % selectivity under such green conditions. No *O*-*tert*-butylated byproducts were formed.

Keywords: *tert*-butylation; 2-*tert*-butyl-*p*-cresol; *p*-cresol; sulfonated ionic liquid.

INTRODUCTION

C-Alkylated phenols have received great attention as industrially important intermediates for the preparation of several antioxidants and agrochemicals. For the synthesis of these materials by alkylation reactions, various alkylating agents, such as olefins, alcohols and ethers, have been used in the presence of a catalyst.[1] In particular, 2-*tert*-butyl-*p*-cresol (TBC) and 2,6-di-*tert*-butyl-*p*-cresol (DTBC), which are commercially known as butylated hydroxyl toluene (BHT), are produced by ortho-*tert*-butylation of *p*-cresol under different reaction conditions. TBC and DTBC have found wide applications as dyes, antioxidants, rubbers, UV-absorbers, agrochemicals, non-ionic detergents, emulsifiers and pharmaceuticals. They have also been used for the preparation of surfactants, phenolic resins, and inhibitors of polymerizable activated olefin monomers.[2,3] Considering these aforementioned applications, the preparation of ortho-*tert*-butylated *p*-cresols *via* efficient approaches has been an active area of research.

There are several literature methods for the ortho-*tert*-butylation of *p*-cresol in the presence of homogeneous or heterogeneous catalytic systems, including Brønsted acids,[4] Lewis acids,[5] cation-exchange resins,[6] mesoporous materials,[7] zeolites,[8] molecular sieves, and also supercritical or near-supercritical water.[9]

* Corresponding author. E-mail: reza_fareghi@yahoo.com
doi: 10.2298/JSC130717072A

Ortho-*tert*-butylation of *p*-cresol was achieved employing various *tert*-butylating agents, particularly *tert*-butyl methyl ether (MTBE) was used in the presence of UDCaT-1 catalyst (a hexagonal mesoporous silica with sulfate modified zirconia).[10] Under the above conditions, the products were obtained in 45 % conversion and 97 % selectivity for TBC. In some cases, the ortho-*tert*-butylation of *p*-cresol was accomplished using *tert*-butanol (TBA) as the C-*tert*-butylating agent. For the promotion of this process, solid-supported catalysts consisting of 12-tungstophosphoric acid (TPA) on zirconia (TPA/ZrO_2),[11] on titania (TPA/ /TiO_2)[12] or on mesoporous silica (TPA/MCM-41),[13] and WO_x/ZrO_2,[14] have been applied. Despite the benefits of these methods, some suffer from disadvantages, such as unsatisfactory conversion, prolonged reaction time, expensive catalyst, low selectivity, use of toxic solvents, tedious work-up, requirement of special equipment, or harsh reaction conditions. Thus, the development of an efficient, easy, highly selective, and environmentally benign method using novel catalysts for the preparation of C-*tert*-butylated phenols is desirable.

During the last two decades, ionic liquids (ILs) have received great attention as catalysts and solvents in organic chemistry due to their environmentally friendly nature, non-volatility, high polarity, and good chemical and thermal stabilities. High yields of the products and high selectivity in short reaction times, and clean reaction procedures are often observed in ILs as reaction media.[15–18] Furthermore, their hydrophobicity/hydrophilicity can be optimized by appropriate modification of the cation or anion part.[19] ILs containing a Lewis or a Brønsted acid group have been used in various chemical transformations.[20] Recently, significant advances in the field have been witnessed, whereby a functional group is covalently bonded to the IL.[21] The incorporation of sulfonic acid groups to ILs significantly increases their acidic property as well as their water solubility. Such SO_3H-functionalized ILs (SFILs) have been used as substitutes for conventional homogenous and heterogeneous acid catalysts.[22] Moreover their polar nature makes them useful for solvent-free conditions.[23–25] Recently, ortho-*tert*-butylation of *p*-cresol was reported in which TBA was used as the *tert*-butylating agent in the presence of SFILs, such as 1-(4-sulfobutyl)pyridinium hydrogensulfate,[26] (4-sulfobutyl)triethylammonium hydrogensulfate,[27] and polysulfonated ILs,[28] whereby TBC was afforded in good to excellent conversion and selectivity.

In continuation of interest in the application of green methodologies in organic synthesis,[29–32] herein an efficient and green procedure for the ortho-*tert*-butylation of *p*-cresol using MTBE in the presence of the SFILs, presented in Fig. 1, as the catalyst–solvent medium, is described (Scheme 1).

EXPERIMENTAL

Commercially available solvents and chemicals were used without further purification. The SFILs **1–3** were prepared according to procedures outlined in the literature[25,33] and were characterized by NMR spectroscopy on a Bruker DPX 3300-300 MHz. Quantitative product analysis was conducted by gas chromatography on a Hewlett Packard HP-5890 instrument equipped with HP-1 column (30 m long, 0.5 mm diameter), and flame ionization detector (FID), using N_2 as the carrier gas at a flow rate of 2 mL min^{-1}.

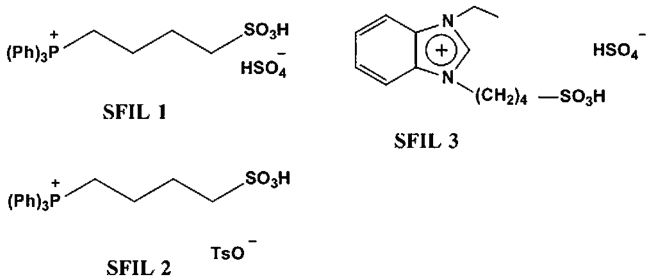

Fig. 1. Structures of the SFILs used in this study; SFIL **1** – triphenyl(4-sulfobutyl)-phosphonium hydrogensulfate ($[Ph_3P(CH_2)_4SO_3H][HSO_4]$), SFIL **2** – triphenyl(4-sulfobutyl)phosphonium tosylate ($[Ph_3P(CH_2)_4SO_3H][TsO]$) and SFIL **3** – 1-ethyl-3-(4--sulfobutyl)-1*H*-benzimidazolium hydrogensulfate ($[bSebim]HSO_4$).

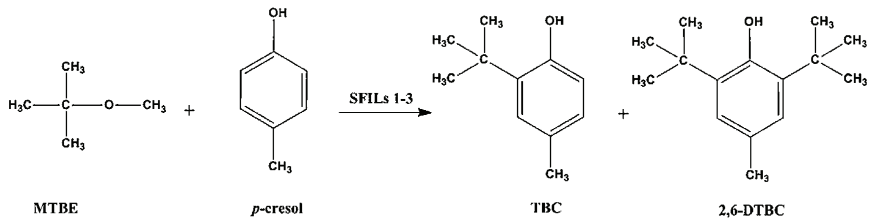

Scheme 1. Ortho-*tert*-butylation of *p*-cresol with MTBE using SFILs **1**–**3**.

Synthesis and characterization of the SFILs

*Synthesis of triphenyl(4-sulfobutyl)phosphonium hydrogensulfate (SFIL **1**) and triphenyl-(4-sulfobutyl)phosphonium tosylate (SFIL **2**).* The triphenyl(4-sulfobutyl)phosphonium hydrogensulfate and triphenyl(4-sulfobutyl)phosphonium tosylate ionic liquids were prepared according to procedures outlined in the literature.[25] Triphenylphosphine was mixed with 1,4-butane sulftone in toluene at 110–120 °C for 12–24 h. After solidification of mass, the product (zwitterion) was washed three times with diethyl ether and then dried *in vacuo*. A stoichiometric amount of *p*-toluenesulfonic acid or sulfuric acid was added to the precursor zwitterion. The mixture was heated at 80 °C for 24 h, during which time the solids liquefied, resulting in the formation of triphenyl(4-sulfobutyl)phosphonium tosylate or triphenyl(4--sulfobutyl)phosphonium hydrogensulfate. The ILs phase were then washed repeatedly with toluene and diethyl ether to remove the non-ionic residues, and dried *in vacuo*.

*$[Ph_3P(CH_2)_4SO_3H][HSO_4]$ (SFIL **1**)*. ^{1}H-NMR (300 MHz, D_2O, δ / ppm): 7.63–7.23 (15H, *m*, Ar-H), 3.05 (2H, *m*, $(CH_2)_3C\mathbf{H}_2SO_3H$), 2.63–2.56 (2H, *t*, J = 7.53 Hz, $C\mathbf{H}_2(CH_2)_3SO_3H$), 1.64 (2H, *m*, $(CH_2)_2C\mathbf{H}_2CH_2SO_3H$), 1.56 (2H, *m*, $CH_2C\mathbf{H}_2(CH_2)_2SO_3H$).

*$[Ph_3P(CH_2)_4SO_3H][TsO]$ (SFIL **2**)*. ^{1}H-NMR (300 MHz, D_2O, δ / ppm); 7.4 (2H, *m*, *p*-TsO), 7.27–7.23 (15H, *m*, Ar-H), 6.82–6.79 (2H, *d*, J = 9.00 Hz, *p*-TsO), 2.83–2.79 (2H, *m*, $(CH_2)_3C\mathbf{H}_2SO_3H$), 2.53–2.48 (2H, *t*, J = 7.56 Hz, $C\mathbf{H}_2(CH_2)_3SO_3H$), 1.87 (3H, *s*, *p*-TsO), 1.57–1.54 (2H, *m*, $(CH_2)_2C\mathbf{H}_2CH_2SO_3H$), 1.32 (2H, *m*, $CH_2C\mathbf{H}_2(CH_2)_2SO_3H$).

*Synthesis of 1-ethyl-3-(4-sulfobutyl)-1*H*-benzimidazolium hydrogensulfate (SFIL **3**)*. The 1-ethyl-3-(4-sulfobutyl)benzimidazolium hydrogen sulfate ionic liquid was prepared according to a procedure outlined in the literature.[33] Under vigorous stirring, the required amounts of benzimidazole and tetrabutylammonium bromide were dissolved in a 30 % aqueous solution of sodium hydroxide, the stoichiometric amount of bromoethane was added dropwise and then the mixture was heated at 45 °C for 12 h until two phases formed. The organic phase (upper phase) was washed with deionized water and ethyl acetate and dried *in vacuo* at 50 °C for 3 h, giving 1-ethylbenzimidazole (Ebim) as a colorless liquid. The required amount of 1,4-butane sulftone was dissolved in toluene under vigorous stirring. The stoichiometric amount of Ebim was added to the solution dropwise and cooling to maintain the temperature at 0–5 °C. After completion of the addition, the mixture was slowly heated up to room temperature and stirred for 2 h, whereby a precipitate formed. The precipitate was recovered by filtration, washed three times with diethyl ether and dried at 100 °C for 5 h, giving 1-ethyl-3-(4-sulfobutyl)-1H-benzimidazolium inner salt (Ebim-BS) as a white powder. An amount of Ebim-BS was dissolved in water and a stoichiometric amount of sulfuric acid was added dropwise at room temperature. After completion of the addition, the mixture was slowly heated to 90 °C and stirred for 2 h and then the water was removed *in vacuo* at 70 °C for 3 h, giving [bSebim]HSO_4 as a colorless solid.

*[bSebim]HSO_4 (SFIL **3**)*. ^{1}H-NMR (300 MHz, D_2O, δ / ppm): 9.07 (1H, *s*, NCHN), 7.61 (2H, *m*, Ar-H), 7.37 (2H, *m*, Ar-H), 4.30 (2H, *m*, $N(CH_2)_3C\mathbf{H}_2SO_3H$), 4.23 (2H, *m*, $NC\mathbf{H}_2CH_3$), 2.74 (2H, *t*, *J* = 6.52 Hz, $NC\mathbf{H}_2(CH_2)_3SO_3H$), 1.90 (2H, *m*, $N(CH_2)_2C\mathbf{H}_2CH_2SO_3H$), 1.59 (2H, *m*, $NCH_2C\mathbf{H}_2(CH_2)_2SO_3H$), 1.38 (3H, *t*, *J* = 7.58 Hz, $NCH_2C\mathbf{H}_3$).

Ortho-tert-*butylation of* p-*cresol with MTBE in the presence of SFILs **1–3***

The SFIL (1 mmol) was added to a mixture of *p*-cresol (1 mmol, 108 mg) and MTBE (1 mmol, 119 μL) in a 25 mL round-bottom flask and the reaction mixture was heated for the required time and at the chosen temperature as indicated (12 h at 90 °C or 7 h at 100 °C). The progress of the reaction was monitored by TLC on silica gel using ethyl acetate/hexane 2:1 as the eluent. After the given time, the mixture was cooled to room temperature and extracted with ethyl acetate (3×5 mL). The recovered SFIL was dried *in vacuo*, and ^{1}H-NMR analysis attested its high purity, showing no traces of reactants or products. The recovered SFIL could be directly reused without further drying.

The ethyl acetate phase containing the products was analyzed by gas chromatography isothermally at 110 °C. Before injecting the sample into the chromatographic column, dichlorobenzene (as an internal standard, 3.40 mmol, 50 mg) was added to all samples. The carrier gas pressure at the beginning of the chromatographic column was about 13 psi*. Total elution time was 31.35 min and the elution times of dichlorobenzene, *p*-cresol, 2-*tert*-butyl-*p*-cresol and 2,6-di-*tert*-butyl-*p*-cresol in the ethyl acetate phase were 4.7, 5.16, 9.3 and 12.19 min, respectively.

RESULTS AND DISCUSSION

*Assessment of SFILs **1**–**3** as catalysts*

The evaluation of the efficiency of SFILs **1**–**3** in the ortho-*tert*-butylation of *p*-cresol for 12 h at 90 °C revealed 1-ethyl-3-(4-sulfobutyl)benzimidazolium

* 1 psi = 6.895 kPa

hydrogensulfate ([bSebim][HSO_4], SFIL **3**) to be the most effective catalyst. As given in Table I, it led to 75.4 % conversion with 93.3 % selectivity for TBC. For optimization purposes, various reaction conditions in the presence of SFIL **3** were examined.

TABLE I. Ortho-*tert*-butylation of *p*-cresol with MTBE using SFILs **1–3**; reaction conditions: 12 h at 90 °C

Entry	Catalyst	Mole ratio *p*-cresol:MTBE:SFIL	Conversion %	Selectivity, %	
				TBC	DTBC
1	$[Ph_3P(CH_2)_4SO_3H][HSO_4]$	1:1:1	56.3	76.3	23.7
2	$[Ph_3P(CH_2)_4SO_3H][TsO]$	1:1:1	35.5	100	0
3	[bSebim][HSO_4]	1:1:1	75.4	93.3	6.7

Effect of the reaction time

The effect of reaction time on the ortho-*tert*-butylation of *p*-cresol with MTBE in the presence of SFIL **3** was studied at 100 °C. Figure 2 shows that increasing the reaction time had a positive impact on enhancing the conversion of *p*-cresol and the selectivity for TBC. The highest conversion and selectivity for TBC were obtained at 7 h and prolonging the reaction time did not lead to any improvement. The maximum conversion of *p*-cresol at 7 h was 85.8 % and the selectivity for TBC 95.2 %.

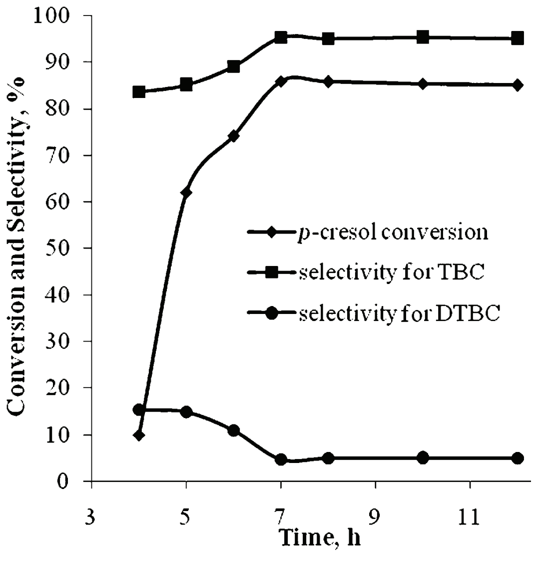

Fig. 2. *p*-Cresol conversion and products selectivity *vs*. reaction time. Reaction conditions: mole ratio of *p*-cresol:MTBE:[bSebim][HSO_4] = 1:1:1; heating at 100 °C.

Effect of the reaction temperature

The ortho-*tert*-butylation of *p*-cresol with MTBE for 7 h was studied at temperatures from 70 to 120 °C. As shown in Fig. 3, conducting the reaction at increasing temperatures up to 100 °C increased the conversion of *p*-cresol and further increases to above 100 °C did not improve this result. Thus, the optimum reaction temperature was 100 °C leading up to 85.8 % conversion and 95.2 % selectivity for TBC.

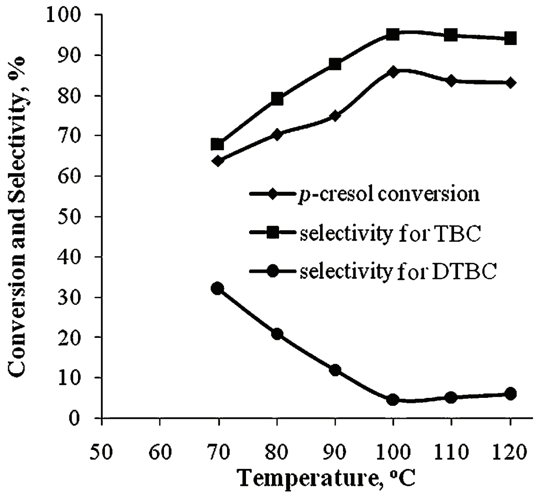

Fig, 3. *p*-Cresol conversion and products selectivity *vs*. reaction temperature. Reaction conditions: mole ratio of *p*-cresol:MTBE:[bSebim][HSO_4] = = 1:1:1; heating for 7 h.

*Effect of the MTBE:*p-*cresol mole ratio*

The influence of MTBE:*p*-cresol mole ratio was studied at 100 °C (reaction for 7 h) while maintaining the [bSebim][HSO_4]:*p*-cresol mole ratio at 1:1 (Fig. 4). Various mole ratios of MTBE:*p*-cresol varying from 0.5–2 were tested. These experiments demonstrated that increasing the mole ratio of MTBE:*p*-cresol

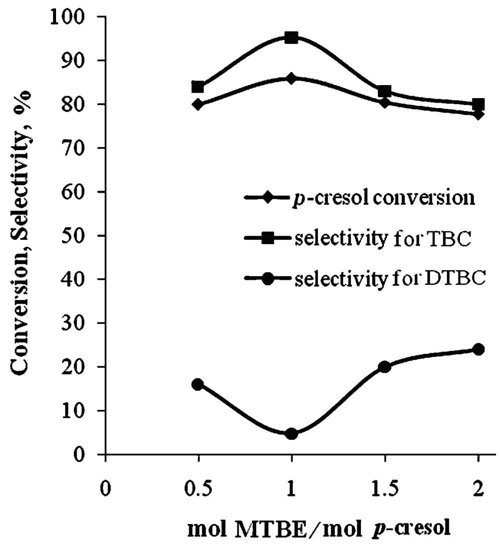

Fig. 4. *p*-Cresol conversion and products selectivity *vs*. amount of MTBE. Reaction conditions: mole ratio of [bSebim][HSO_4]: :*p*-cresol = 1:1; heating for 7 h at 100 °C.

increased the conversion of *p*-cresol, reaching a maximum of 85.8 % from a 1:1 ratio. However, the selectivity for TBC first improved to some extent (a 13 % increase) going from 0.5 to 1 and then decreased. This could be attributed to its transformation into DTBC with more MTBE available. As shown in Fig. 4, the maximum of 85.8 % conversion of *p*-cresol with a 95.2 % TBC selectivity were observed when the MTBE:*p*-cresol ratio was 1:1. Noteworthy, the DTBC selectivity increased when the mole ratio MTBE:*p*-cresol was greater than 1.

*Effect of [bSebim][HSO$_4$]:*p-*cresol mole ratio*

The effect of the mole ratio of [bSebim][HSO$_4$]:*p*-cresol on the reaction was studied under the optimized conditions, *i.e.*, reaction for 7 h at 100 °C with a MTBE:*p*-cresol mole ratio of 1:1. As shown in Fig. 5, with increasing mole ratio of [bSebim][HSO$_4$]:*p*-cresol from 0.5 to 1, both the conversion of *p*-cresol and the selectivity for TBC increased. This is understandable as the progress of catalyzed reactions is proportional to the catalyst loading. However, the best result of 85.8 % conversion and 95.2 % selectivity for TBC was obtained using a [bSebim][HSO$_4$]:*p*-cresol ratio of 1:1, as increasing this ratio did not improve the selectivity.

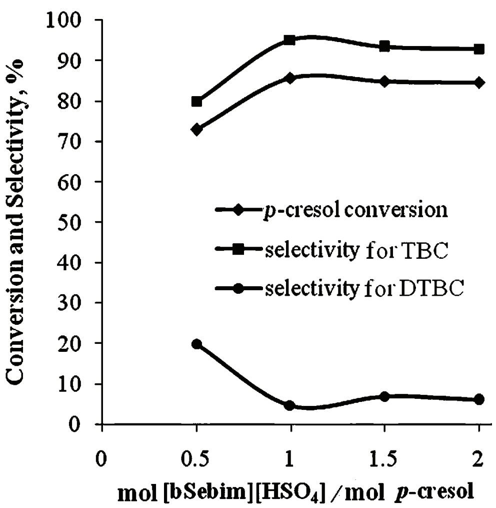

Fig. 5. *p*-Cresol conversion and products selectivity *vs.* amount of [bSebim][HSO$_4$] (SFIL **3**). Reaction conditions: mole ratio of MTBE:*p*-cresol = 1:1; heating for 7 h at 100 °C.

Recycling of SFIL ***3***

In order to examine the recoverability and reusability of [bSebim][HSO$_4$] (SFIL **3**), after completion of the reaction, ethyl acetate (3×5 mL) was added resulting in two layers. The upper phase contained the products and the lower phase the SFIL. After further extractions (2×5 mL ethyl acetate) and phase separation, the SFIL was dried under vacuum for 5 h at 70 °C. Recycle test results for [bSebim][HSO_4] are shown in Table II, indicating no major decrease (< 5 %) in the conversion of *p*-cresol and selectivity for the products in up to three runs.

TABLE II. Recycling of 1-ethyl-3-(4-sulfobutyl)benzimidazolium hydrogensulfate ([bSebim][HSO_4], SFIL **3**); reaction conditions: mole ratios of [bSebim][HSO_4]:*p*-cresol:MTBE = 1:1:1; heating for 7 h at 100 °C

Entry	SFIL **3** Experimental run	Conversion, %	Selectivity, %	
			TBC	DTBC
1	Fresh	85.8	95.2	4.8
2	Recycle 1	81.7	97.8	2.2
3	Recycle 2	80.3	91.8	8.2

*Comparison of efficiencies of SFILs **1**–**3** with those of other SFIL catalysts*

The efficiencies of the prepared SFILs **1**–**3** were compared with those of other literature SFILs for the ortho-*tert*-butylation of *p*-cresol (Table III). As tabulated, all the SFILs led to TBC with high conversion and good selectivity, but the in the literature known di(SO_3H)-functionalized IL based on imidazolium (SFIL **9**) and [bSebim][HSO_4] (SFIL **3**) afforded the best results. The advantage of SFIL **3** is its ease of preparation compared to the former.

TABLE III. Comparison of various SFIL catalysts for the ortho-*tert*-butylation of *p*-cresol with TBA or MTBE

Reactants	Catalyst	Mole ratio *p*-cresol:TBA or MTBE:SFIL	*t* / °C	Conversion %	Selectivity, %		Ref.
					TBC	DTBC	
p-cresol/MTBE	SFIL **1**	1:1:0.5	90	78.4	90.7	9.3	This study
p-cresol/MTBE	SFIL **2**	1:1.25:1	90	44.8	88.6	11.4	This study
p-cresol/MTBE	SFIL **3**	1:1:1	100	85.8	95.2	4.8	This study
p-cresol/TBA	SFIL **4**[a]	1:1:1	70	80.7	90.0	9.5	27
p-cresol/TBA	SFIL **4**[a]	3:1:1	70	85.0	66.8	32.3	27
p-cresol/TBA	SFIL **5**[b]	1:1:1	70	82.6	80.5	16.7	26
p-cresol/TBA	SFIL **6**[c]	1:1:1	70	70.8	70.6	3.5	26
p-cresol/TBA	SFIL **6**[c]	2:1:1	70	84.0	72.0	27.0	27
p-cresol/TBA	SFIL **7**[d]	1:1:1	70	80.0	91.0	8.9	27
p-cresol/TBA	SFIL **8**[e]	1:1:1	70	66.9	69.2	3.9	26
p-cresol/TBA	SFIL **9**[f]	1:1:0.5	70	85.3	95.2	1.4	28

[a]SFIL **4**: (4-sulfobutyl)triethylammonium hydrogensulfate; [b]SFIL **5**: 1-(3-sulfopropyl)pyridinium tosylate; [c]SFIL **6**: 1-(4-sulfobutyl)pyridinium hydrogensulfate; [d]SFIL **7**: 1-methyl-3-(4-sulfobutyl)imidazolium hydrogensulfate; [e]SFIL **8**: 1-(4-sulfobutyl)pyridinium tosylate; [f]SFIL **9**: a di(SO_3H)-functionalized IL based on 1,1′-(1,4-butanediyl)bis[3-(4-sulfobutyl)-1*H*-imidazolium] bis(hydrogensulfate)

*Ortho-*tert*-butylation of* p*-cresol with MTBE in the presence of SFIL **3** on the 50 mmol scale*

To a 1000 mL round-bottom flask containing a mixture of *p*-cresol (50 mmol, 5.4 g) and MTBE (50 mmol, 5.95 ml) was added SFIL **3** (50 mmol, 16.20 g) and the mixture was heated at 100 °C. After 7 h, the reaction mixture was cooled to room temperature and ethyl acetate (3×50 mL) was added leading to the separation of SFIL **3**. The crude product was purified by column chromatography on silica gel using hexane/ethyl acetate 2:1 as eluent that afforded TBC (yellow solid, 6.435 g, 78 % isolated yield) and DTBC (white solid, 0.525 g, 5 % isolated yield). Gas chromatography analysis of the crude product indicated 84.7 % conversion of *p*-cresol and 93.7 % selectivity to TBC.

CONCLUSIONS

A series of SO_3H-functionalized ILs was prepared and their dual catalyst––solvent performances for ortho-*tert*-butylation of *p*-cresol with MTBE examined. The best results were obtained in the presence of [bSebim][HSO_4] (SFIL **3**), and an optimization study was conducted. This Brønsted acidic IL has some advantages, such as up to 85.8 % conversion and 95.2 % selectivity for the mono ortho-*tert*-butylated product TBC, and it could be easily reused avoiding thus the use of solvents and toxic catalysts. The present approach represents an efficient method for the ortho-*tert*-butylation of *p*-cresol to TBC without formation of ortho-*tert*-butylated products and without the use of added solvents.

Acknowledgements. The authors are grateful to Malek Ashtar University of Technology for supporting this work.

ИЗВОД

ЕФИКАСНО И СЕЛЕКТИВНО ОРТО-*ТЕРЦ*-БУТИЛОВАЊЕ *p*-КРЕЗОЛА *ТЕРЦ*-БУТИЛ МЕТИЛ-ЕТРОМ КАТАЛИЗОВАНО СУЛФОНОВАНИМ ЈОНСКИМ ТЕЧНОСТИМА

REZA FAREGHI ALAMDARI, FAEZEH GHORBANI ZAMANI и NEGAR ZEKRI

Department of Chemistry and Chemical Cngineering, Malek Ashtar University of Technology, Tehran, Iran

Утврђено је да серија нових јонских течности типа сулфонских киселина ефикасно катализује орто-*терц*-бутиловање *p*-крезола *терц*-бутил метил-етром (MTBE) као реагенсом за *терц*-бутиловање, без присутног растварача. Моно орто-*терц*-бутиловани производ настаје у приносу до 80,4 % изолованог производа и уз 95,2 % селективности. Не настаје *O*-*терц*-бутиловани производ.

(Примљено 17. априла. 2013, ревидирано 4. јула, прихваћено 9. јула 2014)

REFERENCES

1. A. V. Krishnan, K. Ojha, N. C. Pradhan, *Org. Proc. Res. Dev.* **6** (2002) 132
2. J. Pospisil, *Polym. Degrad. Stab.* **20** (1988) 181
3. J. Murphy, in: Additives *for Plastics Handbook*, 2nd ed., Ch. 2., Elsevier, Amsterdam, 2001
4. L. Tian, F. H. Cao, D. Y. Fang, S. Z. Guo, *Chin. J. Chem. Eng.* **15** (2007) 680
5. T. Zhang, F. Q. Zhang, D. Mei, G. F. Wang, J. G. Wang, *Catal. Commun.* **6** (2005) 385
6. M. A. Harmer, Q. Sen, *Appl. Catal., A* **221** (2001) 45
7. M. Selvaraj, S. Kawi, *Micropor. Mesopor. Mater.* **98** (2007) 143

8. K. Zhang, H. Zhang, G. Xiang, D. Xu, S. Liu, H. Li, *Appl. Catal., A* **207** (2001) 183
9. T. Sato, G. Sekiguchi, T. Adschiri, K. Arai, *Chem. Commun.* **17** (2001) 1566
10. G. D. Yadav, A. A. Pujari, A. V. Joshi, *Green Chem.* **1** (1999) 269
11. B. M. Devassy, G. V. Shanbhag, F. Lefebvre, S. B. Halligudi, *J. Mol. Catal., A* **210** (2004) 125
12. S. M. Kumbar, G. V. Shanbhag, F. Lefebvre, S. B. Halligudi, *J. Mol. Catal., A* **256** (2006) 324
13. G. Kamalakar, K. Komura, Y. Sugi, *Catal. Lett.* **108** (2006) 31
14. S. Sarisha, B. M. Devassy, S. B. Halligudi, *J. Mol. Catal., A* **235** (2005) 44
15. S. Chowdhury, R. S. Mohan, J. L. Scott, *Tetrahedron* **63** (2007) 2363
16. P. Wasserscheid, W. Keim, *Angew. Chem. Int. Ed.* **39** (2000) 3772
17. J. Safaei-Ghomi, M. A. Ghasemzadeh, *J. Serb. Chem. Soc*. **77** (2012) 733
18. a) T. Welton, *Chem. Rev*. **99** (1999) 2071; b) V. I. Parvulescu, C. Hardacre, *Chem. Rev.* **107** (2007) 2615
19. J. L. Anderson, R. Ding, A. Ellern, D. W. Armstrong, *J. Am. Chem. Soc.* **127** (2005) 593
20. W. J. Swindall, *Clean Technol. Envir.* **6** (2004) 149
21. P. Wasserscheid, M. Sesing, W. Korth, *Green Chem.* **4** (2002) 134
22. D. C. Forbes, K. J. Weaver, *J. Mol. Catal., A* **214** (2004) 129
23. Y. Gu, F. Shi, Y. Deng, *J. Mol. Catal., A* **212** (2004) 71
24. J. Gui, X. Cong, D. Liu, X. Zhang, Z. Hu, Z. Sun, *Catal. Commun.* **5** (2004) 473
25. A. C. Cole, J. L. Jensen, I. Ntai, K. L. T. Tran, K. J. Weaver, D. C. Forbes, J. H. Davis, *J. Am. Chem. Soc.* **124** (2002) 5962
26. X. Liu, J. Zhou, X. Guo, M. Lin, X. Ma, C. Song, C. Wang, *Ind. Eng. Chem. Res*. **47** (2008) 5298
27. K. Kondamudi, P. Elavarasan, P. J. Dyson, S. J. Upadhyayula, *J. Mol. Catal., A* **321** (2010) 34
28. S. Bao, N. Quan, J. Zhang, J. Yang, *Chin. J. Chem. Eng,* **19** (2011) 64
29. R. Fareghi-Alamdari, Z. Hosseinabadi, M. Farhadi-Khouzani, *J. Chem. Sci.* **124** (2012) 827
30. N. Zekri, R. Fareghi-Alamdari, A. Khalafi-Nezhad, *Bull. Chem. Soc. Ethiop*. **24** (2010) 299
31. N. Zekri, R. Fareghi-Alamdari, *Can. J. Chem.* **88** (2010) 563
32. A. Khalafi-Nazhad, R. Fareghi-Alamdari, N. Zekri, *Tetrahedron* **56** (2000) 7503
33. Y. Wang, D. Jiang, L. J. Dai, *Catal. Commun.* **9** (2008) 2475.

Journal of the Serbian Chemical Society
JSCS-info@shd.org.rs • www.shd.org.rs/JSCS

J. Serb. Chem. Soc. 79 (11) 1347–1354 (2014)
JSCS–4669

UDC 547.756+542.9+547.574+
547.551:57–188:615.28–188
Original scientific paper

Synthesis, antimicrobial and antioxidative activity of some new isatin derivatives

GAVRILO M. ŠEKULARAC[1#], JASMINA B. NIKOLIĆ[2#], PREDRAG PETROVIĆ[3], BRANKO BUGARSKI[3], BOBAN ĐUROVIĆ[4] and SAŠA Ž. DRMANIĆ[2*#]

[1]*Institute of Chemistry, Technology and Metallurgy, University of Belgrade, Njegoševa 12, Belgrade, Serbia,* [2]*Department of Organic Chemistry, Faculty of Technology and Metallurgy, University of Belgrade, Karnegijeva 4, 11000 Belgrade, Serbia,* [3]*Department of Chemical Engineering, Faculty of Technology and Metallurgy, University of Belgrade, Karnegijeva 4, 11000 Belgrade, Serbia and* [4]*Faculty of Technical Science, Kneza Miloša 7, 38220 Kosovska Mitrovica, Serbia*

(Received 9 July, revised 17 August 2014, accepted 18 August 2014)

Abstract: The isatin derivatives, Schiff bases, were synthesized by the reaction of isatin and various substituted primary amines and characterized by several spectroscopic methods. Investigation of the antimicrobial activity of the synthesized compounds was performed by the agar dilution method, against different strains of bacteria and one fungus. The antioxidative activity of the synthesized compounds was also determined. Some of the compounds showed significant activity against the selected strains of microorganisms and antioxidative activity.

Keywords: isatin derivatives; Schiff bases; antimicrobial activity; antioxidative activity.

INTRODUCTION

The derivatives of isatin (indole-2,3-dione), as well as its Schiff and Mannich bases, have already been reported to show a variety of biological activities, such as antibacterial,[1] antifungal[2] and anti-HIV[3,4] activities. The wide spectrum of isatin derivatives and their various chemical properties has led to their increasingly expanded use as precursors for the preparation of many biologically active compounds.[5–11] Hydrazine derivatives of isatin were found to be active against Walker carcinosarcoma 256.[10,12] Similarly, acetone- and ketone-derivatives of isatin exhibited anticonvulsant activity.[13] Another class of thiosemicarbazone derivates of isatin was found to exhibit interesting applications as research

* Corresponding author. E-mail: drmana@tmf.bg.ac.rs
# Serbian Chemical Society member.
doi: 10.2298/JSC140709084S

tools in physiological studies.[14–18] Similarly, many other isatin-derived compounds possess a wide spectrum of medicinal properties and have thus been studied for activity against tuberculosis,[19,20] leprosy,[21] fungal,[22–26] viral[26] and bacterial[18,27] infections, trypanosomiasis[28] and as anticonvulsants.[29–31] Therefore the antimicrobial activity determination of this class of compounds is of significance and it has already been performed by the diameter of zone of inhibition method.[32,33]

Besides antimicrobial activity, the antioxidative capacities of a compound have become more and more significant nowadays. Oxidation reactions can produce free radicals, which, in turn, can initiate chain reactions. Antioxidants terminate these chain reactions by being oxidized themselves, thereby removing free radical intermediates and inhibiting other oxidation reactions. Such are thiols, ascorbic acid and polyphenols that are also reducing agents.[34] Antioxidants are widely used in dietary supplements and have been investigated for the prevention of diseases such as cancer, or coronary heart disease.[34] Antioxidants also have many industrial uses, *i.e.*, as preservatives in food and cosmetics and even to prevent the degradation of rubber and gasoline.[35]

Taking all this into consideration, it is deemed of interest to test the antimicrobial and antioxidative activity of synthesized isatin derivatives, in order to estimate their activity potential.

In this study, a series of six isatin derivatives, two of them new, which could be classified as Schiff bases, was synthesized, characterized and tested for their antimicrobial and antioxidative activity.

EXPERIMENTAL

Chemistry

The examined Schiff bases were synthesized by the reaction of isatin and the required primary amine, Scheme 1. All employed chemicals were of *p.a.* quality (Fluka–Alrich). The list of synthesized compounds is given in Table I.

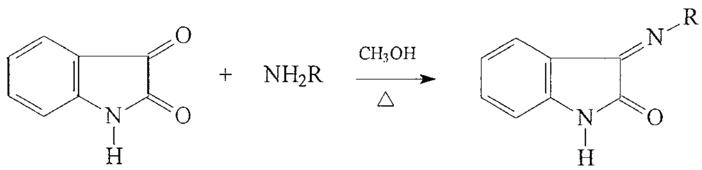

Scheme 1. The synthesis of the isatin derivatives.

Synthesis. Isatin (5 mmol) was dissolved in methanol (40 mL), and corresponding reactants (amine (R–NH_2, 5 mmol) and glacial acetic acid (1 mL) in the given order) were added. Reaction mixture was refluxed at 70 °C for 6 h under stirring at atmospheric pressure. ubsequently, the mixture was left overnight without stirring at room temperature. The obtained crystals were filtered off, dried and recrystallized from methanol. On average, the yield was about 70–79 % (details are given in the Supplementary material).

TABLE I. The synthesized isatin derivatives

Compound	R	Compound name
1	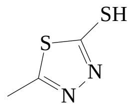	1,3-dihydro-3-[(5-mercapto-1,3,4-thiadiazol-2-yl)imino]-*2H*--indol-2-one
2	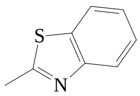	1,3-dihydro-3-(2-benzothiazolylimino)-*2H*-indol-2-one
3	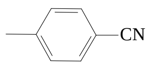	1,3-dihydro-3-[(4-cyanophenyl)imino]-2*H*-indol-2-one
4	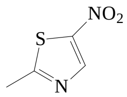	1,3-dihydro-3-[(5-nitro-2-thiazolyl)imino]-2*H*-indol-2-one
5	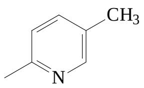	1,3-dihydro-3-[(5-methyl-2-pyridyl)imino]-*2H*-indol-2-one
6	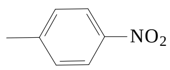	1,3-dihydro-3-[(4-nitrophenyl)imino]-2*H*-indol-2-one

Characterization

Melting points were determined on a Stuart SMP 30 melting point apparatus. The FTIR spectra were recorded on Bomem MB100 spectrometer, using the standard KBr pellet technique. The ^{1}H-NMR and ^{13}C-NMR spectral measurements were performed on a Bruker AC 250 spectrometer at 250 MHz for the ^{1}H-NMR and 62.89 MHz for the ^{13}C-NMR spectra. The spectra were recorded at room temperature in DMSO-d_6. Elemental analysis was realized using an Elemental Vario EL III micro-analyzer.

In vitro *antimicrobial activity*

The antimicrobial activity of all synthesized compounds **1**–**6** was determined on a wide range of different microorganisms by the broth micro-dilution method.[36] The advantage of this method, in comparison to the technique of the diameter of inhibition zones,[32,33] lies in its capability to quantitatively determine antimicrobial activity and give a more precise insight into the effect of every examined compound on the applied bacterial strains.

The broth micro-dilution method[36] was applied to determine the minimal inhibitory concentrations (*MIC*) of the investigated compounds against nine American Type Cell Collection (ATCC) bacterial strains and one strain of yeast, *Candida albicans* (Table II). The method was performed in agreement with Clinical and Laboratory Standard Institute (CLSI 2005).

The active microbial cultures were prepared from lyophilized standard strains by transferring them to test tubes with the appropriate broth. The nutrient broth was used for bacterial strains, except for *L. monocytogenes*, for which the soya triptose broth was used. The malt broth was used for *C. albicans.* The density of microbial suspensions was set approximately at 10^5 CFU (Colony Forming Units), using the appropriate broth.

All examined compounds were first dissolved in 5 % dimethyl sulphoxide to a concentration of 2.5 mg mL^{-1}, and then series of concentrations were prepared by two-fold dilution, using the appropriate broth. The serial concentrations were prepared directly in micro-titre plates and the final volume of specimens was 50 µL. The investigated concentrations were in the range from 0.0024 to 1.25 mg mL^{-1}. In the last column only the appropriate broth was added. Then 50 µL of each microbial suspension were added in each well, so that the final concentrations of the examined extracts were half of those at the beginning, and the final volume was 100 µL in each well. Triphenyltetrazolium chloride (TTC), in concentration of 0.75 vol. % was used as the growth indicator. If growth of a microbial strain occurs, this indicator gives a rosy–red colour to the broth. The plates with bacteria were incubated at 37 °C and that with candida at 32 °C, for 24 h. The results were read the following day and the *MIC* value of each compound on every strain was taken as the concentration at which there was no development of a red colour. All tests were performed in triplicate and the *MIC* values were constant.

TABLE II. The examined bacteria and fungus types

No.	Microorganism	ATCC No.
1	*Staphylococcus aureus*	6538
2	*Lysteria monocytogenes*	19115
3	*Enterococcus faecalis*	29212
4	*Shigella sonnei*	29930
5	*Salmonella enteritidis*	13076
6	*Yersinia enterocolitica*	27729
7	*Escherichia coli*	35150
8	*Proteus hauseri*	13315
9	*Pseudomonas aeruginosa*	27853
10	*Candida albicans*	10259

Antioxidative activity

All the synthesized compounds were screened for their antioxidative activity by the 2,2-diphenylpicrylhydrazyl (DPPH) assay.[37]

DPPH method. A methanolic DPPH solution (0.037 mg mL^{-1}) was prepared and kept in the dark before analysis. Methanolic solutions of the compounds were prepared in various concentrations, depending on the examined compound. 200 µL of each sample was added to 2.8 mL of DPPH solution and reaction mixture was kept in the dark for 20 min. A blind test was performed by adding 200 µL of methanol in 2.8 mL of DPPH solution and the absorbance of both the blind check and the investigated samples was measured at 517 nm. The percent of DPPH reduction, $DPPH_{\mathrm{red}}$, was calculated from the equation:

$$DPPH_{\mathrm{red}} = 100\frac{\left(A_{\mathrm{BT}} - A_{\mathrm{SX}}\right)}{A_{\mathrm{BT}}}$$

where A_{BT} is the absorbance in the blind test, and A_{SX} corresponds to absorbance of a specific sample.

RESULTS AND DISCUSSION

Characterization of the synthesized compounds

The structures of all synthesized compounds **1**–**6** from Table I were confirmed by melting points, FTIR, ^{1}H-,^{13}C-NMR spectra and also by elemental analysis for compounds **1** and **5**. The data for compound characterization are given in the Supplementary material to this paper.

To the best of our knowledge, there are no literature data that compounds **1** and **5** had been hitherto synthesized, therefore they could be classified as new compounds. Compound **2** has already been used for the synthesis of metal complexes,[32] commercial sources exist for compound **3***, and the antimicrobial activities of compounds **4**[38] and **6**[33] have also already been researched. However, no available FTIR or NMR spectra of them could be found in the mentioned studies.

Antimicrobial screening

All the examined compounds showed considerable activity against all the tested strains of microorganism except for compound **3**, which exhibited rather weak activity against *E. coli*, *P. aeruginosa* and *C. albicans* in the range of the investigated concentrations. The overall activity could be described as moderate with some selectivity against Gram-positive (G+) or Gram-negative (G–) strains of bacteria, or the yeast *C. albicans.*

The selectivity to G– bacteria, which is an important property for the pharmacological activity, also appeared in a few cases. This property enables the antibiotic agent based on a G– selective compound to be taken without the support of an agent that recovers the gastrointestinal tract, as the natural bacteria it contains are G+. The activity of certain examined isatin derivatives against the fungus was also important because they could be applied as antifungal agents.

The overall results of the antimicrobial screening are given in Table III.

TABLE III. Antimicrobial activity of the examined compounds (*MIC* / mM)

Cmpd.	Microorganism									
	S. aureus	*L. monocytogenes*	*E. faecalis*	*S. sonnei*	*S. enteritidis*	*Y. enterocolytica*	*E. coli*	*P. hauseri*	*P. aeruginosa*	*C. albicans*
1	0.16	0.32	2.56	1.28	2.56	0.64	2.56	0.64	5.12	2.56
2	2.24	1.12	2.24	1.12	1.12	1.12	1.12	1.12	2.24	2.24
3	2.53	0.63	2.53	5.06	>5.06	2.53	>5.06	5.06	>5.06	>5.06
4	0.57	2.28	0.57	0.57	1.14	1.14	1.14	1.14	2.28	2.28
5	5.27	2.64	2.64	0.66	5.27	0.33	2.64	0.99	2.64	2.64
6	4.68	1.17	4.68	0.59	4.68	0.59	4.68	1.17	2.34	1.17

Some of the isatin derivatives synthesized in this research displayed significant activity against the various examined bacteria and fungus, while some others were only moderately or even weakly active.

Compound **1** exhibited the most prominent overall activity on both G+ (*S. aureus* and *L. monocytogenes*) and G– (*Y. enterocolitica* and *P. hauseri*) bacterial strains. The highest activity of this compound was registered against *S. aureus*

* Scientific Exchange, Inc., 105 Pine River Road, P. O. Box 918, Center Ossipee, NH 03814, USA.

(*MIC* value of 0.16 mM), followed closely by *L. monocytogenes* (*MIC* value of 0.32 mM).

However, compound **1** displayed only moderate activity on *Y. enterocolitica*, unlike compound **5**, which had a rather significant activity against this specific strain (*MIC* value of 0.33 mM). Except for this example, the overall antimicrobial activity of compound **5** was not as strong as that of compound **1**. Besides against *Y. enterocolitica*, it showed moderate activity on *S. sonei* and somewhat slighter on *P. hauseri*.

Compound **6** behaved somewhat similar to compound **5** but without any really prominent antimicrobial activity. It displayed only moderate activity against *Y. enterocolitica* and *S. sonei*.

Compounds **2** and **3** generally showed comparably weak antimicrobial activity. The only observation that could be of interest was the relative selectivity of compound **3** to *L. monocytogenes*. (*MIC* value of 0.63 mM)

Compound **4** exhibited certain moderate activity against *S. aureus*, *E. faecalis* and *S. sonei*.

Antioxidative activity

The results of DPPH analysis showed that compound **1** displayed the most expressed antioxidative activity, while the other investigated compounds, including pure isatin, showed very slight, if any, activity.

With increasing concentration of compound **1**, the absorbance of DPPH decreased, displaying a linear dependence of % $DPPH_{\mathrm{red}}$ in the range of examined concentrations (c, mM), which is described by the following equation:

$$DPPH_{\mathrm{red}}\ [\%] = 5.099 + (101.02 \pm 5.24)c$$

$$R = 0.995,\ s = 3.17,\ n = 6$$

$DPPH_{\mathrm{red}}$ is actually the percent of DPPH reduction and c is the concentration of compound **1**, given in mM. The equation enables the precise determination of the concentration which reduces 50 % of the DPPH concentration (DC_{50}).

Compound **1** showed prominent antioxidative activity, with a DC_{50} value of 0.444 mM. Ascorbic acid was used as a standard, with a DC_{50} value of 0.341 mM (see Fig. S-1 of the Supplementary material), which is quite comparable.

CONCLUSIONS

Six isatin derivatives were synthesized, of which two were new, in order to test their antimicrobial activity. Their structure was confirmed by melting points, and FTIR and NMR spectra. Antimicrobial screening was performed on nine bacterial strains and one yeast strain, by the broth micro-dilution method. Some compounds showed relative selectivity to certain bacterial strains. In several cases, slight selectivity could be noticed against certain bacterial strains. Compounds **1**, **5** and **6** exhibited relative selectivity against the G– bacteria *S. sonei*, *Y. enterocolitica* and *P. hauseri*, shown by the *MIC* values being approximately 4 to 16 times lower than for other examined G– bacteria, which means that the effects of the mentioned compounds were considerably stronger on these three bacterial strains, than on the others tested. Compounds **3** and **6** showed relative selectivity to *L. monocytogenes* – if only the other G+ bacteria were taken into consideration, with approximately 4 times better activity on *L. monocytogenes* than on the other examined G+ bacteria. Compound **1** showed significant activity against both *S. aureus* and *L. monocytogenes.*

Overall effect of the examined compounds on selected bacterial and yeast strains could be described as moderate, with the exception of compounds **1** and **5** which exhibited prominent activity to *S. aureus* and *L. monocytogenes* (**1**) and *Y. enterocolitica* (**5**) and would be of interest for further analysis. Compounds **5** and **6** showed somewhat better activity to certain G– strains than to G+ strains, which makes them interesting from the medicinal point of view.

The DPPH reduction test was performed to investigate the antioxidative activity of the synthesized compounds and compound **1** displayed significant activity, which makes it of highest interest for further study.

SUPPLEMENTARY MATERIAL

Characterization data of the synthesized compounds and graph for antioxidative activity of compound **1** are available electronically from http://www.shd.org.rs/JSCS/, or from the corresponding author on request.

Acknowledgements. Thanks go to the Ministry Education, Science and Technological Development of the Republic of Serbia (Project Nos. 172013 and III 46010) for financial support.

ИЗВОД

СИНТЕЗА, АНТИМИКРОБНА И АНТИОКСИДАТИВНА АКТИВНОСТ ДЕРИВАТА ИЗАТИНА

ГАВРИЛО М. ШЕКУЛАРАЦ[1], ЈАСМИНА Б. НИКОЛИЋ[2], ПРЕДРАГ ПЕТРОВИЋ[3], БРАНКО БУГАРСКИ[3], БОБАН ЂУРОВИЋ[4] и САША Ж. ДРМАНИЋ[2]

[1]*Институт за хемију, технологију и металургију, Универзитет у Београду, Његошева 12, Београд,* [2]*Катедра за органску хемију, Технолошко–металуршки факултет, Универзитет у Београду, Карнегијева 4, 11120 Београд,* [3]*Катедра за хемијско инжењерство, Технолошко–металуршки факултет, Универзитет у Београду, Карнегијева 4, 11120 Београд и* [4]*Факултет техничких наука, Кнеза Милоша 7, 38220 Косовска Митровица*

Деривати изатина, Шифове базе, синтетисани су реакцијом између изатина и различитих супституисаних примарних амина, и затим окарактерисани са неколико спектроскопсих метода. Испитивање антимикробне активности синтетисаних једињења је изведено бујон-микродилуционом методом, на различитим сојевима бактерија и једној гљивици. Такође је испитана и антиоксидативна активност синтетисаних једињења. Нека од њих су показала значајну како антимикробну, тако и антиоксидативну активност.

(Примљено 9. јула, ревидирано 17. августа, прихваћено 18. августа 2014)

REFERENCES

1. R. W. Daisley, V. K. Shah, *J. Pharm. Sci.* **73** (1984) 407
2. E. Piscopo, M. V. Diurno, R. Gogliardi, M. Cucciniello, G. Veneruso, *Boll. – Soc. Ital. Biol. Sper.* **63** (1981) 827
3. S. N. Pandeya, D. Sriram, E. De. Clercq, C. Pannecouque, M. Witvrouw, *Indian J. Pharm. Sci.* **60** (1998) 207
4. V. A. Muthukumar, H. C. Nagaraj, D. Bhattacherjee, S. George, *Int. J. Pharm. Pharm. Sci.* **5** (Suppl. 3) (2013) 95
5. R. S.Varma, I. A. Khan, *Indian J. Med. Res.* **67** (1978) 315
6. F. D. Popp, H. J. Pajouhesh, *Pharm. Sci.* **17** (1988) 1052
7. R. S. Varma, W. L. Nobles, *J. Pharm. Sci* **64** (1975). 881
8. F. D. Popp, R. Parson, B. E. Donigan, *J. Heterocycl. Chem.* **17** (1980) 1329
9. F. Kontz, *Sci. Pharm.* **41** (1973) 123
10. F. P.Silver, F. D. Popp, A. C. Casey, D. P. Chakraborty, E. Cullen, W. R. Kirsch, J. E. McClesky, B. Sinha, *J. Med. Chem.* **10** (1967) 986
11. P. Pakravan, S. Kashanian, M. M. Khodaei, F. J. Harding, *Pharmacol. Rep.* **65** (2013) 313
12. A. C. Padhya, J. J. Meth, V. S. Dighe, S. Somoshkhara, *Sci. Cult.* **39** (1973) 55
13. F. D. Popp, R. Parson, B. E. Donigan, *J. Pharm. Sci.* **69** (1980) 1237
14. F. D. Popp, *J. Heterocycl. Chem* **21** (1984). 289
15. S. K. Shukla, S. P. Singh, *Indian J. Chem., B* **22** (1983). 697
16. J. P. Scovill, D. L. Klayman, C. E. Franchino, *J. Med. Chem.* **25** (1982) 1261
17. H. Schmidhammer, G. Hrovat, M. Reiss, C. Ungerank, *Sci. Pharm.* **64** (1996) 655
18. D. Singh, R. V. Singh, *J. Inorg. Biochem.* **15** (1993) 227
19. R. Protivinsky, *Antibiot. Chemother.* **17** (1971) 101
20. K. C. Joshi, V. N. Pathak, S. K. Jain, *Pharmazie* **35** (1980) 677
21. R. G. Shepherd, in: *Medicinal Chemistry*, A. Burger, Ed., Wiley, New York, 1970, p. 348
22. I. Heinisch, M. Tonew, *Pharmazie* **31** (1976) 840
23. S. P. Sing, S. K. Shukla, L. P. Awasthi, *Curr. Sci.* **52** (1983) 766.
24. A. Danda, V. Kaur, P. Singh, *Indian J. Pharm. Sci.* **55** (1993) 129
25. A. Chattree, N. Singh, *Int. J. Biol. Pharm. Allied Sci.* **1** (2012) 395
26. J. C. Logan, M. P. Fox, J. H. Morgan, A. M. Makohon, C. J. Pfau, *J. Gen. Virol*. **28** (1975) 271
27. A. Omar, M. E. Mohsen, H. Nabil, M. Hassan, *Arch. Pharm.* **317** (1984) 68
28. R. S. Varma, K. R. Pandey, P. Kumar, *Ind. J. Pharm. Sci.* **44** (1982) 132
29. F. D. Popp, R. Parson, B. E. Donigan, *J. Pharm. Sci.* **69** (1980) 1235
30. M. Rajopadhye, F. D. Popp, *J. Med. Chem.* **31** (1988) 1001
31. A. A. El-Gendy, A. A. Nadia, Z. S. El-Taher, A. E. Hosney, *Alex. J. Pharm. Sci.* **7** (1993) 99
32. Z. H. Chohana, H. Perveza, A. Raufb, K. M. Khanc, C. T. Supurand, *J. Enzyme Inhib. Med. Chem.* **19** (2004) 417
33. J. Panda, V. J. Patro, B. Sahoo, J. Mishra, *J. Nanopar.* (2013), Article ID 549502, http://dx.doi.org/10.1155/2013/549502
34. H. Sies, *Exp. Physiol.* **82** (1997) 29
35. C. E. Boozer, G. S. Hammond, C. E. Hamilton, E. Chester, J. N. Sen, *J. Am. Chem. Soc.* **77** (1955) 3233
36. A. Espinel-Ingroff, A. Fothergill, M. Ghannoum, E. Manavathu, L. Ostrosky-Zeichner, M. Pfaller, M. Rinaldi, W. Schell, T. Walsh, *J. Clin. Microbiol.* **43** (2005) 5243
37. K. Shimada, K. Fujikawa, K. Yahara, T. Nakamura, *J. Agric. Food Chem*. **40** (1992) 945
38. E. Piscopo, M. V. Diurno, F. Imperadrice, M. Cucciniello, G. Veneruso, *Boll. – Soc. Ital. Biol. Sper*. **62** (1986) 1441.

Journal of the Serbian Chemical Society
JSCS@tmf.bg.ac.rs • www.shd.org.rs/JSCS
J. Serb. Chem. Soc. 79 (11) S154–S155 (2014) *Supplementary material*

SUPPLEMENTARY MATERIAL TO

Synthesis, antimicrobial and antioxidative activity of some new isatin derivatives

GAVRILO M. ŠEKULARAC[1#], JASMINA B. NIKOLIĆ[2#], PREDRAG PETROVIĆ[3], BRANKO BUGARSKI[3], BOBAN ĐUROVIĆ[4] and SAŠA Ž. DRMANIĆ[2*#]

[1]Institute of Chemistry, Technology and Metallurgy, University of Belgrade, Njegoševa 12, Belgrade, Serbia, [2]Department of Organic Chemistry, Faculty of Technology and Metallurgy, University of Belgrade, Karnegijeva 4, 11000 Belgrade, Serbia, [3]Department of Chemical Engineering, Faculty of Technology and Metallurgy, University of Belgrade, Karnegijeva 4, 11000 Belgrade, Serbia and [4]Faculty of Technical Science, Kneza Miloša 7, 38220 Kosovska Mitrovica, Serbia

J. Serb. Chem. Soc. 79 (11) (2014) 1347–1355

I. CHARACTERIZATION OF THE SYNTHESIZED COMPOUNDS

*1,3-Dihydro-3-[(5-mercapto-1,3,4-thiadiazol-2-yl)imino]-2*H*-indol-2-one* (***1***). Yield: 74 %; m.p.: 183–185 °C; Anal. Calcd. for $C_{10}H_6N_4OS_2$: C, 45.8; H, 2.30; N; 21.4 %. Found: C, 46.0; H, 2.37; N 21.5 %. IR (KBr, cm^{-1}): 3418 (NH), 1743 (C=O), 1733 (C=N), 1616 (C=N); ^{1}H-NMR (250 MHz, DMSO-d_6, δ / ppm): 11.03 (1H, *s*, NH), 7.60–6.90 (4H, *m*, isatin-Ph), 3.4 (1H, *s*, SH); ^{13}C-NMR (62.89 MHz, DMSO-d_6, δ / ppm): 184.0 (C–SH), 180.1 (N–C=N), 162.0 (C=N), 159.1 (C=O), 131.6 (isatin-Ph).

*1,3-Dihydro-3-(2-benzothiazolylimino)-2*H*-indol-2-one* (**2**). Yield: 78 %; m.p.: 164–166 °C; IR (KBr, cm^{-1}): 3315 (NH), 1715 (C=O), 1650 (C=N), 1575 (C=N); ^{1}H-NMR (250 MHz, DMSO-d_6, δ / ppm): 11.05 (1H, *s*, NH), 7.60–6.90 (4H, *m*, isatin-Ph), 7.3–8.2 (4H, *m*, benzothiazol); ^{13}C-NMR (62.89 MHz, DMSO-d_6, δ / ppm): 166.3 (S–C=N), 159.1 (C=N), 152.6 (C=O), 127.9 (isatin-Ph), 136.5 (benzothiazole).

*1,3-Dihydro-3-[(4-cyanophenyl)imino]-2*H*-indol-2-one* (**3**). Yield: 73 %; m.p.: 257–259 °C; IR (KBr, cm^{-1}): 3446 (NH), 2228 (CN), 1742 (C=O), 1727 C=N), 1611 (C=N); ^{1}H-NMR (250 MHz, DMSO-d_6, δ / ppm): 11.05 (1H, *s*, NH), 7.94–6.94 (4H, *m*, isatin-Ph), 7.68 (2H, *d*, *J* = 7.5 Hz, benzene); ^{13}C-NMR (62.89 MHz, DMSO-d_6, δ / ppm): 163.1 (C=N), 153.2 (C=O), 132.4 (isatin-Ph), 128.2 (benzene), 119.2 (C–CN).

* Corresponding author. E-mail: drmana@tmf.bg.ac.rs

*1,3-Dihydro-3-[(5-nitro-2-thiazolyl)imino]-2*H*-indol-2-one* (**4**). Yield: 79 %; m.p.: 178–180 °C. IR (KBr, cm^{-1}): 3431 (NH), 1751 (C=O), 1741 (C=N), 1633 (C=N), 1367 (NO_2); ^{1}H-NMR (250 MHz, DMSO-d_6, δ / ppm): 11.04 (1H, *s*, NH), 8.80 (1H, *s*, CH=C), 7.59–6.87 (4H, *m*, isatin-Ph); ^{13}C-NMR (62.89 MHz, DMSO-d_6, δ / ppm): 184.6 (S–C=N), 173.7 (C=N), 158.3 (N–C=N), 150.7 (C=O), 147.5 (S–C–NO_2), 125.4 (isatin-Ph).

*1,3-Dihydro-3-[(5-methyl-2-pyridyl)imino]-2*H*-indol-2-one* (**5**). Yield: 72 %; m.p.: 204–206 °C; Anal. calcd. for $C_{14}H_{11}N_3O$: C, 71.0; H, 4.6; N; 17.7 %. Found: C, 71.3; H, 4.4; N, 17.5 %; IR (KBr, cm^{-1}): 3447 (NH), 3193 (C=N aromatic), 1753 (C=O), 1733 (C=N), 1626 (C=N); ^{1}H-NMR (250 MHz, DMSO--d_6, δ / ppm): 11.07 (1H, *s*, NH), 7.96–7.23 (4H, *m*, isatin-Ph), 8.33–6.88 (3H, *m*, pyridine), 2.33 (3H, *s*, CH_3); ^{13}C-NMR (62.89 MHz, DMSO-d_6, δ / ppm): 163.6 (C=N), 152 (C=O), 130.6 (isatin-Ph), 138.3 (pyridine), 19.5 (CH_3).

*1,3-Dihydro-3-[(4-nitrophenyl)imino]-2*H*-indol-2-one* (**6**). Yield: 79 %; m.p.: 149–151 °C; IR (KBr, cm^{-1}): 3446 (NH), 1742 (C=O), 1727 (C=N), 1611 (C=N), 1367 (NO_2); ^{1}H-NMR (250 MHz, DMSO-d_6, δ / ppm): 11.02 (1H, *s*, NH), 7.90–7.83 (4H, *m*, isatin-Ph), 6.87 (2H, *d*, *J* = 7.5 Hz, benzene); ^{13}C-NMR (62.89 MHz, DMSO-d_6, δ / ppm): 164.7 (C=N), 155 (C=O), 131.0 (isatin-Ph), 162.3 (C–N), 147.5 (C–NO_2), 141.5 (benzene).

II. ANTIOXIDATIVE ACTIVITY

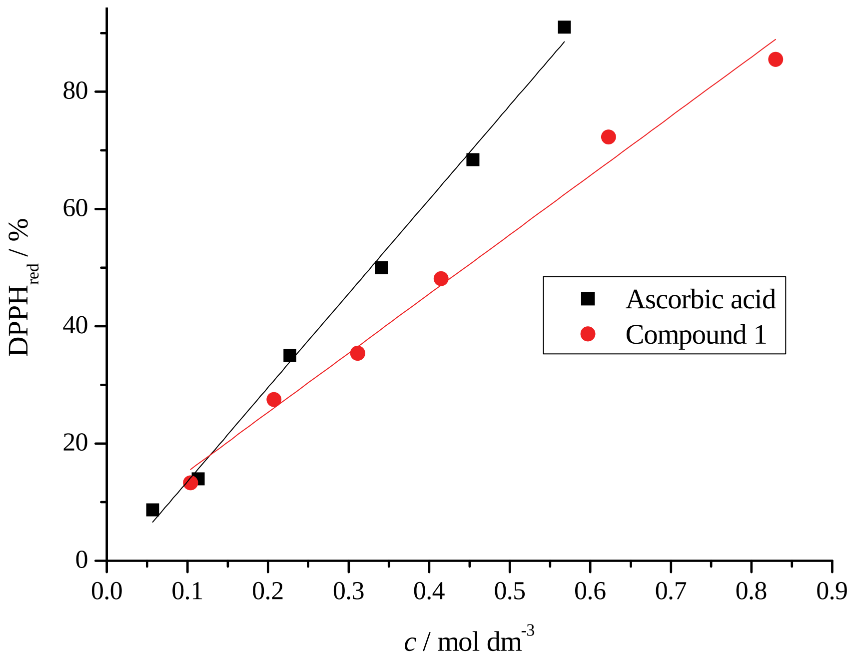

Fig. S-1. DPPH Scavenging activity of compound **1** compared to ascorbic acid.

Journal of the Serbian Chemical Society
JSCS-info@shd.org.rs • www.shd.org.rs/JSCS
J. Serb. Chem. Soc. 79 (11) 1355–1362 (2014)
JSCS–4670
UDC **Centaurea*:547.972:543.422.25
Original scientific paper

Secondary metabolites of three endemic *Centaurea* L. species

VELE TEŠEVIĆ[1]*, IVANA ALJANČIĆ[2], SLOBODAN MILOSAVLJEVIĆ[1#], VLATKA VAJS[1,2], IRIS ĐORĐEVIĆ[3], MILKA JADRANIN[2], NEBOJŠA MENKOVIĆ[4] and VLADO MATEVSKI[5]

[1]*Faculty of Chemistry, University of Belgrade, Studentski trg 12–16, 11158 Belgrade, Serbia,* [2]*Institute of Chemistry, Technology and Metallurgy, Center for Chemistry, University of Belgrade, Njegoševa 12, 11001 Belgrade, Serbia,* [3]*Faculty for Veterinary Medicine, University of Belgrade, Bulevar oslobodenja 18, 11000 Belgrade, Serbia,* [4]*Institute for Medicinal Plant Research, "Dr. Josif Pančić", Tadeuša Košćuška 1, 11000 Belgrade, Serbia and* [5]*Faculty of Natural Sciences and Mathematics, Ss. Cyril and Methodius University in Skopje, Blvd. Goce Delcev 9, 1000 Skopje, FYROM*

(Received 18 March, revised 25 April 2014, accepted 6 May 2014)

Abstract: The aerial parts of three endemic *Centaurea* L. species, namely *C. tomorosii* Micevski, *C. soskae* Hayek and *C. galicicae* Micevski, afforded the sesquiterpene lactone cnicin (**1**) and seven flavonoids: apigenin (**2**), isokaempferide (**3**), hispidulin (**4**), eupatorin (**5**), cirsimaritin (**6**), santoflavone (**7**) and salvigenin (**8**). The structures of the isolated compounds were determined by UV, ^{1}H-NMR and ^{13}C-NMR spectroscopy and HR-ESI-MS spectrometry. ^{1}H-NMR spectroscopy was used as a method for the quantitative analysis of cnicin.

Keywords: *Centaurea*; cnicin; flavonoids.

INTRODUCTION

The genus *Centaurea* L. is one of the largest genera of the Asteraceae family and also one of the most representative genera within the tribe Cardueae Cass. and the subtribe Centaureinae (Cass.) Dumort. with around 250 species.[1] It is mainly distributed in the Mediterranean region and South–East Asia and is characterized by a great degree of endemism,[2] which is usually associated to restricted geographical areas.[3]

The species of the genus *Centaurea* have been used in folk medicine for a long time. Various *Centaurea* species have certain biological activities, such as antifungal,[4] antimicrobial,[5] anti-ulcerogenic,[6] anti-inflammatory,[7] antioxidant,[8] antiviral,[9] anti-*Helicobacter pylori*,[10] anticancer and cytotoxic.[11] The genus was

* Corresponding author. E-mail: vtesevic@chem.bg.ac.rs
# Serbian Chemical Society member.
doi: 10.2298/JSC140318048T

also the subject of interest of several phytochemical investigations for their potentially active constituents, particularly sesquiterpene lactones[12–16] and flavonoids.[17,18]

As a part of ongoing and systematic investigations on the composition of the plants of this genus,[19–24] the chemical constituents of the extracts of the aerial parts of three species: *C. tomorosii* Micevski, *C. soskae* Hayek and *C. galicicae* Micevski, all are endemic to Balkan Peninsula, were investigated. No previous phytochemical study on these species has been reported.

EXPERIMENTAL

General

The UV spectra were recorded on a GBC Cintra 40 UV–Vis spectrometer. The ^{1}H- and ^{13}C-NMR data were acquired on Varian Gemini 2000 NMR spectrometer (200 MHz for ^{1}H- and 50 MHz for ^{13}C-NMR, in $CDCl_3$, with TMS as an internal reference). Dry column flash-chromatography (DCFC) and column chromatography (CC) were performed on silica gel (ICN Silica 12–26 60 Å and 70–230 mesh, ASTM, Merck, respectively). Silica gel 60 F_{254} precoated aluminum sheets (layer thickness 0.25 mm, Merck) for TLC control and preparative TLC plates (2 mm Merck) for preparative purification were used. The high-resolution liquid chromatography/photo-diode array/electrospray ionization/time of flight mass spectra (HRLC/PDA/ESI/TOF MS) were measured on a HPLC instrument (Agilent 1200 Series) equipped with an autosampler, using a Zorbax Eclipse Plus C_{18} analytical column (1.8 μm particle size, 4.6 mm×150 mm i.d., Agilent Technologies), and a PDA detector (DAD) coupled with a 6210 TOF LC/MS system (Agilent Technologies).

Plant materials

The aerial parts of the investigated species were collected during the flowering period (17 July 2010) at the following localities: *C. tomorosii* Micevski at Tomoros (*ca*. 1700 altitude), on Mount Galičica, *C. soskae* Hayek near Lake Ohrid, and *C. galicicae* Micevski close to Lake Prespa. The plants were identified by Vlado Matevski, Institute of Biology, Faculty of Natural Sciences and Mathematics, Ss. Cyril and Methodius University of Skopje, where voucher specimens are deposited at the Macedonian National Herbarium (MKNH) under accession numbers: MKNH135338 (*C. tomorosii*) MKNH135336 (*C. soskae*) and MKNH135337 (*C. galicicae*).

Extraction and isolation

The dried, ground aerial parts of *C. tomorosii* (100 g) were extracted twice with petroleum ether–Et_2O–methanol (1:1:1) at room temperature and re-extracted with Et_2O–MeOH.[25] The crude extract (5 g) was fractionated by dry-column flash chromatography on silica gel using petroleum ether–Et_2O–MeOH with increasing polarity to yield 25 fractions. The fractions eluted with Et_2O–MeOH 9:1 (Fr 19), 8:2 (Fr 20) and 7:3 (Fr 23) contained flavonoids and the sesquiterpene lactone cnicin (according to the ^{1}H-NMR and IR spectra), and were further purified by CC on silica gel. Elution with CH_2Cl_2–MeOH (1:1) afforded cnicin (**1**, 123 mg) from Fr 23, while the combined fractions Fr 19 and Fr 20 yielded apigenin (**2**, 5 mg), isokaempferide (**3**, 3 mg), hispidulin (**4**, 6 mg), cirsimaritin (**6**, 10 mg) and santoflavone (**7**, 8 mg).

HRLC/PDA/ESI/TOF MS analyses

Crude extract of each endemic *Centaurea* species was dissolved in methanol to an approximate concentration of 5 mg mL^{-1}. The HRLC/PDA/ESI/TOF MS analyses were realized under the following conditions: the mobile phase consisted of water containing 0.2 % formic acid (A) and acetonitrile (B). A gradient program was used as follows: 0–1.5 min 5 % B, 1.5––26 min, 5 %–95 % B, 26–35 min, 95 % B. The flow rate of the mobile phase was 1.4 mL min^{-1}, the column temperature was kept at 40 °C and the injection volume was 5 μL. UV spectral data from all peaks were accumulated in the range of 190–450 nm and chromatograms were recorded at 240 nm. MS data were collected by applying the following parameters: ionization, negative ESI capillary voltage 4000 V, gas temperature 350 °C, drying gas 12 L min^{-1}, nebulizer pressure 45 psi*, fragmentor voltage 140 V, mass range 100–2000 *m*/*z*. A personal computer system running MassHunter Workstation software was used for data acquisition and processing.

Quantification of cnicin content

The quantitative analysis of cnicin was performed according to the previously described procedure,[26] using BHT (2,6-bis(1,1-dimethylethyl)-4-methylphenol) as the internal standard. The ^{1}H-NMR spectrum of known amounts of crude plant extract and internal standard was recorded and quantification was performed by calculating the ratio of the peak areas of selected proton signals of the target compound and the internal reference standard.

RESULTS AND DISCUSSION

According to HPLC analysis, all the three studied taxa of *Centaurea* exhibited very similar flavonoid patterns, differing only in the relative amounts of the constituents (Fig. 1).

Exact mass measurements of pseudomolecular ions of the analytes was realized with a time-of-flight (TOF) mass spectrometer operating in the negative polarity mode, which enabled the determination of the molecular formula of most of the constituents. All the identified compounds exhibited a quasi-molecular ion $[M–H]^–$ signal in the negative mode, confirming their molecular masses (Table I).

Peak identification was performed by comparison of their retention time, mass, and UV spectra with those of previously isolated compounds from *C. tomorosii*. From the crude extract of *C. tomorosii*, sesquiterpene lactone cnicin (**1**) and flavonoids apigenin (**2**), isokaempferide (**3**), hispidulin (**4**), cirsimaritin (**6**) and santoflavone (**7**) were isolated and indentified by means of UV, MS and NMR spectral data.[27] Flavonoids eupatorin (**5**) and salvigenin (**8**) were tentatively identified based on their UV and MS spectra, as well as by comparison with the literature data.[21] Formulae of these compounds are represented in Fig. 2.

All compounds represent mainly the characteristic secondary metabolites of the genus that were previously reported from different *Centaurea* species.[18] The observed differences between the taxa is the absence of cirsimaritin (**6**) and predominance of santaflavone (**7**) in *C. soskae* and *C. galicicae*, compared to *C.*

* 1 psi = 6894.757 Pa

tomorosii. Similarly, the germacranolide cnicin (**1**) was detected, as was the case for a large number of *Centaurea* species.[28]

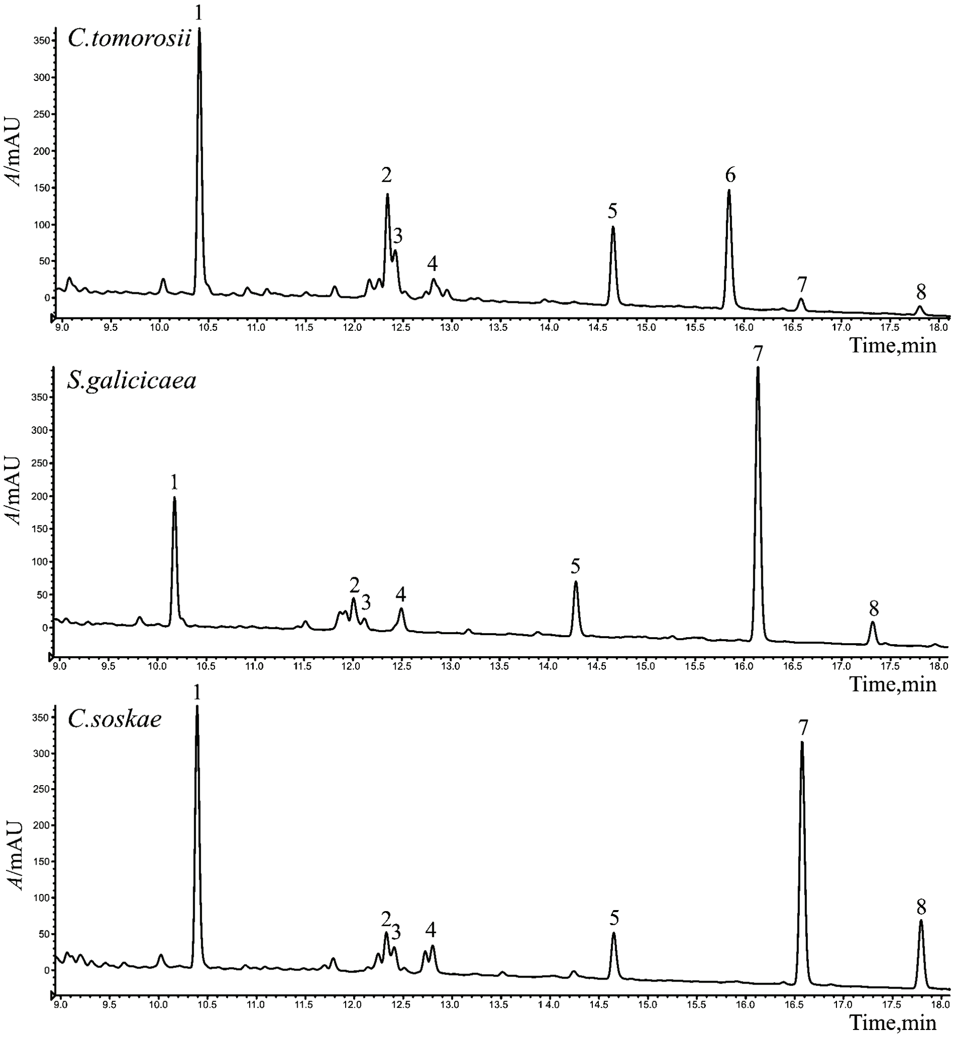

Fig. 1. HPLC profiles of the crude extracts of *C. galicicae, C. soskae* and *C. tomorosii*.

The HPLC chromatograms and ^{1}H-NMR spectra of the crude extracts of the aerial parts of all samples revealed the sesquiterpene lactone cnicin (**1**) as the major constituent (Figs. 1 and 3).

The sesquiterpene lactone cnicin was first isolated from *Cnicus benedictus* (blessed thistle) and found in 83 *Centaurea* species.[28] Since mediaeval times, preparations of blessed thistle (*e.g.*, bitter tonics) have been used to treat various disorders, such as lack of appetite, dyspeptic troubles, liver diseases, and biliousness, while in the form of an external local remedy, blessed thistle was effective against ulcers and chilblains.[29] Nowadays, liver and bile tea compositions contain blessed thistle herb, which is also known to stimulate salivary secretion and gastric juice formation. Cnicin was established as the main active principle in blessed thistle, exhibiting antibacterial, antifungal, and strong anti-inflammatory effects. Known to be cytotoxic as some other sesquiterpene lactones,[30] cnicin exhibited cytotoxic activity against some tumor cell lines including leukemia (HL-60), hepatomas, sarcomas, lymphoid leukemia and multiple myeloma.[31–34]

TABLE I. Composition of flavonoid complex of *C. tomorosii*, *C. soskae* and *C. galicicae*

Compound	$[M–H]^-$ *m/z*	Acc. mass	Molecular formulae	Spectral methods used in identification	*C. tomorosii*	*C. soskae*	*C. galicicae*
Apigenin (**2**)	269.0438	270.0528	$C_{15}H_{10}O_5$	^{1}H-, ^{13}C-NMR, HRMS, UV	+	+	+
Isokaempferide (**3**)	299.0545	300.0633	$C_{16}H_{12}O_6$	^{1}H-, ^{13}C-NMR, HRMS, UV	+	+	+
Hispidulin (**4**)	299.0541	300.0633	$C_{16}H_{12}O_6$	^{1}H-, ^{13}C-NMR, HRMS, UV	+	+	+
Eupatorin (**5**)	343.0811	344.0896	$C_{18}H_{16}O_7$	HRMS, UV	+	+	+
Cirsimaritin (**6**)	313.0702	314.0793	$C_{17}H_{14}O_6$	^{1}H-, ^{13}C-NMR, HRMS, UV	+	–	–
Santoflavone (**7**)	359.1474	360.1209	$C_{19}H_{19}O_7$	^{1}H-, ^{13}C-NMR, HRMS, UV	+	+	+
Salvigenin (**8**)	327.2148	328.0974	$C_{18}H_{16}O_6$	HRMS, UV	+	+	+

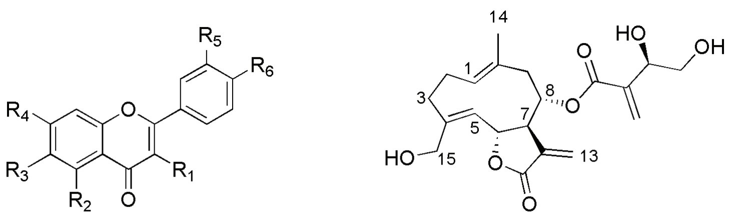

1

Cmpd.	R_1	R_2	R_3	R_4	R_5	R_6
Apigenin (**2**)	H	OH	H	OH	H	OH
Isokaempferide (**3**)	OH	OH	H	OMe	H	OH
Hispidulin (**4**)	H	OH	OMe	OH	H	OH
Eupatorin (**5**)	H	OH	OMe	OMe	OH	OMe
Cirsimaritin (**6**)	H	OH	OMe	OMe	H	OH
Santoflavone (**7**)	H	OH	OMe	OMe	OMe	OMe
Salvigenin (**8**)	H	OH	OMe	OMe	H	OMe

Fig. 2. Chemical structures of the compounds detected in the studied *Centaurea* species.

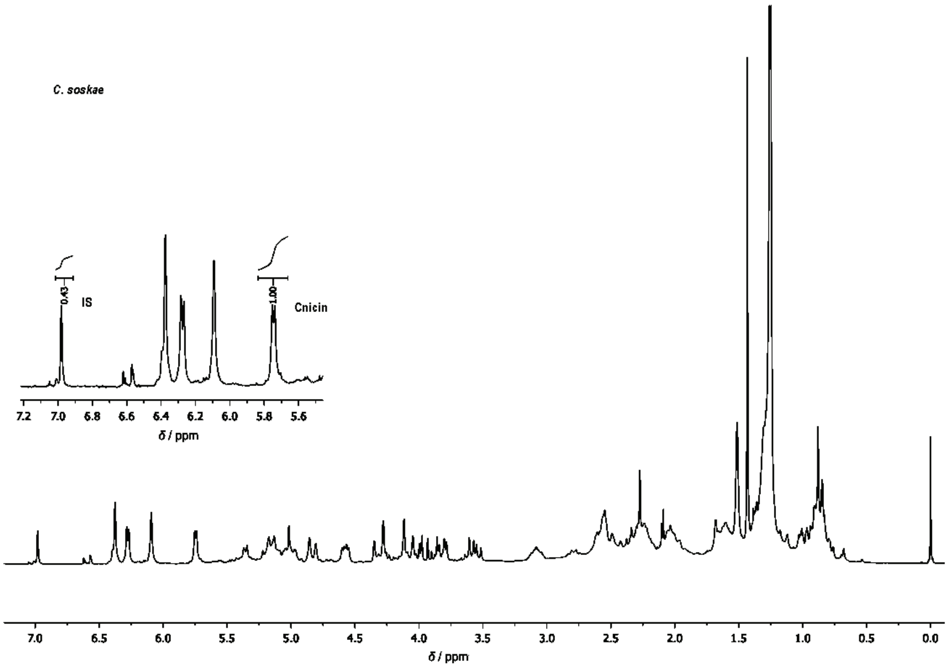

Fig. 3. Representative ^{1}H-NMR spectrum of the crude extract of *C. soskae* with internal standard (IS).

In previous phytochemical studies, the content of cnicin in six *Centaurea species* was analyzed by ^{1}H-NMR spectroscopy. The examined extracts were made from freshly collected plants. The highest content of cnicin was found in *C. affinis* (0.61 %). The content of cnicin in *C. arenaria*, *C. cuneifolia*, *C. glaberrima*, *C. splendens* and *C. stoebe* was lower (0.11–0.55 %).[26] According to quantitative ^{1}H-NMR measurements, based on the integrals of the one-proton doublet of cnicin (centered at δ 5.74 ppm, H-13) and the two-proton singlet (at δ 6.98 ppm) of a known amount of BHT, used as an internal standard, the content of cnicin was 2.9, 9.6 and 3.6 % in the dry plant extracts of *C. tomorosii*, *C. soskae* and *C. galicicae*, respectively (Table II). This amount of cnicin indicates potentially alternative sources of cnicin in these three *Centaurea* species, compared to one of the main natural sources, *i.e.*, *C. benedictus*, in which this metabolite is found at a concentration of 0.5 % of the dry mass.[29]

TABLE II. Content of cnicin in the aerial parts of *C. tomorosii*, *C. soskae* and *C. galicicae*

Specimen	Content±*SD*, % dry plant
C. tomorosii	2.9±0.08
C. soskae	9.6±0.15
C. galicicae	3.6±0.11

CONCLUSIONS

No previous phytochemical study has been performed on these three *Centaurea* species.

Among the three *Centaurea* species examined in this work, *C. soskae* showed the highest content of cnicin 9.6 %, while *C. tomorosii* and *C. galicicae* were found to contain 2.9 and 3.6 % of cnicin, respectively. All isolated compounds represent mainly the characteristic secondary metabolites of the genus. Methoxylated flavones, such as hispidulin (**4**), eupatorin (**5**), cirsimaritin (**6**), santoflavone (**7**) and salvigenin (**8**), as well as apigenin (**2**) and flavonol isokaempferide (**3**) were described previously as constituents of different *Centaurea* species. Similarly, the germacranolide cnicin (**1**) was detected in a large number of *Centaurea* species.

Acknowledgement. This work was financially supported by Ministry of Education, Science and Technological Development of the Republic of Serbia, (Project No. 172053). We thank Andon Bojadži and Oliver Avramoski, National Park Galičica, Ohrid, FYROM for supplying the plant material.

И З В О Д

СЕКУНДАРНИ МЕТАБОЛИТИ ТРИ ЕНДЕМСКЕ ВРСТЕ РОДА *Centaurea* L.

ВЕЛЕ ТЕШЕВИЋ[1], ИВАНА АЉАНЧИЋ[2], СЛОБОДАН МИЛОСАВЉЕВИЋ[1], ВЛАТКА ВАЈС[1,2], ИРИС ЂОРЂЕВИЋ[3], МИЛКА ЈАДРАНИН[2], НЕБОЈША МЕНКОВИЋ[4] и ВЛАДО МАТЕВСКИ[5]

[1]*Хемијски факултет, Универзитет у Београду, Студентски трг 16, 11158 Београд,* [2]*Институт за хемију, технологију и металургију, Центар за хемију, Универзитет у Београду, Његошева 12, 11001 Београд,* [3]*Факултет ветеринарске медицине, Универзитет у Београду, Булевар ослобођења 18, 11000 Београд,* [4]*Институт за лековито биље, „Др Јосиф Панчић" Тадеуша Кошћушка 1, 11000 Београд и* [5]*Faculty of Natural Sciences and Mathematics, Ss. Cyril and Methodius University in Skopje, Blvd. Goce Delcev 9, 1000 Skopje, FYROM*

Из надземног дела три ендемске врсте рода *Centaurea* L., *C. tomorosii* Micevski, *Centaurea soskae* Hayek и *Centaurea galicicae* Micevski, изоловани су сесквитерпенски лактон кницин (**1**) и седам флавоноида: апигенин (**2**), изокемферид (**3**), хиспидулин (**4**), еупаторин (**5**), цирсимаритин (**6**), сантофлавон (**7**) и салвигенин (**8**). Структуре изолата су одређене UV и ^{1}H-NMR спектроскопијим и HR-ESI-MS спектрометријом. ^{1}H-NMR спектроскопија је коришћена као метода за квантитативну анализу сесквитерпенског лактона кницина.

(Примљено 18. марта, ревидирано 25. априла, прихваћено 6. маја 2014)

REFERENCES

1. A. Susanna, N. Garcia-Jacas, in *The families and genera of vascular plants*, J. W. Kadereit, C. Jeffrey, Eds., Springer, Berlin, 2007, p. 123
2. B. Colas, I. Olivieri, M. Riba, *Proc. Natl. Acad. Sci. USA* **94** (1997) 3471
3. V. N. Suárez-Santiago, M. J. Salinas, N. Garcia-Jacas, P. S. Soltis, D. E. Soltis, G. Blanca, *Mol. Phylogenet. Evol.* **43** (2007) 156
4. C. Koukoulitsa, G. D. Geromichalos, H. Skaltsa, *J. Comput.-Aided Mol. Des.* **19** (2005) 617
5. C. Karamenderes, S. Khan, B. L. Tekwani, M. R. Jacob, I. A. Khan, *Pharm. Biol.* **44** (2006) 534

6. E. Yeşilada, E. Sezik, G. Honda, Y. Takaishi, Y. Takeda, T. Tanaka, *J. Ethnopharmacol*. **64** (1999) 195
7. N. Garbacki, V. Gloaguen, J. Damas, P. Bodart, M. Tits, L. Angenat, *J. Ethnopharmacol*. **68** (1999) 235
8. J. F. Severino, K. Stich, G. Soja, *Environ. Pollut*. **146** (2007) 707
9. G. Rusak, M. Krajacic, N. Plese, *Antiviral Res*. **36** (1997) 125–129
10. G. Stamatis, P. Kyriazopoulos, S. Golegou, A. Basayiannis, S. Skaltsas, H. Skaltsa, *J. Ethnopharmacol*. **88** (2003) 175
11. M. Shoeb, S. M. MacManus, M. Jaspars, J. Trevidu, L. Nahar, P. Kong-Thoo-Lin, S. D. Sarker, *Tetrahedron* **62** (2006) 11172
12. A. G. Gonzalez, J. B. Barrera, T. Z. Garcia, F. E. Rosas, *Phytochemistry* **23** (1984) 2071
13. D. Youssef, A. W. Frahm, *Planta Med.* **60** (1994) 572
14. A. M. Fortuna, E. C. de Riscala, C. A. Catalan, T. E. Gedris, W. Herz, *Biochem. Syst. Ecol.* **29** (2001) 967
15. K. Medjroubi, F. Benayache, J. Bermejo, *Fitoterapia* **76** (2005) **744**
16. M. López-Rodriguez, V. P. Garcia, H. Zater, S. Benayache, F. Benayache, *Acta Crystallogr., E* **65** (2009) 1867
17. Z. F. Ahmed, H. Rimpler, A. M. Rizk, F. M. Hammouda, S. I. Ismail, *Phytochemistry* **9** (1970) 1595
18. M. Kaij-A-Kamb, M. Amoros, L. Girre, *Pharm. Acta Helv*. **67** (1992) 178
19. V. Tešević, V. Vajs, P. Janaćković, N. Todorovic, D. Đoković, P. Marin, S. Milosavljević, *Planta Med.* **64** (1998) 488
20. V. Vajs, N. Todorović, M. Ristić, V. Tešević, B. Todorović, P. Janaćković, P. Marin, S. Milosavljević, *Phytochemistry* **52** (1999) 383
21. P. Janaćković, V. Tešević, S. Milosavljević, V. Vajs, P. D. Marin, *Biochem. Syst. Ecol.* **32** (2004) 355
22. V. Tešević, V. Vajs, N. Todorović, D. Đoković, P. Marin, S. Milosavljević, *J. Serb. Chem. Soc.* **63** (1998) 131
23. V. Tešević, D. Đoković, V. Vajs, P. Marin, S. Milosavljević, *J. Serb. Chem. Soc.* **59** (1994) 979
24. V. Tešević, S. Milosavljević, V. Vajs, P. Janaćković, M. Popsavin, *Biochem. System. Ecol.* **31** (2003) 89
25. F. Bohlmann, C. Zdero, H. R. King, E. H. Robinson, *Phytochemistry* **23** (1984) 1979
26. V. Tešević, S. Milosavljević, V. Vajs, P. Janaćković, I. Djordjević, M. Jadranin, I. Vučković, *J. Serb. Chem. Soc.***72** (2007) 1275, and references therein
27. T. J. Mabry, K. R. Markham, M. B. Thomas, *The Systematic Identification of Flavonoids*, Springer, Berlin, 1970
28. M. Bruno, S. Bancheva, S. Rosselli, A. Maggio, *Phytochemistry* **95** (2013) 19
29. S. Berger, D. Sicker, *Classics in Spectroscopy, Isolation and Structure Elucidation of Natural Products*, Wiley–VCH, Weinheim, 2009, p. 443, and references therein
30. M. Bruno, S. Rosselli, A. Maggio, R. A. Raccuglia, K. F. Bastow, C. C. Wu, K. H. Lee, *Planta Med.* **71** (2005) 1176.
31. R. Vanhaelen-Fastré, *Pharm Belg*. **27** (1972) 683
32. R. Vanhaelen-Fastré, M. Vanhaelen, *Planta Med*. **29** (1976) 179
33. K. Johrer, M. Obkircher, D. Neureiter, J. Parteli, C. Zelle-Rieser, E. Maizner, J. Kern, M. Hermann, F. Hamacher, O. Merkel, N. Wacht, C. Zidorn, M. Scheideler, R. Greil, *J. Mol. Med*. **90** (2012) 681
34. M. Bach, M. A. Fortuna, R. Attarian, J. T. de Trimarco, C. A. Catalán, Y. Av-Gay, H. Bach. *Nat. Prod. Commun*. **6** (2011) 163.

Journal of the Serbian Chemical Society
JSCS-info@shd.org.rs • www.shd.org.rs/JSCS

J. Serb. Chem. Soc. *79* (11) 1363–1378 (2014) UDC **Robinia pseudoacacia*:+543.544.5.068.7:
JSCS–4671 615.27/.28–188:577.18
Original scientific paper

Antimicrobial and antioxidant activity of the vegetative and reproductive organs of *Robinia pseudoacacia*

IOANA C. MARINAS[1], ELIZA OPREA[2]*, ELISABETA-IRINA GEANA[3], CARMEN CHIFIRIUC[1] and VERONICA LAZAR[1]

[1]University of Bucharest, Faculty of Biology, Microbiology Department, 1–3 Portocalilor Way, Bucharest, Romania, [2]University of Bucharest, Faculty of Chemistry, 4–12 Regina Elisabeta, 030018 Bucharest, Romania and [3]National R & D Institute for Cryogenics and Isotopic Technologies – ICIT Rm. Valcea, 4 Uzinei Street, PO Raureni, 240050 Rm. Valcea, Romania

(Received 4 March, revised 30 April, accepted 7 May 2014)

Abstract: This study was aimed at investigating the antimicrobial and antioxidant activity of ethanol extracts obtained from the leaves, seeds and sheaths of *Robinia pseudoacacia*. Total phenolic content (*TPC*, Folin–Ciocalteu method), antioxidant activity (trolox equivalent antioxidant capacity (*TEAC*) assay) and antimicrobial activity (agar disk diffusion method and broth dilution method) of the vegetative and reproductive organs of *R. pseudoacacia* were determined. The highest content of polyphenols (expressed as gallic acid equivalents, GAE) was found in the extract of *R. pseudoacacia* leaves (266.7 μg GAE mL^{-1} extract) followed by the extract of the seeds (232.2 μg GAE mL^{-1} extract). HPLC analysis showed the presence of catechin (0.925 μg mL^{-1}), rutin (0.831 μg mL^{-1}), resveratrol (0.664 μg mL^{-1}) and quercetin (0.456 μg mL^{-1}) in the leaf extract, and catechin (0.127 μg mL^{-1}), epicatechin (0.239 μg mL^{-1}) and rutin (0.231 μg mL^{-1}) in the seed extract. The results showed that the studied extracts exhibited a selective antimicrobial effect directed against Gram-positive (*Staphylococcus aureus* and *Bacillus subtilis*) and Gram-negative (*Pseudomonas aeruginosa*, *Klebsiella pneumoniae* and *Escherichia coli*) bacterial strains. The combination leaf extract/antibiotic had the highest synergistic effect when compared to combinations with seed and sheath extracts. The same extract with penicillin G, kanamycin and rifampin had highest synergetic effect against methicillin-resistant *S. aureus* strain (MRSA), a strain that has gained great interest of microbiologists within the past decades. The chemical characterization of ethanol extracts from the vegetative and reproductive organs of *R. pseudoacacia*, the synergistic effects of certain antibiotics and acacia extracts and the potential to increase the antimicrobial activity of some commercial antibiotics against MRSA were investigated for the first time.

* Corresponding author. E-mail: eliza.oprea@g.unibuc.ro
doi: 10.2298/JSC140304049M

Keywords: antimicrobial activity; antioxidant activity; *Robinia pseudoacacia*; antibiotics.

INTRODUCTION

Robinia pseudoacacia (black locust) is an invasive species transformer that is gaining increasing abundance throughout Europe. It is included on the list of the most dangerous invasive species due to its ability to spread quickly and its high growth rate, forming mono-dominant forests. Few species are tolerant to the allelopatic substances (robetrin, myricetin and quercetin) found in the ethanol extracts from the leaves of acacia.[1,2] Acacia plants (species) are still spreading and invading spontaneous vegetation types which are important and valuable. This species was brought from North America and planted for ornamental and melliferous purposes due to its quality in stabilizing eroded field slopes and sands.[1]

According to the literature, *R. pseudoacacia* contains polyphenolic compounds, such as tannins[3] and taxon specific monoterpenes (robinlin).[4] In addition, some natural compounds with antibacterial activity have been identified in the leaves.[5,6] Some phytocompounds of this species play a vital role in protecting against pathogen or other biotic attacks, being responsible for the natural durability of the solid wood of *R. pseudoacacia*.[7] It was reported that acacia bark has exceptional resistance to biodegradation, this property being assigned to its concentration of dihydrobinetin and robinetin.[8] Essentially the flavonoids with allelopatic properties were detected in high concentrations in willow bark including the chalcones: robtein (2′,3,4,4′,5-pentahydroxychalcone), butein (2′,3,4,4′-tetrahydroxychalcone) and 2′,4,4′-trihydroxychalcone; the flavanones: L-robtin ((2*S*)-3′,4′,5′,7-tetrahydroxyflavanone), ((2S)-3′,4′,7-trihydroxyflavanone) and liquiritigenin ((2S)-4′,7-dihydroxyflavanone); flavanonols: D-dihydrorobinetin ((2*R*,3*R*)-3,3′,4′,5′,7-pentahydroxyflavanone), which is the major component of the bark, and D-fustin ((2*R*,3*R*)-3,3′,4′,7-tetrahydroxyflavanone); flavonols: robinetin (3,3′,4′,5′,7-pentahydroxyflavone) and fisetin (3,3′,4′,7-tetrahydroxyflavanone), flavan-3-ol: L-robinetinidol (3,3′,4′,5′,7-pentahydroxy-2,3-*trans*-flavan), flavan-3,4-diols: leucorobinetinidin (3,3′,4,4′,5′,7-tetrahydroxyflavanhexol) and D-3,3′,4,4′,7-pentahydroxy-2,3-*trans*-3,4-*cis*-flavan. In addition, heartwood contains β-resorcylic acid and methyl β-resorcylate.[9–11] Traditionally, *R. pseudoacacia* flowers are used in medicine as antispasmodic agents, for soothing the feelings of heartburn, to reduce gastric hyperacidity, as a mild sedative and a cholagogue.[12] In addition, the content of polyphenols present in the flowers create a strong antioxidant potential.[13]

The antimicrobial effect of polyphenols could be caused or facilitated by a significant electrical charge, the redox potential or through the free radical scavenging activity of antioxidants.[14,15] This hypothesis demonstrated that the antimicrobial effects of the derived polyphenols cause structural or functional damage to the bacterial cell membrane.[14] Microbial cells are negatively affected by derived substances from plants *via* various mechanisms of action that attack the phospholipid bilayer of the cell membrane and disrupt enzyme systems.[16] According to the literature,[17,18] a number of polyphenols (catechin, epicatechin, rutin and quercetin) that have been identified in some vegetal extracts show antimicrobial activity.

There are not data on HPLC analysis or the total phenol content of ethanolic extracts of *R. pseudoacacia*. Data on the chemical composition of acacia extracts are scarce. An aqueous extract was used to isolate five compounds from acacia leaves: luteolin 7-*O*-*β*-D-glucuronopyranosyl-(1→2)[*α*-L-rhamnopyranosyl-(1→6)]-*β*-D-glucopyranoside, apigenin 7-*O*-*β*-D-glucuronopyranosyl-(1→2)[*α*-L-rhamnopyranosyl-(1→6)]-*β*-D-glucopyranoside, acacetin 7-*O*-*β*-D-glucuronopyranosyl-(1→2)[*α*-L-rhamnopyranosyl-(1→6)]-*β*-D-glucopyranoside, acacetin 7-O-*β*-D-glucopyranosyl-(1→2)[*α*-L-rhamnopyranosyl-(1→6)]-*β*-D-glucopyranoside and acacetin 7-O-*β*-D-xylopyranosyl-(1→2)[*α*-L-rhamnopyranosyl-(1→6)]-*β*-D-glucopyranoside. These compounds were characterised by spectroscopic and chemical methods.[19]

In 2000, secundiflorol, mucronulatol, isomucronulatol, and isovestitol, identified by spectral analyses, were reported for the first time from this species in an ethanolic extract of the whole plant of *R. pseudoacacia*.[20]

Some literature data concerning antimicrobial activity were found. A low molecular weight cationic peptide was isolated from *R. pseudoacacia* seed and its *in vitro* antibacterial activity was investigated. The peptide inhibited the growth of the tested strains and *S. aureus* was found to be the most sensitive strain compared with others strains (*Corynebacterium michiganense*, *Bacillus subtilis*, *Erwinia carotovora*, *Pseudomonas syringae*, *Xanthomonas campestris* and *Escherichia coli*).[21]

Poor data on the antioxidant activity of *R. pseudoacacia* extracts exists. The antioxidant activity of lyophilized extracts of acacia leaves was evaluated by the oxygen radical absorbance capacity (ORAC) assay. The extract had a lower antioxidant capacity (1940 μmol trolox equivalent g^{-1}) compared with the other tested plants *Rhus typhina* (4651), *Acer rubrum* (3805) and *Rosa multiflora* (2533).[22]

Therefore, the aim of this study was to obtain and determine the antimicrobial and antioxidant activity of plant extracts from different vegetal and reproduction organs of the species *R. pseudoacacia* and to demonstrate potential synergistic effects with antibiotics commonly used in the clinic. The chemical characterization of the ethanol extracts from the vegetative and reproductive organs of *R. pseudoacacia*, synergistic effects of certain antibiotics and acacia extracts were realized for the first time. The potential to increase antimicrobial activity of some commercial antibiotics against MRSA is very important because these strains produce nosocomial infections, which has become an area of great interest for microbiologists in the past decades.

EXPERIMENTAL

Plant material. The plants were harvested during the physiological maturity period (July–September) from a hilly area (Calimanesti – Valcea). The vegetative and reproductive organs taken into consideration for the *R. pseudoacacia* species were the leaves, seeds and sheaths. The plants were manually sorted and dried at room temperature. The species was identified by the Department of Botany and Microbiology from the Faculty of Biology, University of Bucharest. A voucher specimen was deposited in the Herbarium of the Botanical Gardens "Dimitrie Brandza" of the University of Bucharest (No. 400636).

Alcoholic extracts. 4g of dried plant material was extracted with 50 mL 70% ethanol. The extraction was performed without heating using an ultrasonic bath (Elma Sonic 80H), with frequencies ranging from 20 kHz to 2000 kHz, which increases the permeability of the cell walls causing cell lysis, thereby enabling the extraction of the biologically active compounds. The extract thus obtained was filtered. The plant material residual was extracted for three times and brought to 300 mL with the same solvent. The extracts were stored in tightly closed containers at 4 °C and away from sunlight.

Determination of total phenols (TPC). The total phenols content (TPC) was determined by the Folin–Ciocalteu method[23] by mixing 0.5 mL of sample or standard (gallic acid) with 5 mL of Folin–Ciocalteu reagent and 4 mL of 1 M sodium carbonate solution. The absorbance was measured at wavelength of 746 nm. The calibration curve was constructed using standard solutions of gallic acid in the concentration range from 5 to 150 mg L^{-1}. The equation of the standard curve was $y = 0.0061x + 0.0057$ ($R^2 = 0.9988$). The TPC was expressed as mg of gallic acid equivalents (GAE) in one gram of the plant and in 1 mL extract.

HPLC analysis. All standards (gallic acid, (+)-catechin, (−)-epicatechin, syringic acid, vanillin, *p*-coumaric acid, resveratrol, rutin and quercetin) were purchased from Sigma–Aldrich (Steinheim, Germany). Stock solutions of all the standards were prepared in methanol. Working standards were made by diluting the stock solutions with a mixture of methanol and water (50:50, *V*/*V*). Both stock and working standards were stored at 4 °C until further use. Formic acid, acetonitrile and methanol (LC grade) were obtained from Merck. Double distilled and demineralised water from a Milli-Q Millipore system (Bedford, MA, USA) was used for the preparation of the aqueous solutions. The phenolic compounds were evaluated by reversed phase-high performance liquid chromatography (RP-HPLC) with direct injection. Chromatographic analysis was performed with a Thermo Finnigan Surveyor Plus instrument equipped with a Surveyor Photodiode Array Detector (PDA), a Surveyor autosampler, a Surveyor LC Pump (Quaternary gradient) and a Chrome Quest Chromatography workstation. The separation was performed at 30 °C with Accuacore PFP (2.6 μm, 100 mm×2.1 mm) column. The flow rate was 0.4 mL min^{-1} and an injection volume 1 μL. Gradient elution of two solvents was used: solvent A consisted of water with 0.1 % formic acid and solvent B: acetonitrile with 0.1 % formic acid. The gradient programme used is given Table I. Detection was made at 280 nm.

The *R. pseudoacacia* extracts were injected into HPLC system after filtering through a 0.45 μm pore size membrane filter. The amount of phenolic compounds in the extracts were calculated as mg L^{-1} extract using external calibration curves, which were obtained for each phenolic standard. The linearity of the method was between 0 – 50 mg/L, for each compound.

Each determination was realized in triplicate and the mean is reported. Blank solution and control samples were analyzed in order to monitor performance related to variable factors or random error.

TABLE I. Solvent gradient conditions with linear gradients

Time, min	Solvent A content, %	Solvent B content, %
Initial	98	2
30	70	30
35	25	75
40	98	2
50	98	2

TEAC assay (trolox equivalent antioxidant capacity). The method is based on the ability of antioxidants to quench the long-lived $ABTS^{\bullet +}$, a blue–green chromophore with a characteristic absorption at 734 nm. The addition of antioxidants to the preformed radical cation reduces it to ABTS, causing a decolourization. A stable stock solution of $ABTS^{\bullet +}$ was produced by reacting an aqueous solution of ABTS with potassium persulphate. Then, the mixture was left standing in the dark at room temperature for 12–16 h before use. An $ABTS^{\bullet +}$ working solution was obtained by dilution of this solution with ethanol to an absorbance of around of 0.70, according to Pellegrini *et al*.[24]. The results for the test compounds were expressed relative to trolox, in mmol of trolox per mL extract.

Evaluation of the antimicrobial activity of the studied phytochemical mixtures. The antimicrobial activity was tested using reference and clinically isolated microbial strains, belonging to Gram-positive, (*Staphylococcus aureus*, *Bacillus subtilis* and *Enterococcus faecalis*), Gram-negative (*Pseudomonas aeruginosa*, *Escherichia coli*, *Klebsiella pneumoniae* and *Acinetobacter baumannii*) bacteria and yeasts (*Candida famata*, *C. utilis* and *C. albicans*). These strains are part of the collection of the Laboratory of Microbiology, Faculty of Biology, University of Bucharest, Romania.

Qualitative screening of the antimicrobial activity. In order to test the degree of antimicrobial activity, microbial suspensions were adjusted to 1.5×10^{8} CFU mL^{-1} 0.5 McFarland standard from 18–24 h cultures grown on solid medium. The antimicrobial activity was determined by the disc diffusion method. Stock solutions that were used to test the quality of antimicrobial activity were the alcoholic plant extracts and also solvent control, ethanol 70 %. The obtaining of a mixed inhibition area at the spot level of the culture area was interpreted as a positive result.

*Quantitative assessment of the minimal inhibitory concentration (*MIC*).* Quantitative analysis was performed by the binary serial microdilution method in liquid medium (broth for bacteria and Sabouraud for yeasts) in 96-well plates. The concentration range of the working stock solutions for alcoholic extracts was from 0.78 to 400 μL mL^{-1}. Simultaneously, serial dilutions were made with 70 % ethanol under the same working conditions in order to obtain a negative control. Each well was inoculated with 10 μL microbial suspension adjusted to 1.5×10^{8} CFU mL^{-1} 0.5 McFarland standard from 18–24 h grown cultures. The *MIC* values were established both macroscopically, as the last concentration at which no microbial growth was observed, and spectrophotometrically. The absorbance of the microbial cultures was measured at 620 nm using an Apollo LB 911 spectrophotometer. An amount of 5 μL of the *R. pseudoacacia* leaves extracts of different concentrations from 200 to 6.25 μL mL^{-1} were spotted on solid medium to identify the minimal microbicidal concentration after 18–24 h.

Influence of plant extracts on the microbial adherence capacity to an inert substrate. Following the quantitative analysis protocol of the antimicrobial effect on adherence, the adherence of a biofilm biomass was assessed after fixation with cold methanol (5 min) and crystal violet staining (0.1 % concentration for 15 min) using the microtitre method. The optical density of the biological material resuspended in 33 % CH_3COOH (under stirring with Optic Ivymen System at 150 rpm for 15 min) was determined by reading the absorbance at 490 nm. The inert substrate was 96-well plates.

Sensitivity of bacterial strains to the alcoholic extracts and antibiotics commonly used in clinic. The antibiotic discs alone or with 10 μL of the stock solution of alcohol extracts were placed on the previously seeded solid media, as for a classic antibiogram*, using as controls simple antibiotic and antibiotic impregnated with 70% ethanol. Standard antibiotic discs were chosen according to the Clinical and Laboratory Standards Institute (CLSI)** and literature data.[25,26]

RESULTS AND DISCUSSION

The results concerning the total phenols and total antioxidant capacity are presented in Table II.

TABLE II. Content of total phenols (*TPC*) and the *TEAC* value of the *R. pseudoacacia* extracts

No.	Parameter	*R. pseudoacacia* leaf extract	*R. pseudoacacia* sheath extract	*R. pseudoacacia* seed extract
1	*TP* / μg GAE mL^{-1} extract	266.7	56.7	232.2
2	*TEAC* / mmol trolox mL^{-1} extract	902.17	172.91	625.23

The highest content of polyphenols was found in the leaf extract of *R. pseudoacacia* (266.7 μg mL^{-1} plant extract), compounds known for their strong antioxidant activity. HPLC chromatograms for the standard solution and for *R. pseudoacacia* leaf extract are presented in Figs. 1 and 2, respectively. By HPLC, four polyphenolic compounds were identified in the leaf extract, which represent 1.078 % of the TPCs quantified by the Folin–Ciocalteu method, and three compounds in the seed extract, which represent 0.257 % of the quantified TPCs. (These percentages were calculated by dividing the amount of phenols as determined by HPLC analysis at the total quantity of phenols obtained by Folin–Ciocalteu method). The identified polyphenolic compounds were catechin, rutin, resveratrol and quercetin in the leaf extract, and catechin, epicatechin and rutin in the seed extract, Table III). The major components are catechin for leaves extract and epicatechin for seeds extract. None of these compounds were identified in the sheath extract. Besides identified phenols in *R. pseudoacacia* leaf extract, HPLC analysis shows chromatographic separation of other compounds with a

* I. Marinas, A. M. Grumezescu, C. Saviuc, C. Chifiriuc, D. Mihaiescu, V. Lazar, *Biointerf. Res. Appl. Chem.* **2** (2012) 271.

** CLSI. Performance Standards for Antimicrobial Susceptibility Testing, M100-S24, Clinical and Laboratory Standards Institute, Wayne, PA, 2014.

significant peak area whose identification was not possible due to the lack of the standards. In our future studies, we will increase the number of identified and quantified phenolic compounds in plant extracts.

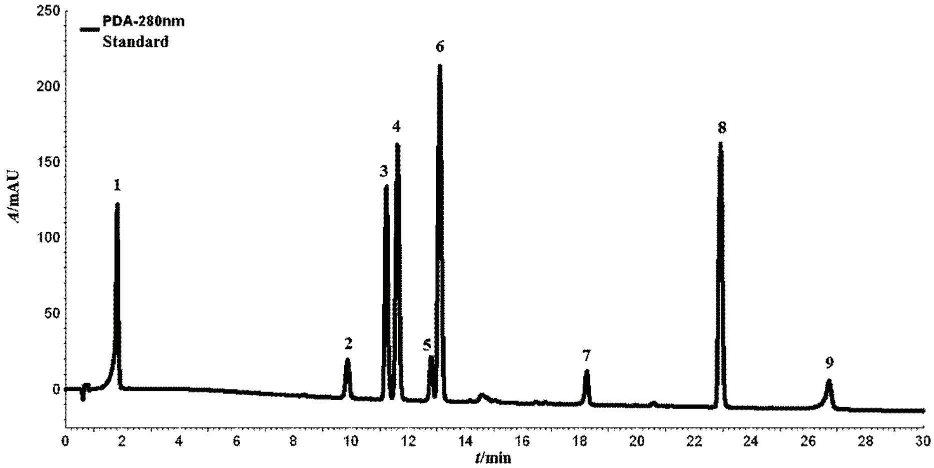

Fig. 1. HPLC chromatogram of standard solution. Peaks identification: 1 – gallic acid; 2 – (+)-catechin; 3 – syringic acid; 4– vanillin; 5 – (–)-epicatechin; 6 – *p*-coumaric acid; 7 – rutin; 8 – resveratrol; 9 – quercetin. Separation conditions: Accuacore PFP (2.6 μm, 100 mm×2.1 mm) column, temperature: 30 °C, flow rate: 0.4 mL min^{-1}, injection volume: 1 μL, gradient elution: solvent A consisted of water with 0.1 % formic acid and solvent B: acetonitrile with 0.1 % formic acid.

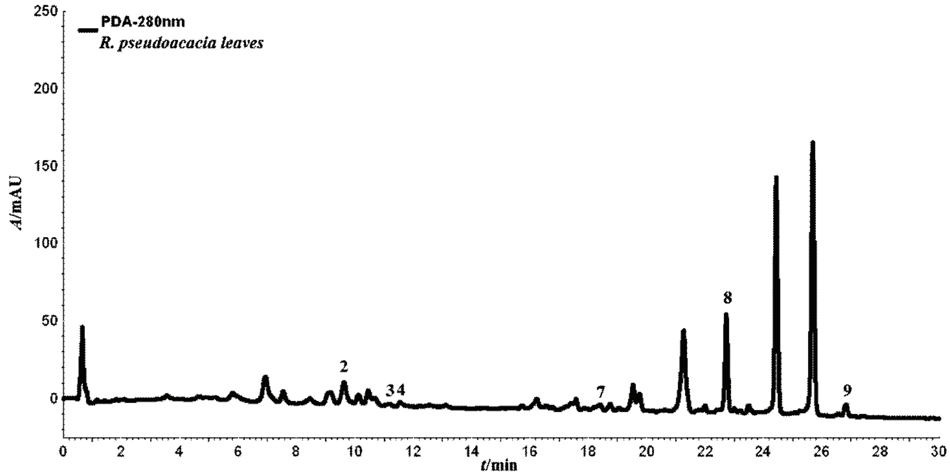

Fig. 2. HPLC chromatogram of *R. pseudoacacia* leaf extract. Peaks identification: 2 – (+)-catechin; 3 – syringic acid; 4 – vanillin; 7 – rutin; 8 – resveratrol; 9 – quercetin. Separation conditions: as in the legend to Fig. 1.

TABLE III. The concentration of polyphenols derivatives (μg mL^{-1} extract) in the hydroalcoholic extracts of the vegetative and reproduction organs of *R. pseudoacacia*; bdl – below the instrumental detection limit

R. pseudoacacia sample	Derivative								
	Gallic acid	Catechin	Syringic acid	Vanillin	Epicatechin	*p*-Coumaric acid	Rutin	Resveratrol	Quercetin
Leaves	bdl	0.925	bdl	bdl	bdl	bdl	0.831	0.664	0.456
Sheaths	bdl	bdl	bdl	bdl	bdl	bdl	bdl	bdl	bdl
Seeds	bdl	0.127	bdl	bdl	0.239	bdl	0.231	bdl	bdl

The results of the qualitative assessment of the antimicrobial activity of the alcoholic extracts are given in Table IV. According to the qualitative assay, the alcoholic extracts showed different diameters of the inhibition zones for *K. pneumoniae* (14–16 mm for the leaf extract), *S. aureus* (8–12 mm for the leaf extract), *P. aeruginosa* (7–10 mm for the sheath extract) and *Candida* sp. (8–14 mm for all extracts) and lower than 6 mm for the solvent control. In addition, the 70 % ethanol solvent control showed some activity against *K. pneumoniae* strains, *A. baumannii* and *Candida* sp. These results are in accordance with literature data, *i.e.*, a 90 % ethanolic extracts of *R. pseudoacacia* leaves and barks were shown to be active against *E. coli*, *P. aeruginosa*, *Proteus vulgaris*, *Salmonella choleraesuis* and *C. albicans* strains.[27]

TABLE IV. Qualitative and quantitative assessment of the antimicrobial activity of alcoholic extracts obtained from different parts of the species *R. pseudoacacia*; –: 5 mm (disc diameter); +: 6–10 mm; ++: 11–20 mm

Microbial strain	Leaves		Sheaths		Seeds		Solvent control (ethanol 70 %)	
	Qualit. (5 μL)	*MIC* μL mL^{-1}	Qualit. (5 μL)	*MIC* μL mL^{-1}	Qualit. (5 μL)	*MIC* μL mL^{-1}	Qualit. (5 μL)	*MIC* μL mL^{-1}
S. aureus ATCC 6538	++	50	–	–	–	–	–	200
S. aureus MRSA 1263	+	200	–	–	–	–	–	400
B. subtilis 6683[a]	+	100	+	100	+	100	–	200
B. subtilis 12488[a]	+	200	+	200	+	400	–	400
E. coli ATCC 8739	–	–	–	–	–	–	–	200
E. coli $O_{126}B_{16}$	+	200	–	–	–	–	–	400
K. pneumoniae 134202[a]	++	50	–	–	–	–	+	200
K. pneumoniae 11[a]	++	50	–	–	+	–	+	200

TABLE IV. Continued

Microbial strain	Leaves		Sheaths		Seeds		Solvent control (ethanol 70 %)	
	Qualit. (5 μL)	*MIC* μL mL^{-1}	Qualit. (5 μL)	*MIC* μL mL^{-1}	Qualit. (5 μL)	*MIC* μL mL^{-1}	Qualit. (5 μL)	*MIC* μL mL^{-1}
P. aeruginosa ATCC 27853	++	50	+	100	+	50	–	200
P. aeruginosa 13202[a]	+	200	+	200	+	100	–	400
E. fecalis ATCC 29212	+	100	+	100	–	–	–	200
A. baumannii 77 sc	+	200	++	50	++	25	+	200
C. utilis	++	50	++	100	++	100	+	200
C. famata	++	50	+	200	+	200	–	200
C. albicans 945[a]	++	50	+	100	+	100	+	200
C. albicans 393[a]	+	200	+	100	+	100	+	200

[a]The clinical microbial strains were introduced in our laboratory collection from hospital units where they received these registration codes

Strains that were shown to be susceptible to the studied extracts in the qualitative screening were used for *MIC* determination of the extracts. Comparisons between *MIC* values of the extracts from vegetative and reproductive organs and also the differences between them and the solvent used are given in Table IV. Quantitative analysis indicated a moderate antibacterial activity of the alcoholic extracts of *R. pseudoacacia* (the *MIC* values ranged between 50–400 μL mL^{-1}) but only the leaf extract, which had the most active compounds, showed antibacterial activity on the MRSA strain. In case of the alcoholic extracts obtained from *R. pseudoacacia* leaves, a precipitate was observed which prevented both macroscopic and spectrophotometric determination of the *MIC* value. Thus, for the *MIC* determination, the microbial culture grown in the presence of the *R. pseudoacacia* leaf extract concentrations of 200 to 6.25 μL mL^{-1} was spotted on solid medium.

Microorganisms involved in invasive infections usually produce extracellular capsular polysaccharides known as capsules, slime or glycocalyx. The slime term is usually used to refer to closely related bacterial cell exopolysaccharides, which increase the viscosity of the liquid culture medium seeded with strains possessing the virulence factor. The production of slime is involved in the adhesion and colonization of medical devices.[28] Regarding the influence on the ability of adhesion, there was a significant decrease in absorbance measured at the wavelength of 490 nm. The influence of plant extracts on the microbial adherence to an inert substrate resulted in inhibition of microbial biofilm development. These results suggest the ability of the alcoholic extracts to interfere with the expression of microbial adhesions involved in the initial step of colonization, essential for the initiation of an infectious process; thus, the synthesis of adhesins is therefore an important virulence factor for pathogenic microorganisms. Adhesion is a major ecologic advantage for the pathogenic bacteria in terms of provision of nutrients, protection from antibodies and lysozyme, *etc*. Microbial growth after adhesion occurs at a rate much higher than that of non-adherent cells.[29] The ability of adhesion to an inert substrate was inhibited by extract concentrations ranging from 12.5 to 100 μL mL^{-1} (Table V). The main virulence factor involved in the microbial pathogenesis lies in their ability to adhere to various cellular and inert surfaces, by microbial adhesins. Numerous studies showed that the inhibition of a single adhesin may often be sufficient to produce non-virulent pathogenic microorganisms. This led to the exploration of the interference with the activity of adhesins, as a strategy for the treatment of bacterial infections.[30] The development of a biofilm is closely related to the pathogenicity of the microorganisms and their sensitivity to antibiotics, and is also influenced by other factors, such as enzymatic factors, hydrophobicity *etc*.[31]

TABLE V. Quantification of the inhibitory effect of alcoholic extracts from various parts of *R. pseudoacacia* species on the adherence capacity (μL mL^{-1}) of the studied strains to the inert substratum

Microbial strains	*R. pseudoacacia* leaves	*R. pseudoacacia* sheaths	*R. pseudoacacia* seeds	Solvent control (ethanol 70%)
S. aureus (S.a.) ATCC 6538	12.5	–	–	100
MRSA 1263	100	–	–	200
B. subtilis (B.s.) 6683	50	50	50	100
B. subtilis (B.s.) 12488	50	100	100	200
E. coli (E.c.) $O_{126}B_{16}$	100	–	–	200
K. pneumoniae (KPN) 134202	25	–	–	100
K. pneumoniae (KPN) 11	25	–	–	100
P. aeruginosa (P.a.) ATCC 27853	25	50	25	100
P. aeruginosa (P.a.) 13202	50	100	50	200
E. faecalis ATCC 29212	25	50	–	100
A. baumannii 77	100	25	12.5	100
C. utilis	25	50	50	100
C. famata	25	100	100	100
C. albicans 945	12.5	50	50	100
C. albicans 393	50	50	50	100

The alcoholic extract of the *R. pseudoacacia* leaves potentiated the antimicrobial activity of currently used antibiotics against the nine tested bacterial strains: *E. coli*, *K. pneumoniae*, *B. subtilis*, *S. aureus* and *P. aeruginosa*. The most significant potentiation effects were observed in case of *E. coli* $O_{126}B_{16}$ for trimethoprim–sulfamethoxazole (SXT), ticarcillin–clavulanic acid (TIM) and piperacillin–tazobactam (TZP); *K. pneumoniae* 134202 for cefotaxime (CTX), aztreonam (ATM) and cephalexin (LEX); *P. aeruginosa* 13202 for ciprofloxacin (CIP), piperacillin (PIP) and colistin (CST); *P. aeruginosa* ATCC for CIP, PIP, CST, ceftriaxone (CRO) and ofloxacin (OFX); *S. aureus* ATCC for CIP, erythromycin (ERY) and penicillin (PEN); MRSA for rifampin (RIF), kanamycin (KAN), ERY and PEN); *B. subtilis* 6683 for KAN and PEN); *B. subtilis* 12488 for cefaclor (CEC) and vancomycin (VAN). On the contrary, in the case of the *K. pneumoniae* 11 strain, the plant extracts decreased the activity of the used antibiotics. Noteworthy, for kanamycin, a very strong potentiation effect was observed in case of the MRSA strain (Table VI).

TABLE VI. Quantification of the differences between the diameters (mm) of the inhibition zones of microbial growth caused by *R. pseudoacacia* leaf extract and an antibiotic; solvent: ethanol 70 %; –: resistant strain; negative values: the combination solvent:antibiotic was more active than the combination extract:antibiotic; positive values: the combination extract:antibiotic was more active than the combination solvent:antibiotic

Antibiotic	MRSA	S.a. ATCC	B.s. 6683	B.s. ATCC	E.c. $O_{126}B_{16}$	KPN ATCC	KPN 11	P a. ATCC	P.a. 132404
Amoxicillin (AM)						–	–		
Aztreonam (ATM)						3	–1		
Cefaclor (CEC)			0	4					
Cefotaxime (CTX)					–2	2	14		
Ceftriaxone (CRO)								8	8
Cephalexin (LEX)						4	0		
Chloramphenicol (CHL)			0	2					
Ciprofloxacin (CIP)	0	2			–2	–2	18	17	12
Colistin (CST)CL								5	4
Erythromycin (ERY)	4	10							
Kanamycin (KAN)	22	0	2	0					
Ofloxacin (OFX)						2	–2	1	0
Oxacillin (OXA)	9	0						–	–
Penicillin G (PEN)	18	8	3	0					
Piperacillin (PIP)					–4			7	8
Piperacillin–tazobactam (TZP)					2				
Rifampin (RIF)	13	2							
Ticarcillin–clavulanic acid (TIM)					9			–	0
Trimethoprim–sulfamethoxazole (SXT)					15				
Vancomycin (VAN)			–2	1					

Among the tested antibiotics, the penicillin activity (acting on the synthesis of bacterial cell wall) and kanamycin activity (active on bacterial protein synthesis) were significantly improved on the MRSA strain by the active substances found in the alcoholic extract of *R. pseudoacacia* leaves. Oxacillin for *S. aureus* is often associated with resistance mechanisms that determine the deactivation of other classes of antibiotics (aminoglycosides, fluoroquinolones, macrolides, lincosamides, ketolides, phosphomycin and rifampicin).[32,33]

Alcoholic extracts of *R. pseudoacacia* sheaths and seeds had a lower synergistic effect than the leaf extract. An improvement observed in the antimicrobial effect of seeds extracts was obtained for *B. subtilis* strains in combination with PEN, CHL, CEC, KAN, VAN and teicoplanin (TEC); *P. aeruginosa* 13202 for PIP, CRO, norfloxacin (NOR), ATM and TIM, and *K. pneumoniae* 11 for TIM and ATM (Tables VII and VIII).

TABLE VII. Quantification of the differences between the diameters (mm) of the inhibition zones of microbial growth caused by antibiotic: *R. pseudoacacia* seed extract plus the antibiotic; solvent: ethanol 70 %; –: resistant strain; negative values: the combination solvent:antibiotic was more active than the combination extract:antibiotic; positive values: the combination extract:antibiotic was more active than the combination solvent:antibiotic

R. pseudoacacia seeds and:	Microbe				
	B.s. 6683	B.s. ATCC	KPN 11	P.a. ATCC	P.a. 132404
Amoxicillin (AMX)			–		
Aztreonam (ATM)			5		
Cefaclor (CEC)	8	10			
Cefotaxime (CTX)			–1		
Ceftriaxone (CRO)				1	1
Cephalexin (LEX)			–5		
Chloramphenicol (CHL)	2	0			
Colistin (CST)				–3	–4
Kanamycin (KAN)	–2	–7			
Nalidixic acid (NAL)			–2		
Norfloxacin (NOR)				0	0
Ofloxacin (OFX)			–8	–	–
Oxacillin (OXA)					
Penicillin G (PEN)	0	–7			
Piperacillin (PIP)				–1	3
Teicoplanin (TEC)	–1	–4			
Ticarcillin–clavulanic acid (TIM)				9	2
Vancomycin (VAN)	–2	–3			

The alcoholic extract of *R. pseudoacacia* sheaths proved to be less effective on the synergistic effect of the antibiotics tested, the differences between the diameters of the inhibition zone for the extract:antibiotic and solvent:antibiotic ranging between –6 and 9 mm and no change from resistant to susceptible category being noticed (Table VIII).

TABLE VIII. Quantification of the differences between the diameters (mm) of the inhibition zones of microbial growth caused by antibiotic: *R. pseudoacacia* sheaths extract and antibiotic; solvent: ethanol 70 %; –: resistant strain; negative values: the combination solvent:antibiotic was more active than the combination extract:antibiotic; positive values: the combination extract:antibiotic was more active than the combination solvent:antibiotic

R. pseudoacacia sheath extract and:	Microbe			
	B.s. 6683	*B.s.* ATCC	*P.a.* ATCC	*P.a.* 132404
Cefaclor (CEC)	4	6		
Ceftriaxone (CRO)			1	2
Chloramphenicol (CHL)	–2	0		
Colistin (CST)			–3	–4
Kanamycin (KAN)	5	–3		
Norfloxacin (NOR)			–2	–1
Oxacillin (OXA)			–	9
Penicillin G (PEN)	1	–5		
Piperacillin (PIP)			1	1
Teicoplanin (TEC)	–4	–6		
Ticarcillin–clavulanic acid (TIM)			9	1
Vancomycin (VAN)	–5	–3		

According to recent data,[34] antibiotics can produce genetic changes in different ways, including an increase in free radicals within the cell. These results demonstrate that polyphenolic compounds could have a double effect of increasing the antimicrobial activity and neutralizing the free radicals formed by the use of antibiotics.

CONCLUSIONS

Ethanol extracts from the vegetative and reproductive organs of *R. pseudoacacia* were chemically characterised and the synergistic effects of certain antibiotics and the acacia extracts were investigated for the first time.

The phytochemical extract of *R. pseudoacacia* leaves (0.27 mg GAE mL^{-1} extract) proved to be the richest in polyphenols, known for their strong antioxidant capacity and possible antimicrobial activity. Through HPLC, four compounds from the leaf extract, which represented 1.078 % of the TPC, and three compounds from the seed extract, which represented 0.257 % of the TPC, were identified for the first time.

The alcoholic extracts of *R. pseudoacacia* showed antimicrobial activity towards the tested strains belonging to the Gram-positive (*S. aureus*, *B. subtilis* and *E. faecalis*) and Gram-negative (*P. aeruginosa*, *E. coli*, *K. pneumoniae* and *A. baumannii*) bacterial and the yeasts (*Candida* sp.) strains. The minimum inhibitory concentrations of stock solutions from the studied phytochemical alcoholic mixtures ranged from 25–400 μL mL^{-1}. The *R. pseudoacacia* active principles extracted from the leaves were proved to be the most active in terms of antimicrobial activity. The tested plant extracts also inhibited adherence of the microbial cells and their ability to form biofilms on an inert substrate. However, further studies are required in order to establish their efficiency on pre-formed biofilms. The antimicrobial activities of antibiotics commonly used in the clinic were enhanced in the presence of the studied vegetative plant extracts. Among the tested antibiotics, the activities of penicillin, kanamycin and rifampin on an MRSA strain were significantly improved by the active substances from the alcoholic extract obtained from the leaves of *R. pseudoacacia* and furthermore conversion from resistant to susceptible was obtained. These results are of special interest nowadays because MRSA has become resistant to many antimicrobial agents, and currently represents a large problem in clinical infections.

This study has proved that the tested vegetative extracts could be used as therapeutic agents complementing antibiotherapy; such an approach enables potentiation of the activity of antibiotics with different mechanisms of action, highlighting the necessity for molecular studies in order to establish the influence of vegetal extracts upon gene expression on certain genes involved in microbial virulence and resistance. The results also demonstrated that polyphenolic compounds can have a dual effect, *i.e.*, increasing the antimicrobial activity and neutralizing the free radicals formed by the employed antibiotics.

Acknowledgements. This work was supported by the strategic grant POSDRU/159/ /1.5/S/133391, Project “Doctoral and Post-doctoral Programs of Excellence for Highly Qualified Human Resources Training for Research in the Field of Life Science, Environment and Earth Science” cofinanced by the European Social Found within the Sectorial Operational Program Human Resources Development 2007–2013.

ИЗВОД

АНТИМИКРОБНА И АНТИОКСИДАТИВНА АКТИВНОСТ ВЕГЕТАТИВНИХ И РЕПРОДУКТИВНИХ ОРГАНА БИЉКЕ *Robinia pseudoacacia*

IOANA C. MARINAS[1], ELIZA OPREA[2], ELISABETA-IRINA GEANA[3], CARMEN CHIFIRIUC[1] и VERONICA LAZAR[1]

[1]*University of Bucharest, Faculty of Biology, Microbiology Department, Bucharest, Romania,* [2]*University of Bucharest, Faculty of Chemistry, Bucharest, Romania* и [3]*National R & D Institute for Cryogenics and Isotopic Technologies - ICIT Rm. Valcea, Romania*

Испитивана је антимикробна и антиоксидативна активност етанолних екстраката добијених из лишћа, семена и изданака биљке *Robinia pseudoacacia*. Одређени су укупни феноли (TPC, Folin–Ciocalteu метод), антиоксидативна активност (TEAC тест) и антимикробна активност (метод дифузије на агару) вегетативних и репродуктивних органа *R. pseudoacacia*. Највећи садржај полифенола (изражен као еквивалент галне киселине, GAE) нађен је у екстракту лишћа (266,7 μg GAE mL^{-1} екстракта), а затим у екстракту семена (232,2 μg GAE mL^{-1} екстракта). HPLC анализа је показала присуство катехина (0,925 μg mL^{-1}), рутина (0,831 μg mL^{-1}), резвератрола (0,664 μg mL^{-1}) и кверцетина (0,456 μg mL^{-1}) у екстракту лишћа, односно катехина (0,127 μg mL^{-1}), епикатехина (0,239 μg mL^{-1}) и рутина (0,231 μg mL^{-1}) у екстракту семена. Екстракти су показали селективни антимикробни ефекат спрам Грам-позитивних (*Staphylococcus aureus* и *Bacillus subtilis*) и Грам-негативних (*Pseudomonas aeruginosa*, *Klebsiella pneumoniae* и *Escherichia coli*) бактерија. Најјачи синергистички антибактеријски ефекат имао је екстракт лишћа у комбинацији са антибиотиком. Екстракт лишћа, у комбинацији са пеницилином, канамицином и рифампицином испољио је највећи синергистички ефекат спрам метицилин-резистентног соја *S. aureus* (MRSA). У овом раду је, по први пут, извршена хемијска карактеризација етанолних екстраката вегетативних и репродуктивних органа *R. pseudoacacia* и испитан синергистички ефекат неких антибиотика и екстраката, показујући да екстракти могу повећати антимикробну активност комерцијалних антибиотика спрам MRSA.

(Примљено 4. марта, ревидирано 30. априла, прихваћено 7. маја 2014)

REFERENCES

1. R. Benesperi, C. Giuliani, S. Zanetti, M. Gennai, M. M. Lippi, T. Guidi, J. Nascimbene, B. Foggi, *Biodivers. Conserv*. **21** (2012) 3555
2. H. Nasir, Z. Iqbal, S. Hiradate, Y. Fujii, *J. Chem. Ecol.* **31** (2005) 2179
3. D. D. Rakesh, T. K. Bhat, B. Singh, *J. Gen. Appl. Microbiol.* **46** (2000) 99
4. F. Tian, C. J. Chang, J. B. Grutzner, D. E. Nichols, J. L. McLaughlin, *Bioorg. Med. Chem. Lett.* **11** (2001) 2603
5. E. J. Kupchik, M. A. Pisano, A. M. Carroll, J. R. Lumpp, J. A. Feiccabrin, *J. Pharm. Sci.* **69** (1980) 340
6. T. Kamo, T. Takemura, N. Wasano, Y. Fujii, S. Hieadate, *Biosci. Biotechnol. Biochem.* **76** (2012) 1416
7. H. Pereira, J. Graca, J. C. Rodrigues, in *Wood chemistry in relation to wood quality*, in *Wood Quality and Its Biological Basis*, J. R. Barnett, G. Jeronimidis, Eds., Blackwell Publishing, Oxford, 2003, p. 53
8. P. Rudman, *Holzforschung* **17** (1963) 183
9. A. Hemmerlin, J. L. Harwood, T. J. Bach, *Prog. Lipid Res.* **51** (2012) 95
10. S. K. Hosseinihashemi, V. Safdari, S. Kanani, *Asian J. Chem*. **25** (2013) 929
11. J. V. F. Latorraca, O. Dunisch, G. Koch, *An. Acad. Bras. Cienc.* **83** (2011) 1059
12. M. Temelie, *Encyclopedia of Spontaneous Medicinal Plants from Romania*, Rovimed Publishers, Bacau, 2006, p. 373 (in Romanian)
13. H. F. Ji, A. Du, L. Zhang, C. Y. Xu, M. Yang, F. F. Li, *J. Med. Plants Res*. **6** (2012) 3233
14. V. Sendamangalam, O. K. Choi, Y. Seo, D. S. Kim, *Free Radicals Antioxid.* **1** (2011) 48
15. L. Barbosa-Pereira, A. Bilbao, P. Vilches, I. Angulo, J. L. Luis, B. Fité, P. Paseiro-Losada, J. M. Cruz, *Food Chem*. **145** (2014) 191
16. J. Oh, H. Jo, A. R. Cho, S. J. Kim, J. Han, *Food Control* **31** (2013) 403
17. T. P. T. Cushnie, A. J. Lamb, *Int. J. Antimicrob. Agents* **26** (2005) 343
18. P. Srinivas, S. R. Reddy, *Asian Pac. J. Trop. Biomed*. **2** (2012) 838
19. N. C. Veitch, P. C. Elliott, G. C. Kite, G. P. Lewis, *Phytochemistry* **71** (2010) 479
20. F. Tian, J. L. McLaughlin, *Pharm. Biol*. **38** (2000) 229
21. T. Talas-Ogras, Z. Ipekci, K. Bajrovic, N. Gozukirmizi, *Fitoterapia* **76** (2005) 67
22. L. M. Katiki, J. F. S. Ferreira, J. M. Gonzalez, A. M. Zajac, D. S. Lindsay, A. C. S. Chagas, A. F. T. Amarante, *Vet. Parasitol*. **192** (2013) 218

23. V. L. Singleton, J. A. Rossi, *Am. J. Enol. Viticul*. **16** (1965) 144
24. N. Pellegrini, D. Del Rio, B. Colombi, M. Bianchi, F. Brighenti, *J. Agric. Food Chem*. **51** (2003) 260
25. S. Balakrishnan, K. R. John, M. R. George, *Indian J. Mar. Sci*. **32** (2003) 81
26. V. Sivakumari, G. Shanthi, *Adv. BioTech* **8** (2009) 10
27. A. F. Rosu, A. Bita, D. Calina, L. Rosu, O. Zlatian, V. Calina, *Eur. J. Hosp. Pharm*. **19** (2012) 216
28. C. Chifiriuc, G. Mihăescu, V. Lazăr, *Medical Microbiology and Virology*, Univ. Bucharest Press, Bucharest, 2011, p. 389 (in Romanian)
29. V. Lazăr, *Microbial Adhesion*, Romania Academy Press, Bucharest, 2003, p. 96 (in Romanian)
30. P. Klemm, M. A. Schembri, *Int. J. Med. Microbiol*. **290** (2000) 27
31. G. Qiao, H. Li, D. H. Xu, S. II Par, *J. Bacteriol. Parasitol*. **3** (2012) 130
32. A. Mărculescu, M. Cernea, V. Nueleanu, N. A. Oros, R. Chereji, *Med. Vet./Vet. Drug* **1** (2007) 44
33. G. Mihăescu, M. C. Chifiriuc, L. M. Ditu, *Antibiotics and Antimicrobial Chemotherapeutic Substances*, Romania Academy Press, Bucharest, 2007, p. 24 (in Romanian)
34. A. Rodríguez-Rojas, J. Rodríguez-Beltrán, A. Couce, J. Blázquez, *Int. J. Med. Microbiol*. **303** (2013) 293.

Journal of the Serbian Chemical Society
JSCS-info@shd.org.rs • www.shd.org.rs/JSCS

J. Serb. Chem. Soc. *79* (11) 1379–1393 (2014)
JSCS–4672

UDC 546.48–38+541.8:544.478–44+ 543.552:541.134.5
Original scientific paper

Syntheses, characterization and electrocatalytical comparison of two cadmium-containing mono-lacunary Wells–Dawson polyoxometalates, α_1- and α_2-$[P_2W_{17}Cd(H_2O)O_{61}]^{8-}$

FARROKHZAD MOHAMMADI ZONOZ[1*], ALI JAMSHIDI[2], FATEME HAJIZADEH[1] and KHADIJEH YOUSEFI[3]

[1]Department of Chemistry, Hakim Sabzevari University, Sabzevar, 96179-76487, Iran, [2]School of Chemistry, Damghan University, Damghan, Iran and [3]Payamnoor University of Sari, Sari, Iran

(Received 18 January, revised 18 May, accepted 28 May 2014)

Abstract: Two new cadmium-containing Wells–Dawson polyoxometalates $K_8[\alpha_1\text{-}P_2W_{17}Cd(H_2O)O_{61}]\cdot 14H_2O$ (α_1-$P_2W_{17}Cd$) and $K_8[\alpha_2\text{-}P_2W_{17}Cd(H_2O)\text{-}O_{61}]\cdot 16H_2O$ (α_2-$P_2W_{17}Cd$) were synthesized as water-soluble potassium salts. The cadmium-substituted complexes were characterized by IR, ^{31}P-NMR, ^{113}Cd-NMR spectroscopy and cyclic voltammetry (CV). Redox activities for the tungsten and cadmium centers were observed by cyclic voltammetry. It was found that the presence of cadmium decreased the electrocatalytic activity of the $[\alpha_1\text{-}LiP_2W_{17}O_{61}]^{9-}$ and α_2-$[P_2W_{17}O_{61}]^{10-}$ heteropolyanions.

Keywords: polyoxometalates; Wells–Dawson; electrocatalytic; cadmium; cyclic voltammetry.

INTRODUCTION

Polyoxometalates (POMs), as a rich class of inorganic metal oxide cluster compounds, have different applications in molecular materials,[1] medicine, biology[2,3] and catalysis[4,5] due to their molecular, structural, and electronic versatility. The Dawson-type heteropolyanions with highly symmetric structures are famous as one kind of POMs. Their formula is $[X_2W_{18}O_{62}]^{n-}$, where X is a heteroatom such as phosphorus.[6] Removal of a WO unit from a cap WO_6 polyhedron of the $(\alpha\text{-}P_2W_{18}O_{62})^{6-}$ (Wells–Dawson structure) results in the lacunary $(\alpha_2\text{-}P_2W_{17}O_{61})^{10-}$ isomer that has C_s symmetry, and removal of a WO unit from a belt WO_6 polyhedron results in the lacunary $(\alpha_1\text{-}P_2W_{17}O_{61})^{10-}$ isomer, that has C_1 symmetry (Fig. 1).[7,8] An important structural characteristic of Dawson-type heteropolyanions is the possibility of replacing one of the tungsten atoms by a

* Corresponding author. E-mail: f.zonoz@hsu.ac.ir; fzmohamadi@yahoo.com
doi: 10.2298/JSC140118057Z

transition metal cation, which possesses five bridging oxygens and a sixth oxo-group, which is occupied by a water molecule. For instance, transition metal *mono*-substituted Dawson anions with the general formula $K_8[\alpha_2\text{-}P_2W_{17}M\text{-}(H_2O)O_{61}]$ (M= Zr(IV), Hf(IV), Mn(II), Zn(II), Fe(II), Co(II), Cu(II) or Ni(II)) were investigated.[9,10] Furthermore, these compounds have also been used as heterogeneous catalysts.[11–13]

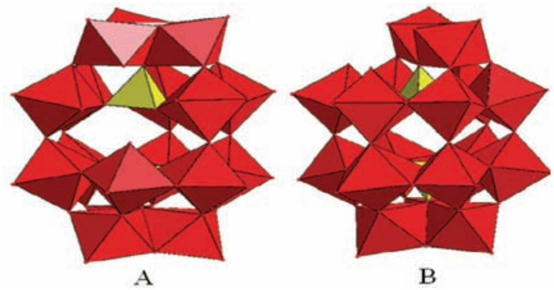

Fig. 1. A) The monovacant α_1-$[LiP_2W_{17}O_{61}]^{9-}$ unit obtained by removing a WO_6 octahedron in the equatorial site of the parent Wells–Dawson structure, B) The monovacant α_2-$[P_2W_{17}O_{61}]^{10-}$ unit obtained by removing a WO_6 octahedron in the capping region of the parent Wells–Dawson structure.

Until now, only a few cadmium-containing polyoxometalates have been reported. The first cadmium-containing heteropolyanions, related to the mono-lacunary anion of the Keggin structure (XW11) were presented by Contant.[14] In 1995, Kirby and Baker[15] reported the first sandwich-type heteropolyanions including Cd^{2+} based on the $[P_2W_{15}O_{56}]^{12-}$ defect structure, and later Bi *et al.*[16] prepared a series of dimeric polytungstates by reacting $[As_2W_{15}O_{56}]^{12-}$ with M^{2+} (M = Cu(II), Mn(II), Co(II), Ni(II), Zn(II) or Cd(II)). Subsequently, Alizadeh *et al.*[17] synthesized and structurally characterized $[Cd_4(H_2O)_2(PW_9O_{34})_2]^{10-}$. In 2005, Kortz *et al.*[18] reported another cadmium containing polyxoxometalate, $[Cd_4Cl_2(B\text{-}\alpha\text{-}AsW_9O_{34})_2]^{12-}$. Finally, Zhao *et al.*[19] prepared and characterized $[Cd_4(H_2O)_2(B\text{-}\alpha\text{-}SiW_9O_{34})_2]^{12-}$.

Over past years, electrochemical methods were shown to be an inexpensive and effective method for the determination of some inorganic and organic substrates.[20–23] In particular, POMs exhibited multi-electron reversible redox characteristics, which enables them to be redox electrocatalysts for some irreversible electrochemical processes.[24–26] In electrochemistry, the main processes include the reduction of protons or the oxidation of hydrogen, the reduction of dioxygen, and the electrochemical processes of nitrogen oxides NO_x and carbon oxides CO_x, complemented by the electrocatalysis of bromate, iodate and so forth. All of these reactions have important implications in environmental problems and/or are potentially considered to be abundant, inexpensive sources for the production of useful chemicals.[27] In this paper, the syntheses of two new cadmium-containing

α_1- and α_2-mono-lacunary Dawson-type polyoxometalates, $K_8[\alpha_1\text{-}P_2W_{17}Cd(H_2O)O_{61}]\cdot14H_2O$ (α_1-$P_2W_{17}Cd$) and $K_8[\alpha_2\text{-}P_2W_{17}Cd(H_2O)O_{61}]\cdot16H_2O$ (α_2-$P_2W_{17}Cd$), are described. Several attempts to prepare single crystals of α_1-$P_2W_{17}Cd$ and α_2-$P_2W_{17}Cd$ failed. Therefore, these compounds were characterized by elemental analysis, and FT-IR, ^{31}P-NMR and ^{113}Cd-NMR spectroscopic methods. The electrochemical properties of these compounds and the electrocatalytic reductions of nitrite were investigated in detail by cyclic voltammetry.

EXPERIMENTAL

All reagents were of analytical grade and were used as received from commercial sources without further purification. The mono-lacunary POMs $K_{10}[\alpha_2\text{-}P_2W_{17}O_{61}]\cdot20H_2O$ and $K_9[\alpha_1\text{-}LiP_2W_{17}O_{61}]\cdot20H_2O$ were prepared according to the literature and characterized accordingly.[28] FT-IR spectra were recorded in the range 400–4000 cm^{-1} on an Alpha Centaurt FT-IR spectrophotometer using the KBr pellet technique. The NMR spectrum was recorded on a Bruker BRX-300 Avance spectrometer. The resonance frequencies for the ^{31}P and ^{113}Cd nuclei are at 202.46 and 110.92 MHz, respectively. The chemical shifts for the ^{31}P- and ^{113}Cd-NMR spectra were externally referenced relative to 85 % H_3PO_4 and 0.1 M cadmium perchlorate, respectively. Elemental analyses were realized using an Integra XL inductively coupled plasma spectrometer. The water used for all electrochemical measurements was obtained by passing through a Millipore Q water purification set. The solutions were deaerated thoroughly for at least 30 min by bubbling with pure N_2 and kept under N_2 atmosphere during the whole experiment. The electrochemical set-up was a Metrohm 797VA computrace polarographic analyzer. A conventional three-electrode system was used. The working electrode was a glassy carbon electrode. A platinum electrode was used as the counter electrode and an Ag/AgCl (3 M KCl) electrode was employed as the reference electrode. All potentials were measured and reported *vs*. the Ag/AgCl electrode. All voltammetric experiments were performed at room temperature.

Synthesis of $K_8[\alpha_1\text{-}P_2W_{17}Cd(H_2O)O_{61}]\cdot14H_2O$

$Cd(NO_3)_2\cdot4H_2O$ (0.72 g, 2.33 mmol) was dissolved in 40 mL of sodium acetate buffer (0.25 M, pH 4.7). The solution was heated to 80 °C and then, 10 g (2.08 mmol) of $K_9[\alpha_1\text{-}LiP_2W_{17}O_{61}]\cdot20H_2O$ was added gradually. After 2 h, the solution was cooled to room temperature, and precipitate was removed by filtration. This solid was recrystallized from boiling water and dried under vacuum. Yield: 41.58 %; Anal. Calcd. for $CdH_{30}K_8O_{76}P_2W_{17}$: Cd, 2.31; K, 6.43; P, 1.27; W, 64.32; H_2O, 5.18 %. Found: Cd, 2.28; K, 6.30; P, 1.23; W, 64.35; H_2O, 5.24 %; IR (KBr, cm^{-1}): 1084, 1060, 1014 (P–O stretching bonds), 948 (W–O_{term} stretching bonds), 898 (W–O_b stretching bonds), 784, 738 (W–O_c stretching bonds).

Synthesis of $K_8[\alpha_2\text{-}P_2W_{17}Cd(H_2O)O_{61}]\cdot16H_2O$

A 0.72 g (2.33 mmol) of $Cd(NO_3)_2\cdot4H_2O$ was dissolved in 40 mL of sodium acetate buffer (0.25 M, pH 4.7). The solution was heated to 90 °C and then 10 g (2.03 mmol) of $K_{10}[\alpha_2\text{-}(P_2W_{17}O_{61})]\cdot20H_2O$ was added gradually. After 2 h, the solution was cooled to room temperature and precipitate was removed by filtration. This solid was recrystallized from boiling water and dried under vacuum. Yield: 61.4 %; Anal. Calcd. for $CdH_{34}K_8O_{78}P_2W_{17}$: Cd, 2.29; K, 6.39; P, 1.26; W, 63.85; H_2O, 5.88 %. Found: Cd, 2.24; K, 5.45; P, 1.16; W, 64.81; H_2O, 5.82 %. IR (KBr, cm^{-1}): 1085, 1053, 1016 (P–O stretching bonds), 945 (W–O_{term} stretching bonds), 889 (W–O_b stretching bonds), 800, 730 (W–O_c stretching bonds).

RESULTS AND DISCUSSION

IR spectra

The compounds α_1-P_2W_{17}Cd and α_2-P_2W_{17}Cd, synthesized in this work, showed typical bands of transition metal-substituted Wells–Dawson heteropolyanion in the range of 700–1200 cm^{-1}.[29] The solid-state FT-IR measurements of $K_6[\alpha$-$P_2W_{18}O_{62}]$, $K_9[\alpha_1$-$LiP_2W_{17}O_{61}]$, α_1-P_2W_{17}Cd, $K_{10}[\alpha_2$-$P_2W_{17}O_{61}]$ and α_2-P_2W_{17}Cd (Fig. 2, curves a–e, respectively) show the spectral patterns characteristic of the Dawson POM framework.

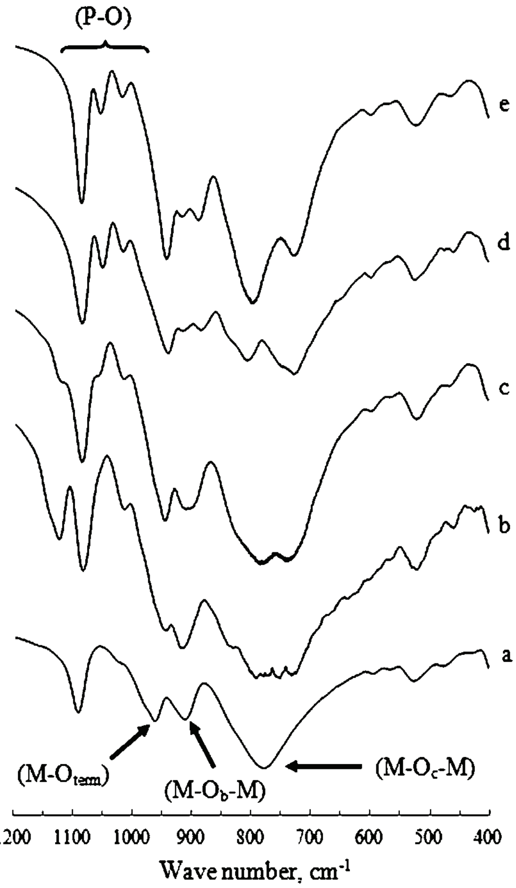

Fig. 2. IR spectra of: a) $K_6[\alpha$-$P_2W_{18}O_{62}]$; b) $K_9[\alpha_1$-$LiP_2W_{17}O_{61}]$; c) α_1-P_2W_{17}Cd, d) $K_{10}[\alpha_2$-$P_2W_{17}O_{61}]$; e) α_2-P_2W_{17}Cd.

As seen in Fig. 2, it is remarkable that only two bands of (P–O) stretching vibration were observed within the range of 1000–1200 cm^{-1} in the $[\alpha$-$P_2W_{18}O_{62}]^{6-}$ heteropolyanion,[30] whereas three bands were observed within the range of 1000–

–1200 cm^{-1} in the $[\alpha_1\text{-}LiP_2W_{17}O_{61}]^{9-}$ heteropolyanion. In α_1-$P_2W_{17}Cd$, by replacing Cd^{2+} in the mono-lacunary $[\alpha_1\text{-}LiP_2W_{17}O_{61}]^{9-}$ polyoxometalate, significant changes were observed in the (P–O) stretching region. As seen in Fig. 2, curve c, the 1122 cm^{-1} band was observed as a shoulder and therefore, the pattern of the spectrum of α_1-$P_2W_{17}Cd$ was approximately similar to that of $[\alpha\text{-}P_2W_{18}O_{62}]^{6-}$. It was surmised that removal of the bands was due to the increase in the symmetry of PO_4 unit caused by transition metal substitution.[31] Moreover, the FT-IR spectra of α_1-$P_2W_{17}Cd$ in the (M–O) region are very similar to that of $K_9[\alpha_1\text{-}LiP_2W_{17}O_{61}]$, especially with regards to the ($M–O_{term}$) oxygen atoms (948 cm^{-1} for α_1-$P_2W_{17}Cd$ and 945 cm^{-1} for $K_9[\alpha_1\text{-}LiP_2W_{17}O_{61}]$), the bands assignable to corner-sharing ($M–O_b–M$) oxygen atoms (898 cm^{-1} for α_1-$P_2W_{17}Cd$ and 912 cm^{-1} for $K_9[\alpha_1\text{-}LiP_2W_{17}O_{61}]$) and the bands assignable to edge-sharing ($M–O_c–M$) oxygen atoms (784 and 738 cm^{-1} for α_1-$P_2W_{17}Cd$; 790 and 732 cm^{-1} for $K_9[\alpha_1\text{-}LiP_2W_{17}O_{61}]$). The FT-IR spectra of α_2-$P_2W_{17}Cd$ in the polyoxometalate region were very similar to that of $K_{10}[\alpha_2\text{-}P_2W_{17}O_{61}]$, especially with regards to the multiple (P–O) bands (1085, 1053 and 1016 cm^{-1} for α_2-$P_2W_{17}Cd$; 1083, 1047, and 1016 cm^{-1} for $K_{10}[\alpha_2\text{-}P_2W_{17}O_{61}]$), the bands assignable to ($M–O_{term}$) oxygen atoms (943 cm^{-1} for α_2-$P_2W_{17}Cd$ and 939 cm^{-1} for $K_{10}[\alpha_2\text{-}P_2W_{17}O_{61}]$), the bands assignable to corner-sharing ($M–O_b–M$) oxygen atoms (889 cm^{-1} for α_2-$P_2W_{17}Cd$ and 885 cm^{-1} for $K_{10}[\alpha_2\text{-}P_2W_{17}O_{61}]$) and the bands assignable to edge-sharing ($M–O_c–M$) oxygen atoms (800 and 730 cm^{-1} for α_2-$P_2W_{17}Cd$; 868 and 736 cm^{-1} for $K_{10}[\alpha_2\text{-}P_2W_{17}O_{61}]$).

^{31}P-NMR

^{31}P-NMR spectroscopy is a very sensitive technique to characterize polyoxometalates and evaluate the purity of these compounds. The ^{31}P-NMR data obtained in this study work and the data for some transition-metal substituted Dawson-type polyoxometalates are given in Table I. In this table, P (1) refers to

TABLE I. ^{31}P-NMR chemical shift patterns (δ / ppm) for some phosphotungstate Dawson-type polyoxometalates; P (1) refers to the resonance attributed to the phosphorus atom nearer to the site of substitution (or defect); P (2) refers to the P atom far away from the site of substitution (or defect)

Compond	P (1)	P (2)	Ref.
$K_6[\alpha\text{-}P_2W_{18}O_{62}]$	–12.50	–12.5	28
$K_9[\alpha_1\text{-}LiP_2W_{17}O_{61}]$	–9.00	–13.1	28
$K_{10}[\alpha_2\text{-}P_2W_{17}O_{61}]$	–6.90	–13.70	32
$K_8[\alpha_1\text{-}P_2W_{17}Zn(H_2O)O_{61}]$	–8.56	–13.45	33
$K_8[\alpha_2\text{-}P_2W_{17}Zn(H_2O)O_{61}]$	–8.65	–14.15	33
$K_7[\alpha_1\text{-}P_2W_{17}La(H_2O)_4O_{61}]$	–10.58	–13.64	34
$K_7[\alpha_1\text{-}P_2W_{17}Lu(H_2O)_4O_{61}]$	–10.57	–13.55	34
$K_7[\alpha_2\text{-}P_2W_{17}Lu(H_2O)_4O_{61}]$	–10.58	–13.61	34
$K_8[\alpha_1\text{-}P_2W_{17}Cd(H_2O)O_{61}]$	–7.99	–14.19	This work
$K_8[\alpha_2\text{-}P_2W_{17}Cd(H_2O)O_{61}]$	–6.72	–13.00	This work

the resonance attributed to the P atom nearer to the site of substitution (or defect) and P (2) refers to the P atom far away from the site of substitution (or defect). In addition, ^{31}P-NMR spectra of α_1-P_2W_{17}Cd and α_2-P_2W_{17}Cd are shown in Fig. 3. The two-line ^{31}P-NMR spectra strongly suggest the presence of a single species in solution, thereby precluding the presence of even minor, phosphorus-containing impurities in α_1-P_2W_{17}Cd or α_2-P_2W_{17}Cd. Finally, the integrated intensity of P (1) appears smaller than that of P (2) because of a slow relaxation rate (large T_1).

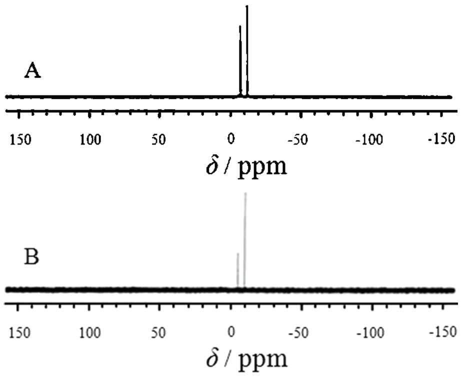

Fig. 3. ^{31}P-NMR spectra of A) α_1-P_2W_{17}Cd and B) α_2-P_2W_{17}Cd.

^{113}Cd-NMR

The ^{113}Cd-NMR spectra in D_2O show clean, single spectra with a resonance at δ = 63.34 ppm for α_1-P_2W_{17}Cd (Fig. 4A) and at δ = –22.86 ppm for α_2-P_2W_{17}Cd (Fig. 4B). As shown in Fig. 4, a considerable difference was observed between the chemical shifts in the ^{113}Cd-NMR spectra of α_1-P_2W_{17}Cd and α_2-P_2W_{17}Cd. Francesconi *et al.*[35] reported that the basic oxygen of the α_1 structure is bound to one tungsten atom, while the corresponding oxygen of the α_2 structure is bound to two tungsten atoms. This observation is ascribed mainly to

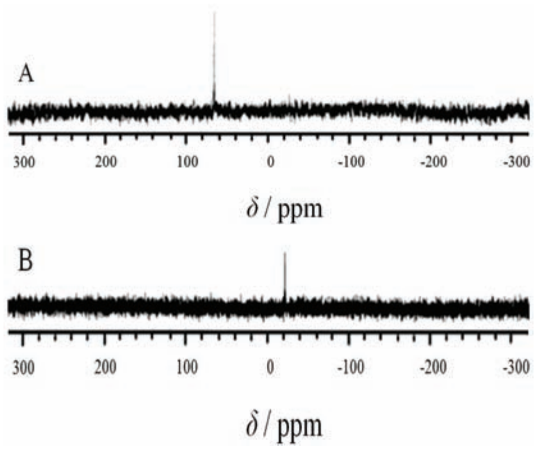

Fig. 4. ^{113}Cd-NMR spectra of A) α_1--P_2W_{17}Cd and B) α_2-P_2W_{17}Cd.

the large framework distortion induced by the vacancy in the α_1 site, and to the nature of the cadmium substituent, which could be considered as not filling the vacancy completely and hence, its resonance moves to an upfield value. On the other hand, for the α_2 site, the cadmium substituent fills the vacancy perfectly and therefore its resonance is downfield shifted.

Electrochemical behavior of α_1-$P_2W_{17}Cd$ *and* α_2-$P_2W_{17}Cd$

Electrochemical behavior of α_1-$P_2W_{17}Cd$. The electrochemical behavior of α_1-$P_2W_{17}Cd$ was studied in 0.5 M acetate buffer solution by cyclic voltammetry (CV), and the obtained results are compared in Fig. 5 with those for $[\alpha_1$--$LiP_2W_{17}O_{61}]^{9-}$. As can be clearly seen in Fig. 5, four quasi-reversible redox peaks appeared in the potential range –1.1 to –0.3 V at a scan rate of 75 mV s^{-1}. The cathodic peak potentials were at –0.97 V (tungsten center), –0.84 V (tungsten center), –0.61 V (tungsten and cadmium centers) and –0.46 V (tungsten center) for α_1-$P_2W_{17}Cd$ while the corresponding peaks were found at –0.97, –0.7, –0.6 and –0.43 V, respectively, for $[\alpha_1$-$LiP_2W_{17}O_{61}]^{9-}$. On considering these data, when cadmium replaced in polyoxometalate vacancy, the cadmium potential would be shifted toward negative potential and the current intensity at –0.6 V would be increased considerably, however the oxidation and reduction of Cd^{2+}/Cd, in the free ion state, occurs at –0.4 V.[36]

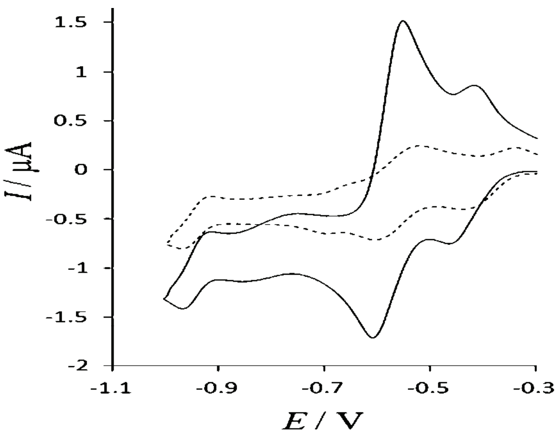

Fig. 5. Cyclic voltammograms of α_1-$P_2W_{17}Cd$ (solid line) and $K_9[\alpha_1$--$LiP_2W_{17}O_{61}]$ (dashed line).

The cyclic voltammograms of α_1-$P_2W_{17}Cd$ in 0.5 M acetate buffer solution at different scan rates are shown in Fig. 6. When the scan rate was varied from 25 to 750 mV s^{-1}, the cathodic peak potentials shifted in the negative direction and the corresponding anodic peak potentials shifted in the positive direction with increasing scan rate. The plots of peak (III) current *vs*. scan rate are shown in the inset of Fig. 6. At scan rates slower than 100 mV s^{-1}, the anodic currents were proportional to the square root of the scan rate, which indicates that the redox process was diffusion-controlled; however, at scan rates higher than 100 mV/s, the anodic currents were proportional to the scan rate, suggesting that the redox process was surface-confined.

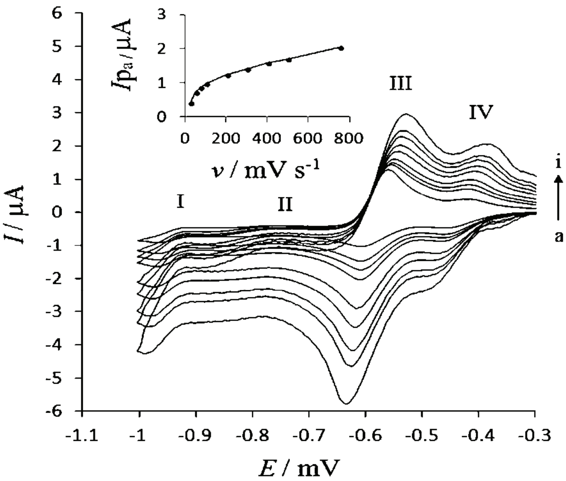

Fig. 6. Cyclic voltammograms of α_1-$P_2W_{17}Cd$ in 0.5 M acetate buffer solutions at different scan rates of a) 25, b) 50, c) 75, d) 100, e) 200, f) 300, g) 400, h) 500 and i) 750 mV s^{-1}. The inset shows plots of the anodic peak current of III against scan rate.

Electrochemical behavior of α_2-$P_2W_{17}Cd$. The electrochemical behavior of α_2-$P_2W_{17}Cd$ was studied in 0.5 M acetate buffer solution by cyclic voltammetry (CV). The obtained results are compared with the corresponding results for $[\alpha_2\text{-}P_2W_{17}O_{61}]^{10-}$ in Fig. 7, from which it can be clearly seen that in the potential range –1.1 to –0.3 V, three quasi-reversible redox peaks appeared and the cathodic peak potentials for a scan rate of 75 mV s^{-1} were at –0.87 (tungsten center), –0.61 (tungsten and cadmium centers) and –0.47 V (tungsten center) for α_2-$P_2W_{17}Cd$ and at –0.95, –0.67 and –0.54 V, respectively, for $[\alpha_2\text{-}P_2W_{17}O_{61}]^{10-}$. Similar to α_1-$P_2W_{17}Cd$, on substituting cadmium in the polyoxometalate vac-

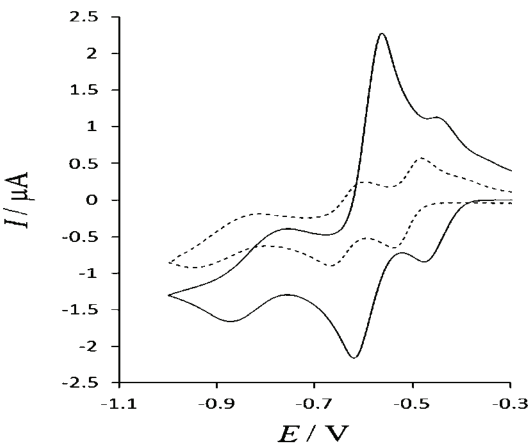

Fig. 7. Cyclic voltammograms of α_2-$P_2W_{17}Cd$ (solid line) and $K_{10}[\alpha_2\text{-}P_2W_{17}O_{61}]$ (dashed line).

ancy, the cadmium potential was shifted toward negative potentials and the current intensity at –0.6 V increased considerably, although the oxidation and reduction of Cd^{2+}/Cd in the free ion state occurs at –0.4 V.[36]

On comparison of cathodic potential data between α_1-P_2W_{17}Cd and [α_1-$LiP_2W_{17}O_{61}$]$^{9–}$, and between α_2-P_2W_{17}Cd and [α_2-$P_2W_{17}O_{61}$]$^{10–}$, it is obvious that when cadmium replaced the vacancy in [α_1-$LiP_2W_{17}O_{61}$]$^{9–}$, no significant changes in the cathodic potentials for α_1-P_2W_{17}Cd were observed. However, when cadmium replaced the vacancy in [α_2-$P_2W_{17}O_{61}$]$^{10–}$, considerable changes in these potentials were observed for α_2-P_2W_{17}Cd. These results indicate that cadmium, which substituted completely in the [α_2-$P_2W_{17}O_{61}$]$^{10–}$ vacancy affects the redox potentials of the tungsten centers of the polyoxometalate, while cadmium in α_1-P_2W_{17}Cd does not fill the vacancy of [α_1-$LiP_2W_{17}O_{61}$]$^{9–}$ completely.

Figure 8 shows the cyclic voltammograms of α_2-P_2W_{17}Cd at different scan rates in the 0.5 M acetate buffer solution. When the scan rate was varied from 10 to 750 mV $s^{–1}$, the cathodic peak potentials were shifted in the negative direction and the corresponding anodic peak potentials shifted in the positive direction with increasing scan rate. The plots of peak (III) current *vs*. scan rate are shown in the inset of Fig. 8. At scan rates lower than 75 mV $s^{–1}$, the anodic currents were proportional to the square root of the scan rate, which indicates that the redox process was diffusion-controlled; however, at scan rates faster than 75 mV $s^{–1}$, the anodic currents were proportional to the scan rate, suggesting that the redox process is surface-confined.

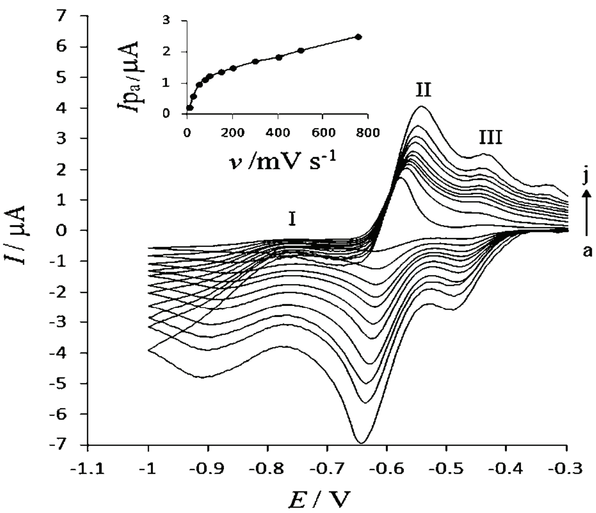

Fig. 8. Cyclic voltammograms of α_1-P_2W_{17}Cd in 0.5 M acetate buffer solutions at different scan rates of a) 10, b) 25, c) 50, d) 75, e) 100, f) 200, g) 300, h) 400, i) 500 and j) 750 mV s^{-1}. The inset shows plots of the anodic peak current of III against scan rate.

Electrocatalysis of $NO_2^–$ reduction

As is known, POMs have been exploited extensively in electrocatalytic reductions.[37] For example, Keita *et al.* reported the first examples of efficient participation of selected metal-ion-substituted heteropolyanions in the electrocatalytic reduction of nitrate and that vanadium-substituted Dawson-types are versatile electrocatalysts.[38,39]

Electrocatalysis of $NO_2^–$ reduction by α_1-$P_2W_{17}Cd$

The polyoxometalates $[\alpha_1\text{-LiP}_2W_{17}O_{61}]^{9–}$ and α_1-P_2W_{17}Cd were tested at pH 4.7 for their activity in the reduction of nitrite ion. The CVs for the electrocatalytic reduction of $NO_2^–$ by glassy carbon electrode in the 0.5 M acetate buffer solution are shown in Fig. 9.

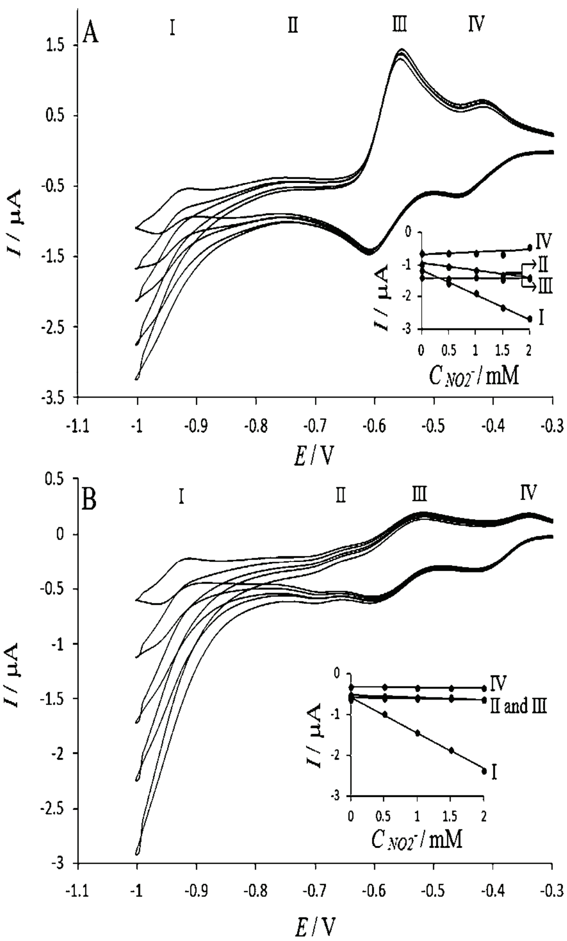

Fig. 9. A) Cyclic voltammograms (scan rate: 75 mV s^{-1}) for the electrocatalytic reduction of NO_2^- with a 5×10^{-4} M solution of α_1-P_2W_{17}Cd in a 0.5 M acetate buffer solution (from top to bottom γ = 0, 1, 2, 3 and 4). B) Cyclic voltammograms (scan rate: 75 mV s^{-1}) for the electrocatalytic reduction of NO_2^- with a 5×10^{-4} M solution of $K_9[\alpha_1\text{-LiP}_2W_{17}O_{61}]$ in a 0.5 M acetate buffer solution (from top to bottom γ = 0, 1, 2, 3 and 4). The excess parameter defined as γ = $= c^0_{(NO_2^-)}/c^0_{(POM)}$ Inset: the relationship between catalytic current and the NO_2^-concentration.

Clearly, with the addition of $NaNO_2$ to the solution, even for small values of the excess parameter, γ, which is defined here as:

$$\gamma = \frac{c^0_{(NO_x)}}{c^0_{(POM)}}$$

the cathodic current of all waves increased and the corresponding anodic current decreased. The catalytic efficiency *CAT* for waves I and II of $[\alpha_1\text{-LiP}_2W_{17}O_{61}]^{9-}$ varied from 53.20 to 274.02 % and 4.53 to 19.84 %, respectively (Table II), when γ increase from 1 to 4, while the *CAT* for $\alpha_1\text{-P}_2W_{17}Cd$ varied from 34.74 to 127.9 % (wave I) and 9.26 to 43.6 % (wave II), Table III. *CAT* is defined as:

$$CAT = 100 \times \frac{\left[I_p(\text{POM,NaNO}_2) - I_p(\text{POM})\right]}{I_p(\text{POM})}$$

where I_p(POM) and I_p(POM,$NaNO_2$) are the cathodic peak currents in the absence and in the presence of $NaNO_2$, respectively.

TABLE II. Catalytic efficiency for $[\alpha_1\text{-LiP}_2W_{17}O_{61}]^{9-}$; $CATw_x$ refers to catalytic efficiency for the x^{th} wave

γ	$CATw_1$ / %	$CATw_2$ / %	$CATw_3$ / %	$CATw_4$ / %
1	53.20	4.53	2.80	3.52
2	123.78	10.39	6.84	8.01
3	191.07	11.34	5.78	6.73
4	274.02	19.84	10.87	1.21

TABLE III. Catalytic efficiency for $\alpha_1\text{-P}_2W_{17}Cd$; $CATw_x$ refers to catalytic efficiency for the x^{th} wave

γ	$CATw_1$ / %	$CATw_2$ / %	$CATw_3$ / %	$CATw_4$ / %
1	34.74	9.26	3.57	4.51
2	61.01	19.66	0.71	1.61
3	99.15	35.27	5.00	6.29
4	127.90	43.60	2.10	4.03

It is noticeable from Tables II and III that the electrocatalytic activity of $[\alpha_1\text{-LiP}_2W_{17}O_{61}]^{9-}$ was greater than that of $\alpha_1\text{-P}_2W_{17}Cd$ in wave I, while this behavior was *vice versa* for wave II. This trend may be attributed to the presence of Cd^{2+}. However, the electrocatalytic activity of $[\alpha_1\text{-LiP}_2W_{17}O_{61}]^{9-}$ decreased on cadmium ion substitution.

The inset of Fig. 9 presents four straight lines over a wide range of concentrations with different slopes, indicating that wave I had a higher catalytic activity than the other waves.

Electrocatalysis of NO_2^- reduction by α_2-$P_2W_{17}Cd$

The polyoxometalates $[\alpha_2\text{-}P_2W_{17}O_{61}]^{10-}$ and α_2-P_2W_{17}Cd were tested at pH 4.7 for their activity in the reduction of nitrite ion. The CVs for the electrocatalytic reduction of NO_2^- by GC in 0.5 M acetate buffer solution are shown in Fig. 10.

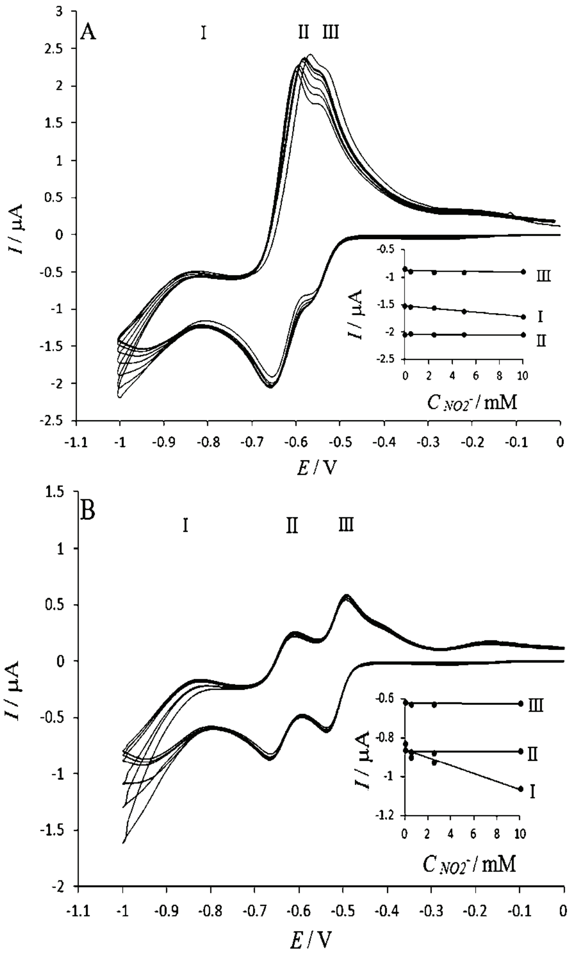

Fig. 10. A) Cyclic voltammograms (scan rate: 75 mV s^{-1}) for the electrocatalytic reduction of NO_2^- with a 5×10^{-4} M solution of α_2-P_2W_{17}Cd in a 0.5 M acetate buffer solution (from top to bottom γ = 0, 1, 5, 10 and 20). B) Cyclic voltammograms (scan rate: 75 mV s^{-1}) for the electrocatalytic reduction of NO_2^- with a 5×10^{-4} M solution of $K_{10}[\alpha_2\text{-}P_2W_{17}O_{61}]$ in a 0.5 M acetate buffer solution (from top to bottom γ = = 0, 1, 5 and 20). The excess parameter defined as $\gamma = c^0_{(NO2^-)}/c^0_{(POM)}$. Inset: the relationship between catalytic current and NO_2^-concentration.

Clearly, with the addition of $NaNO_2$ to the solution, even for small values of the excess parameter γ, cathodic current of all waves increased and the corresponding anodic current decreased. The catalytic efficiency *CAT* for wave I of $[\alpha_2\text{-}P_2W_{17}O_{61}]^{10-}$ varied from 8.34 to 28.17 % (Table IV) when γ = 1, 5 and 20, while the *CAT* variations for α_2-P_2W_{17}Cd were from 0.65 to 10.46 % when γ = 1, 5, 10 and 20 (Table V).

TABLE IV. Catalytic efficiency for $[\alpha_2\text{-}P_2W_{17}O_{61}]^{10-}$; *CAT*w$_x$ refers to catalytic efficiency for the x^{th} wave

γ	*CAT*w$_1$ / %	*CAT*w$_2$ / %	*CAT*w$_3$ / %
1	8.34	1.27	1.45
5	11.60	1.74	1.94
20	28.17	0.69	0.97

TABLE V. Catalytic efficiency for $\alpha_2\text{-}P_2W_{17}Cd$; *CAT*w$_x$ refers to catalytic efficiency for the x^{th} wave

γ	*CAT*w$_1$ / %	*CAT*w$_2$ / %	*CAT*w$_3$ / %
1	0.65	0.00	0.22
5	2.61	0.00	0.55
10	6.53	0.49	1.00
20	10.46	0.49	0.33

It is noticeable from Tables IV and V that the electrocatalytic activity of $[\alpha_2\text{-}P_2W_{17}O_{61}]^{10-}$ was greater than that of $\alpha_2\text{-}P_2W_{17}Cd$ in wave I, due to the presence of Cd^{2+} ion.

The inset of Fig. 10 presents four straight lines over a wide range of concentrations with different slopes, indicating that wave I had a higher catalytic activity than the other waves.

CONCLUSIONS

Two new cadmium-containing Wells–Dawson polyoxometalates were synthesized as water-soluble potassium salts. ^{113}Cd-NMR indicated that cadmium was substituted completely in the $[\alpha_2\text{-}P_2W_{17}O_{61}]^{10-}$ vacancy, whereas cadmium in $[\alpha_1\text{-}LiP_2W_{17}O_{61}]^{9-}$ did not fill completely the vacancy. Moreover, electrochemical investigations were in good agreement with this result because remarkable differences in the redox peaks were not observed between the $\alpha_1\text{-}P_2W_{17}Cd$ and $[\alpha_1\text{-}LiP_2W_{17}O_{61}]^{9-}$ compounds.

The electrochemistry of $\alpha_1\text{-}P_2W_{17}Cd$ and $\alpha_2\text{-}P_2W_{17}Cd$ was studied. First, these polyoxoanions exhibited four- and three-step redox waves attributed to the tungsten–oxo and cadmium–oxo redox processes in pH 4.7 solutions. The best electrocatalytic activity for $\alpha_1\text{-}P_2W_{17}Cd$ and $\alpha_2\text{-}P_2W_{17}Cd$ was observed in wave I, which is related to tungsten–oxo redox centers. In addition, decreases in the electrocatalytic activity of mono-lacunary Dawson-type ($[\alpha_1\text{-}LiP_2W_{17}O_{61}]^{9-}$ and $[\alpha_2\text{-}P_2W_{17}O_{61}]^{10-}$) follows from the presence of cadmium metal ion in these compounds. The presence of cadmium metal ion in the mono-lacunary Dawson--type ($[\alpha_1\text{-}LiP_2W_{17}O_{61}]^{9-}$ and $[\alpha_2\text{-}P_2W_{17}O_{61}]^{10-}$) caused decreases in electrocatalytic activity of these compounds.

ИЗВОД

СИНТЕЗА, КАРАКТЕРИЗАЦИЈА И УПОРЕЂИВАЊЕ ЕЛЕКТРОКАТАЛИТИЧКЕ АКТИВНОСТИ ДВА МОНОЛАКУНАРНА WELLS–DAWSON ПОЛИОКСОМЕТАЛАТА КОЈИ САДРЖЕ КАДМИЈУМ, α_1- И α_2-$[P_2W_{17}Cd(H_2O)O_{61}]^{8-}$

FARROKHZAD MOHAMMADI ZONOZ[1], ALI JAMSHIDI[2], FATEME HAJIZADEH[1] и KHADIJEH YOUSEFI[3]

[1]*Department of Chemistry, Hakim Sabzevari University, Sabzevar, 96179-76487, Iran,* [2]*School of Chemistry, Damghan University, Damghan, Iran и* [3]*Payamnoor University of Sari, Sari, Iran*

У овом раду су синтетизоване калијумове соли два Wells–Dawson полиоксометалата који садрже кадмијум, $K_8[\alpha_1$-$P_2W_{17}Cd(H_2O)O_{61}]\cdot 14H_2O$ (α_1-$P_2W_{17}Cd$) и $K_8[\alpha_2$-$P_2W_{17}Cd(H_2O)O_{61}]\cdot 16H_2O$ (α_2-$P_2W_{17}Cd$). Синтетизовани комплекси су окарактерисани применом IR, ^{31}P- и ^{113}Cd-NMR спектроскопије, док су редокс потенцијали волфрама и кадмијума у овим једињењима одређени применом цикличне волтаметрије (CV). Добијени резултати су показали да присуство јона кадмијума утиче на смањење електрокаталитичке активности $[\alpha_1$-$LiP_2W_{17}O_{61}]^{9-}$ и α_2-$[P_2W_{17}O_{61}]^{10-}$ хетерополианјона.

(Примљено 18. јануара, ревидирано 18. маја, прихваћено 28. маја 2014)

REFERENCES

1. L. Ouahab, *Chem. Mater.* **9** (1997) 1909
2. M. T. Pope, A. Muller, *Angew. Chem. Int. Ed. Engl.* **30** (1991) 34
3. M. Witvrouw, H. Weigold, C. Pannecouque, D. Schols, E. D. Clercq, G. Holan, *J. Med. Chem.* **43** (2000) 77
4. C. L. Hill, R. B. Bown, *J. Am. Chem. Soc.* **108** (1986) 536
5. A. Watzenberger, G. Emig, D.T. Lynch. *J. Catal.* **124** (1990) 247
6. D. Mansuy, J. F. Bartoli, P. Battioni, D. K. Lyon, R. G. Finke, *J. Am. Chem. Soc.* **113** (1991) 7222
7. R. Contant, J.-P. Ciabrini, *J. Chem. Res. Synop.* **222** (1997) 2601
8. Z. Zhang, Y. Li, Y. Wang, Y. Qi, E. Wang, *Inorg. Chem.* **47** (2008) 7615
9. D. K. Lyon, W. K. Miller, T. Novet, P. J. Domaille, E. Evitt, D. C. Johnson, R. G. Finke, *J. Am. Chem. Soc.* **113** (1991) 7209
10. M. N. Sokolov, N. V. Izarova, E. V. Peresypkina, D. A. Mainichev, V. P. Fedin, *Inorg. Chim. Acta* **362** (2009) 3756
11. J. Choi, J. K. Kim, S. Park, J. H. Song, I. K. Song, *Appl. Catal. A,* **427–428** (2012) 84
12. G. Absillis, T. N. Parac-Vogt, *Inorg. Chem.* **51** (2012) 9902
13. S. Vanhaecht, G. Absillis, T. N. Parac-Vogt, *Dalton Trans*. **41** (2012) 10028
14. R. Contant, *J. Chem. Res., Synop.* (1984) 120
15. J. F. Kirby, L. C. V. Baker, *J. Am. Chem. Soc.* **117** (1995) 10010
16. L. H. Bi, E. B. Wang, J. Peng, R. D. Hung, L. Xu, C. W. Hu, *Inorg. Chem.* **39** (2000) 671
17. M. H. Alizadeh, H. Razavi, F. Mohammadi Zonoz, M. R. Mohammadi, *Polyhedron* **22** (2003) 933
18. F. Hussain, L. H. Bi, U. Rauwald, M. Reicke, U. Kortz, *Polyhedron* **24** (2005) 847
19. L. Chen, D. Shi, J. Zhao, Y. Wang, P. Ma, J. Wang, J. Niu, *Cryst. Growth Des.* **11** (2011) 1913
20. S. Q. Liu, D. Volkmer, D. G. Kurth, *J. Cluster Sci.* **14** (2003) 405
21. M. Green, J. Harries, G. Wakefield, R. Tayor, *J. Am. Chem. Soc.* **127** (2005) 12812
22. L. Cheng, J. A. Cox, *Electrochem. Commun.* **3** (2001) 285
23. G. G. Gao, L. Xu, W. J. Wang, W. J. An, Y. F. Qiu, Z. Q. Wang, E. B. Wang, *J. Phys. Chem., B* **109** (2005) 8948

24. J. Y. Qu, X. Q. Zou, B. F. Liu, S. J. Dong, *Anal. Chim. Acta* **599** (2007) 51
25. A. Kuhn, F. C. Anson, *Langmuir* **12** (1996) 5481
26. X. Xi, S. Dong, *J. Mol. Catal., A* **114** (1996) 257
27. W. R. Epperly, *Chemtech* (1991) 429
28. R. Contant, *Inorg. Synth.* **27** (1990) 104
29. Y. Saku, Y. Sakai, K. Noniya, *Inorg. Chim. Acta* **363** (2010) 967
30. I. M. Mbolmekalle, Y. W. Lu, B. Keita, L. Nadjo, *Inorg. Chem. Commun.* **7** (2004) 86
31. K. Kim, M. T. Pope, G. J. Gama, M. H. Dickman, *J. Am. Chem. Soc.* **32** (1976) 11164
32. R. Contant, M. Abbessi, J. C. A. Belhouari, B. Keita, L. Nadjo, *Inorg. Chem.* **36** (1997) 4961
33. J. Bartis, Y. Kunina, M. Blumenstein, L. C. Francesconi, *Inorg. Chem.* **35** (1996) 1497
34. J. Bartis, M. Dankova, J. J. Lessmann, Q. Luo, W. Horrocks, L. C. Francesconi, *Inorg. Chem.* **38** (1999) 1042
35. D. McGregor, B. P. Burton-Pye, R. C. Howell, I. M. Mbomekalle, W. W. Lukens Jr., F. Bian, E. Mausolf, F. Poineau, K. R. Czerwinski, L. C. Francesconi, *Inorg. Chem.* **50** (2011) 1670
36. www.csudh.edu, http://www.csudh.edu/oliver/chemdata/data-e.htm (18/01/2014)
37. M. T. Pope, A. Muller, E. Papaconstantinou, A. Ioannidis, A. Hiskia, P. Argitis, D. Dimoticali, S. Korres, *Polyoxometalates: from Platonic Solids to Antiretroviral Activity*, Kluwer, Dordrecht, 1994, p. 327
38. B. Keita, E. Abdeljalil, L. Nadjo, R. Contant, R. Belgiche, *Electrochem. Commun.* **3** (2001) 56
39. B. Keita, I. Mbomekalle, L. Nadjo, P. Oliveira, A. Ranjbari, R. Contant, *C. R. Chim.* **8** (2005) 1057.

Journal of the Serbian Chemical Society
JSCS-info@shd.org.rs • www.shd.org.rs/JSCS

J. Serb. Chem. Soc. 79 (11) 1395–1404 (2014) UDC 546.3:577.1+541.132+54.05:504.53:628
JSCS–4673 *Original scientific paper*

The migration of some biometal ions in the systems mineral tissue of teeth–soil and teeth–water media

RUŽICA S. NIKOLIĆ[1], NATAŠA V. RADOSAVLJEVIĆ-STEVANOVIĆ[2], TATJANA D. ANĐELKOVIĆ[1#], MAJA N. STANKOVIĆ[1] and NENAD S. KRSTIĆ[1*#]

[1]Department of Chemistry, Faculty of Sciences and Mathematics, University of Niš, Višegradska 33, 18000 Niš, Serbia and [2]The National Crime-Technical Centre, Ministry of Interior of the Republic of Serbia, Kneza Miloša 103, 11000 Belgrade, Serbia

(Received 7 February, revised 30 May, accepted 30 May 2014)

Abstract: This paper outlines the changes in the mineral tissue of teeth that had been exposed to the influence of the agents of natural media. Such mineral tissue could be used as a potentially important forensic material that is gradually altered under the influence of external media. The biometal content was determined using the ICP-OES technique. According to the quantitative changes of the biometals in teeth tissue after its exposure to different media, the migration of Ca^{2+}, Mg^{2+}, Fe^{2+}, Cu^{2+} and Zn^{2+} in teeth–soil and teeth–water media was observed. The content of Ca^{2+} and Mg^{2+} in the mineral tissue increased, but the Cu^{2+} content decreased. The migration of Fe^{2+} and Zn^{2+} depended on the content and type of the soil media and differed for clay soil, limestone enriched soil and urban area soil. The changes that occurred in the mineral matrix of teeth were detected by the SEM–EDS technique. The intensity of the biometal content and the mineral matrix changes are a potentially significant subject matter for forensic examination, because they indicate the kind of medium to which the material was exposed.

Keywords: biometal ions; migration; teeth; soil; water media.

INTRODUCTION

The hard mineral tissue of bones and teeth represents readily available biopsy material that is relatively easy to analyze and could be used in forensics, especially in examination of bones. It is potentially important and convenient in cases of exposure to the influence of different external media.[1] Tooth enamel consists of 96 % hydroxyapatite (HAp).[2] Through the influence of agents in ambient media, the mineral tissue of teeth changes, and the change is manifested, among other things, in an alteration of the elemental composition of the HAp.[3–5]

* Corresponding author. E-mail: nenad.krstic84@yahoo.com
# Serbian Chemical Society member.
doi: 10.2298/JSC140207058N

In the structure of the HAp, the Ca^{2+} are surrounded by the oxygen from the phosphate and they can, under certain conditions, be replaced in the crystal lattice by other M^{2+} (metal ions) with an appropriate radius.

The efficiency of the substitution depends on the strength of the interaction between the cations and the oxygen found in the immediate environment, as well as on the ionic potential.[6,7] According to data found in the literature, during ionic replacement processes, the Ca^{2+} in synthetic HAp were almost completely replaced by Ba^{2+} and Pb^{2+} and somewhat less effectively by Cd^{2+} and Sr^{2+} from diluted solutions of their salts.[8–10] During contact between teeth and environment media, and in natural HAp tissue, similar processes occur (substitution, diffusion, ionic exchange and others), during which the Ca^{2+} are replaced by the cations of other M^{2+}. In addition, sorption of ions from the ambient environment into the HAp of natural teeth is possible. These processes occur in living human bodies during contact between teeth and food, water and oral fluids.[11] Similar processes occur in bones exposed to the influence of the natural environment, and probably in teeth. Unfortunately, not enough data exists on the changes that occur in teeth.[4]

Soil represents natural ground, a multiphase system with a mineral matter content of approximately 40 % and an organic matter content of approximately 6 %.[12] The organic soil content, in which humic acids are found, influences the possibility of adsorption, desorption, absorption, buffer capacity and exchange of constituent ions of soil with materials from the external environment, both of natural and anthropological origin.[13] Forensic examinations of soil samples are based on a qualitative comparison of undisputed and disputed samples through the application of different methods of analysis.[14–16] It was shown that the soil components interact with metal ions; especially with the ions of heavy metals, and that these interactions depend on the soil pH, buffer capacity, humic matter content, ionic radius and charge, and atmospheric conditions.[17,18]

There are multiple possibilities (adsorption, desorption, diffusion, ionic exchange, precipitation and co-precipitation) in the natural environment for ionic exchange in a system of soil-exposed anthropogenic material. This has already been used in practice for the determination of time of death.[2,19] The intensity of ion migration into or out of mineral tissue could be an indicator of tissue exposure time to the environment, as well as the type of environment. According to data found in the literature, the current studies in forensic practices have focused on the examination of the content of hard mineral bone tissue that had been exposed to soil.[20] No detailed studies were found regarding how the mineral content of hard teeth tissue reacts in the natural environment and in different types of soil and water.

Based on the qualitative and quantitative changes that occurred in the mineral tissue of teeth after it had been exposed to different types of soil and to water, the aim of the study was to obtain potentially useful information for forensic experts. With the aim of examining the changes in the mineral content of hard teeth tissue, changes in the contents of the biometal ions, Ca^{2+}, Mg^{2+}, Fe^{2+}, Cu^{2+} and Zn^{2+}, in teeth were also studied, as well as the migration trend of these metal ions in a teeth–natural environment system. The calcium ion was chosen as the basic constituent of the HAp, Fe and Mg as metals present in soil in high concentrations, and Zn and Cu as biometals the M^{2+} of which are readily mobile. Data regarding changes in the mineral tissue were also obtained by the characterization of the mineral tissue using inductively coupled plasma-optical emission spectroscopy (ICP-OES) and scanning electron microscopy–energy dispersive spectroscopy (SEM–EDS).

EXPERIMENTAL

Model system. The model system for the study of the interaction between soil and anthropogenic material consisted of human teeth exposed to the influence of different natural environment media (soil and water). The soil media from the natural environment consisted of three different types of soil: urban city soil samples from a park (SM1), soil with a predominant clay content (SM2) and soil samples with a mostly limestone content (SM3) from the city of Niš and its surrounding area.[21,22] The aqueous media from the natural environment consisted of: a commercial bottled water "*Aqua viva*" (WM1) and a solution of a "rainwater model system" (WM2). The anthropogenic material exposed to the influence of the aforementioned media consisted of human teeth extracted due to health and orthodontic reasons in the Dental Hospital of the Medical Faculty of the University of Niš.

The teeth were exposed to the aforementioned media in a mass ratio of 100:1 and left for three months at room temperature (22–25 °C). The migration of biometal ions in the studied model systems was examined by measuring the biometal content using the ICP-OES method at the beginning and at the end of the experiment. The changes in the teeth mineral tissue and its structural characterization were examined by SEM–EDS analyses.

Preparation of the media. Approximately 2 kg of soil was sampled from the selected locations, at 30 cm from the surface.[23] The specimen samples were measured in the form of dried soils samples (SM1, SM2 and SM3), and were later moistened with deionized water in glass beakers, while the subjected anthropogenic material was placed into the beakers. The influence of the aqueous media on human teeth was examined in the same mass ratio and under the same conditions.

Preparation of the human material. The extracted teeth were treated with saline solution, washed with deionized water, dried to a constant mass at 70 °C and then measured. One part of the anthropogenic material was separated as the control sample and the rest was divided into five samples that were exposed to each medium for three months. After this period, one part of the anthropogenic material was used for the determination of the contents of the studied biometal and the other part for the study of changes in the mineral tissue through application of techniques that are usually used for the characterization of inorganic material.

Determination of the biometal contents. The biometal contents in the media and in samples of mineral tissue of teeth were determined using a Spectroflame ICP-OES instrument with an argon plasma. The teeth samples, *i.e.*, the control (untreated) sample and the group of samples that had been exposed to the influence of the various media, were solubilized in the same way and under the same conditions. The precisely measured mass of the dried samples was dissolved twice in 6 mol dm^{-3} HNO_3 acid. The obtained dry residue was treated twice with the same concentration HCl acid and the final dried residue was dissolved in deionized water to a definite volume.[24,25] The biometal content was determined from the solutions. In the same way, and according to the same procedure, the soil samples were treated and prepared for metal content determination.

Mineralogical examination of the mineral material of teeth. The structural characterization of the mineral matrix of teeth of both the control sample and the group of samples exposed to the influence of external environment media was realized by SEM–EDS analyses. The SEM–EDS examination of *in situ* teeth tissue (covered by a vapor of colloidal gold) was performed using a FEI Quanta 200 microscope.

Statistical interpretation of the results. For the statistical interpretation of results, the Student's *t*-test (Microsoft Office Excel) was applied. All of the results of the chosen measurement of the biometal contents are given as the mean value ±*SD*. Statistically important results are shown as $p < 0.01$, $p < 0.05$ and $p < 0.1$.

RESULTS AND DISCUSSION

The results of the determination of the organic matter (OM) content, given as the content of organic carbon, the pH results and the results of biometal determination in the media to which mineral tissue of teeth had been exposed are given in Table I. The results represent the mean value ± *SD* ($n = 5$, n – the number of probes).

TABLE I. The pH values and contents of organic matter and biometals in the employed media (mg g^{-1}); SM1 – urban city soil, SM2 – clay enriched soil and SM3 – limestone enriched soil; WM1 – "*Aqua viva*" commercial bottled water and WM2 – rain water model; n.d. – not detected

Parameter	SM1	SM2	SM3	WM1	WM2
pH	7.23±0.74	4.55±0.39	7.06±0.82	7.22±0.68	6.13±0.58
Organic C	12.71±1.50	59.58±6.79	21.45±2.47	–	–
Ca^{2+}	48.23±5.16	0.21±0.04	88.44±8.30	120.00±11.56	1.20±0.15
Mg^{2+}	58.00±6.38	0.54±0.09	8.84±0.90	45.20±5.12	0.43±0.09
Cu^{2+}	$(0.03\pm5.8)\times10^{-3}$	$0.04\pm6.4\times10^{-3}$	0.15±0.03	<0.1	n.d.
Fe^{2+}	$(0.02\pm3.9)\times10^{-3}$	0.26±0.05	24.98±2.95	<0.05	n.d.
Zn^{2+}	$(0.62\pm1.1)\times10^{-3}$	$0.03\pm5.4\times10^{-3}$	0.38±0.07	<0.1	n.d.

These results showed that the soil enriched with clay was the most acidic (pH 4.55) and contained the highest content of organic matter. The limestone-enriched soil used in the present study contained the highest level of calcium and about one hundred times more iron than the other types of soil. The urban soil samples contained the highest levels of magnesium and zinc in comparison to the other soil types. In the analyzed soil samples, the level of copper was the mean value of the metal in the soil samples.[12]

The results of the interaction and the change in the biometal ion content in the system "medium–anthropogenic material" during a three-month period are presented in the Table II. The results represent the mean value ±*SD* ($n = 5$).

TABLE II. The content of biometals in the teeth samples that had been exposed to the influence of different media; SM1 – urban city soil, SM2 – clay enriched soil and SM3 – limestone enriched soil; WM1 – "*Aqua viva*" commercial bottled water and WM2 – rain water model; *: $p < 0.01$, **: $p < 0.05$, ***: $p < 0.1$

Specimen	Ca^{2+}	Mg^{2+}	Cu^{2+}	Fe^{2+}	Zn^{2+}
	Concentration, mg g^{-1}		Concentration, μg g^{-1}		
Control	293.94±34.47	5.50±1.20	37.93±5.96	36.52±6.05	0.53±0.08
SM1	477.52±19.17*	8.63±1.56*	14.47±3.41*	105.24±10.34*	0.22±0.02*
SM2	327.5±11.55***	8.74±1.09*	31.56±4.41***	21.52±2.55*	0.55±0.02**
SM3	372.00±15.37*	6.58±0.37***	22.85±2.96*	117.80±17.32*	0.368±0.02**
WM1	332.00±15.01***	8.12±0.68*	12.04±2.38*	34.84±3.99	0.36±0.02**
WM2	401.78±11.64*	6.00±0.46***	11.98±2.28*	33.26±3.09	–

The percentage of biometals ion migration *IN* or *OUT* of the mineral tissue of teeth that had been exposed to different soil and aqueous medium was calculated by Eqs. (1) and (2), respectively:

$$IN = \frac{(X - Y)}{Y} \times 100 \quad (1)$$

$$OUT = \frac{(Y - Z)}{Y} \times 100 \quad (2)$$

where X is the increase in the value of the metal content compared to the control, Y is the metal content of untreated teeth tissue and Z is decrease in the value of metal content compared to control. The results of these calculations are shown in Fig. 1.

According to the results, it could be concluded that the calcium and magnesium contents increased during teeth exposure to the influence of all the soils and aqueous media from *ca*. 9 to 60 % (Fig. 1). Thus, Ca^{2+} and Mg^{2+} have the same, statistically important, tendency of migration from the soil ($p < 0.01$) and the aqueous media ($p < 0.1$) into teeth. The reasons for this are probably because the media in these experiments contained high concentrations of these two metals and a large relative quantity of the media was used (mass ratio of the medium:teeth = 100:1). The highest quantity of Ca^{2+} (477.52 mg g^{-1}) was adsorbed from the urban soil samples, where probably the limestone-enriched soil contained calcium in the form of insoluble salts. A number of factors affect the migration of calcium and magnesium ions from the soil: the acidity of the medium, the concentration of the other ions present, the organic material, the mineral matrix of the soil samples, temperature, etc.

Copper is a bioelement present in the body in small quantities of 1.0–2.0 mg dm^{-3} of serum, but after a number of years and in contact with food and oral fluids, it begins to accumulate, among other tissues, in the mineral tissue of the teeth (37.93 μg g^{-1}).[25] When such a mineral biomaterial is exposed to the exter-

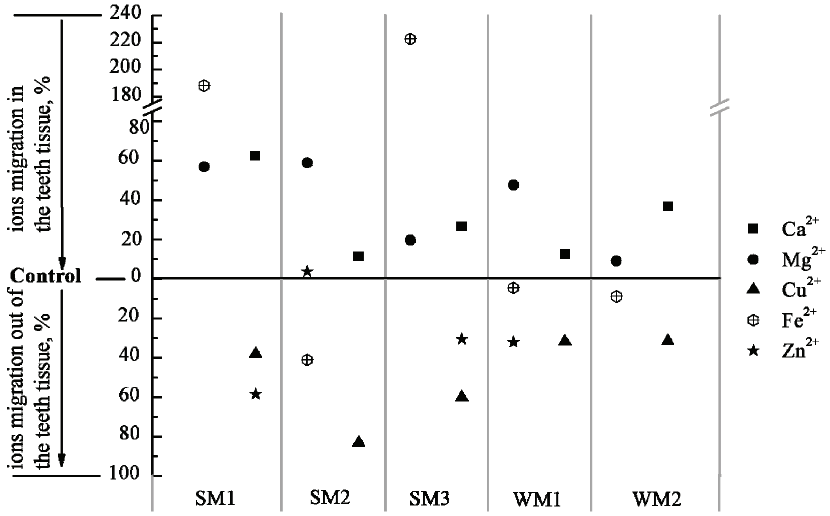

Fig. 1. Percentage of migration of biometal ions: Ca^{2+}, Mg^{2+}, Fe^{2+}, Cu^{2+} and Zn^{2+}, in the systems mineral tissue of teeth–soil and teeth–water media; SM1 – urban city soil, SM2 – clay enriched soil and SM3 – limestone enriched soil; WM1 – "*Aqua viva*" commercial bottled water and WM2 – rain water model.

nal environment, statistically significant leaching occurs and the level of Cu^{2+} decreases ($p < 0.01$). Since Cu^{2+} is of small volume, it can easily be assimilated in the structure of HAp, which further contributes to its migration.[26] The results of the measurement of this metal content in the samples of teeth mineral tissue indicated that the copper content decreased, or in other words, it migrated from the teeth to the outer environment regardless to the medium (from *ca*. 30 to 80 %), as shown in Fig. 1. This migration tendency of copper ions occurs with the aim of establishing equilibrium, because of potential interactions and complex reactions of copper ions with the soil components and the possible exchangeable adsorption of this metal.[25]

Iron from a soil with predominantly limestone content, which was analyzed in this study, is relatively available and is adsorbed by biological material in greater amounts. Thus, the content of Fe in the mineral tissue increased in a statistically significant way ($p < 0.01$), up to three times (from 36.52 to 117.80 μg g^{-1}). The content of the clay mineral kaolinite and smectite in addition to feldspar and other minerals in the soil is convenient for the binding of higher charged ions because of the special structure of the aluminum silicates. Thus, it led to a decrease in the iron content in the mineral matrix of the analyzed biomaterial, 41 % for medium SM2, less than 10 % of the aqueous media (Fig. 1), and probably to the formation of a more stable aluminum silicate matrix.[21,22] This type of soil was the one with a higher content of organic matter in comparison to the other types of soil and hence, it potentially has a greater ability for the interaction of iron ions with O-donor atoms of the organic matter of the soil and for the formation of complexes and sparingly soluble iron compounds.[27] Since the difference in the iron content in the mineral tissue and the aqueous media is the greatest, during the three-month period of exposure to the influence of these media, the content of the iron ions in the mineral tissue decreased because of the diffusion of the metal ions into the surrounding medium. These different migration tendencies of iron ions in the studied model systems, natural medium–teeth, are potentially important for forensic examination and the application of teeth as a forensic material. Research showed that the divalent cation exchange in synthetic HAp depended on the M^{2+}–O interaction (O nearest atoms from the PO_4^{3-} group in HAp) and that the processes of Ca^{2+} replacement by larger cations (Pb^{2+} and Cd^{2+}) in a weakly basic environment is more convenient in terms of energy, whereas the exchange of small ions occurred with a lower tendency in a weakly acidic environment.[7–10]

Zinc is a biometal found in small quantities in the human body, but due to ingestion through food and oral fluids, it starts to accumulate in the mineral tissues. The mean value of this metal in the analyzed biomaterial was 0.53 mg g^{-1}.[25] The study presented in this paper shows that the zinc ions migrate *ca*. 4 % into the mineral content of teeth tissue from the clay mineral enriched soils (kaolinite and smectite near quartz, brookite and feldspar)[21,22] with a higher content of organic matter and lower pH values ($p < 0.05$). In the other studied model systems, the leaching of zinc ions from the mineral content of teeth tissue into the outer medium occurred ($p < 0.01$), as shown in Fig. 1.

The SEM micrographs of the untreated teeth sample and the samples of teeth that had been exposed to the influence of the soil medium SM1 and the aqueous medium WM2 are shown in Fig. 2.

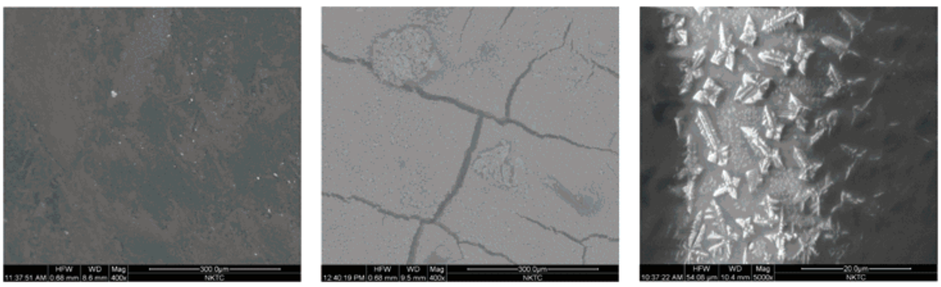

a) b) c)

Fig. 2. SEM micrographs; a) untreated teeth, b) teeth exposed to the urban city soil medium SM1 and c) to the rain water medium WM2.

Based on a comparison of the results of the SEM–EDS analyses of the untreated and the treated samples that had been exposed to different types of soil media, changes in the content and the surface appearance of the mineral content of the hard dental tissue were noted, while no significant changes were noticed in the samples exposed to water (Fig. 2 and Table III). The EDS spectra indicate local changes in the metals in the studied mineral tissue, which occurred due to adsorption. Al, Mg, Si and traces of Fe could be noticed in the teeth tissue that had been exposed to the urban city soil samples; the adsorption of Mg and Na occurred in the clay enriched medium and the increase in Ca, Si, Mg and Na. Significant changes in the Ca^{2+}/P ratio were noticed for teeth samples that had been exposed to the limestone enriched soil (Table III). The ratio of the Ca^{2+}/P content was altered probably as the result of the adsorption of Ca^{2+} from the surrounding environment or adsorption of an excessive amount of phosphates on the crystal surface or substitution of Ca^{2+} by the ions from the surrounding environment.[28–32] The small diameters of Na^{+}, Mg^{2+} and Al^{3+} enable them to migrate easily into internal dental tissue.[25]

Table III. Dependence of the Ca^{2+}/P ratio in teeth tissue on the investigated soil and water media; SM1 – urban city soil, SM2 – clay enriched soil and SM3 – limestone enriched soil; WM1 – "*aqua viva*" commercial bottled water and WM2 – rain water model

Specimen	Ca^{2+} (wt. %)	P (wt. %)	Ca^{2+}/P, [%]
Control	15.98	8.27	1.93
SM1	26.75	11.56	2.29 (19.68)
SM2	22.29	10.53	2.12 (9.85)
SM3	44.78	9.35	4.79 (147.69)
WM1	20.74	13.13	1.59 (17.61)
WM2	24.30	13.37	1.82 (5.70)

Cracks on the teeth surface were noticed, which originated from the interaction of the teeth with all the surrounding soil environments (Fig. 2).

CONCLUSIONS

This study of the interaction between environmental media and anthropogenic material (teeth) on the model systems of soil and water of different composition showed that after a three-month exposure period, statistically significant changes in the biometals contents in the mineral content of dental tissue occurred due to different physicochemical processes and interactions of the mineral tissue with the surrounding environment. The intensity and direction of the changes in the biometal ions (Ca^{2+}, Mg^{2+}, Cu^{2+}, Fe^{2+} and Zn^{2+}) content could potentially be important in forensic examinations because they could allow focus to be directed on the type of the environmental medium in which the dental material was stored. The SEM–EDS analysis showed differences between the samples exposed to the soil media, on the one hand, and the aqueous medium, on the other. Although the information obtained by the application of the ICP-OES is more reliable, its mutual application with the SEM–EDS technique used in this study could help end conclusion to be reached and a combination of these methods could allow for a potential differentiation of the environmental medium in which the mineral tissue had been stored.

Acknowledgements. This research was partly realized with the financial help of the Ministry of Education, Science and Technological Development of the Republic of Serbia within the projects III45017 and TR34008. The authors would also like to thank Marta Dimitrijević, MA, for proofreading the text of this paper.

ИЗВОД

МИГРАЦИЈА ПОЈЕДИНИХ ЈОНА БИОМЕТАЛА У СИСТЕМУ МИНЕРАЛНО ТКИВО ЗУБА–ЗЕМЉИШТЕ И МИНЕРАЛНО ТКИВО ЗУБА –ВОДЕНА СРЕДИНА

РУЖИЦА С. НИКОЛИЋ[1], НАТАША В. РАДОСАВЉЕВИЋ-СТЕВАНОВИЋ[2], ТАТЈАНА Д. АНЂЕЛКОВИЋ[1], МАЈА Н. СТАНКОВИЋ[1] и НЕНАД С. КРСТИЋ[1]

[1]*Департман за хемију, Природно-математички факултет, Универзитет у Нишу, Вишеградска 33, 18000 Ниш и* [2]*Национални криминалистичко-технички центар, Министарство унутрашњих послова Републике Србије, Кнеза Милоша 103, 11000 Београд*

У раду су описане промене у минералном ткиву зуба које је било изложено утицају агенаса природних средина. Такође, минерално ткиво може послужити као потенцијално важан форензички материјал који подлеже постепеним променама под утицајем спољашњих средина. Садржај биометала је испитиван применом ICP-OES методе. На основу квантитативних промена садржаја биометала у ткиву зуба након његовог излагања различитим срединама, уочена је миграција јона биометала, Ca^{2+}, Mg^{2+}, Fe^{2+}, Cu^{2+} и Zn^{2+}, у системима зуб–земљиште и зуб–водена средина. Садржај Ca^{2+} и Mg^{2+} у минералном ткиву је повећан, док је садржај Cu^{2+} смањен. Миграција Fe^{2+} и Zn^{2+} зависи од њиховог садржаја и типа земљишта, и различита је за глинено, кречњачко и градско земљиште. Промене у минералној матрици зуба су детектоване SEM–EDS техником. Интензитет промене садржаја биометала и промене у минералној матрици су потенцијално значајни за форензичка испитивања, јер могу указати на тип средине у којој је испитивани материјал био одложен.

(Примљено 7. фебруара, ревидирано 30. маја, прихваћено 30. маја 2014)

REFERENCES

1. B. Nowak, *Analyst* **120** (1995) 747
2. M. Yoshino, T. Kimijuma, S. Miyasaka, H. Sato, S. Seta, *Forensic Sci. Int.* **49** (1991) 143
3. B. M. Kaličanin, R. S. Nikolić, *Connect. Tissue Res.* **51** (2010) 31
4. W. Castro, J. Hoogewerff, C. Latkoczy, J. R. Almirall, *Forensic Sci. Int.* **195** (2010) 17
5. A. Bigi, G. Cojjazi, S. Panzavolta, A. Ripamonti, N. Roveri, M. Romanello, K. N. Suarez, L. Moro, *J. Inorg. Biochem.* **68** (1997) 45
6. B. Wopenkia, J. D. Pasteris, *Mater. Sci. Eng., C* **25** (2005) 131
7. K. Matsunaga, H. Inamori, H. Murata, *Phys. Rev., B* **78** (2008) 094101
8. S. Sugiyama, H. Matsumoto, H. Hayashi, J. B. Moffat, *Colloids Surfaces, A* **169** (2000) 17
9. S. Sugiyama, T. Ichii, H. Matsumoto, H. Hayashi, *Adv. Environ. Res.* **6** (2002) 285
10. A. Yasukawa, T. Yokoyama, K. Kandory, T. Ishikawa, *Colloids Surfaces, A* **317** (2008) 123
11. B. Kaličanin, R. Nikolić, in *Wide Spectra of Quality Control*, I. Akyar, Ed., InTech, Rijeka, 2011, Ch. 12, p. 211

12. L. D. Sparks, *Environmental Soil Chemistry*, 2nd ed., Academic Press, Elsevier, London, 2003
13. M. Jakovljević, M. Pantović, *Chemistry of Soils and Waters*, Naučna knjiga, Belgrade, 1991 (in Serbian)
14. N. Petraco, T. A. Kubic, *J. Forensic Sci*. **45** (2000) 872
15. N. Petraco, T. A. Cubic, N. D. K. Petraco, *Forensic Sci. Int.* **178** (2008) 23
16. W. C. McCrone, *Microscope* **30** (1982) 17
17. A. Dube, R. Zbytniewski, T. Kowalkowski, E. Curkovska, B. Buszewski, *Pol. J. Environ. Stud.* **10** (2001) 1
18. T. D. Anđelković, J. M. Perović, M. M. Purenović, S. D. Blagojević, R. S. Nikolić, D. Anđelković, A. Lj. Bojić, *Anal. Sci.* **22** (2006) 1553
19. A. A. Vass, W. M. Bass, J. Wolt, J. Ammons, *J. Forensic Sci.* **37** (1992) 1236
20. T. Shinomiya, K. Shinomiya, C. Orimoto, T. Minami, Y. Tohno, M. Yamada, *Forensic Sci. Int.* **98** (1998) 1098
21. D. A. Spears, *Int. J. Coal Geol.* **94** (2012) 22
22. W. F. Outerbridge, *Geol. Soc. Am. Bull.* **108** (1996) 120
23. M. Pansu, J. Gautheyrou, *Handbook of Soil Analysis, Mineralogical, Organic and Inorganic Methods*, Springer, Berlin, 2006
24. S. Cazalbou, D. Eichert, C. Crouet, C. Combes, C. Rey, *C. R. Palevol* **3** (2004) 563
25. R. Nikolić, B. Kaličanin, N. Krstić, *Connect. Tissue Res.* **53** (2012) 229
26. A. F. Wells, *Nature* **157** (1946) 192
27. A. Kabata-Pendias, A. B. Mukherjee, *Trace Elements from Soil to Human*, Springer, Berlin, 2007
28. J. Andjić, *Oral Physiology and Biochemistry Fundamentals*, Naučna knjiga, Belgrade, 1990 (in Serbian)
29. C. Drouet, M. T. Carayon, C. Combes, C. Rey, *Mat. Sci. Eng., C* **28** (2008) 1544
30. P. D. Frazier, *Arch. Oral Biol.* **12** (1967) 25
31. W. H. Arnold, P. Gaengler, *Ann. Anat.* **189** (2007) 183
32. S. Kannan, F. Goetz-Neunhoeffer, J. Neubauer, J. M. F. Ferreira, *J. Am. Ceram. Soc.* **91** (2008) 1.

Journal of the Serbian Chemical Society
JSCS-info@shd.org.rs • www.shd.org.rs/JSCS

J. Serb. Chem. Soc. 79 (11) 1405–1411 (2014) UDC 547.587.51+532.14:544.176:544.18
JSCS–4674 *Original scientific paper*

Density functional theory: ^{1}H- and ^{13}C-NMR spectra of some coumarin derivatives

SELMA ŠPIRTOVIĆ-HALILOVIĆ[1]*, MIRSADA SALIHOVIĆ[2], SNEŽANA TRIFUNOVIĆ[3], SUNČICA ROCA[4], ELMA VELJOVIĆ[1], AMAR OSMANOVIĆ[1], MARIJANA VINKOVIĆ[4] and DAVORKA ZAVRŠNIK[1]

[1]Department of Pharmaceutical Chemistry, Faculty of Pharmacy, University of Sarajevo, Zmaja od Bosne 8, 71000 Sarajevo, Bosnia and Herzegovina, [2]Department of Organic Chemistry, Faculty of Pharmacy, University of Sarajevo, Zmaja od Bosne 8, 71000 Sarajevo, Bosnia and Herzegovina, [3]Faculty of Chemistry, University of Belgrade, Studentski trg 12–16, 11000 Belgrade, Serbia and [4]NMR Centre, Ruđer Bošković Institute, Bijenička cesta 54, 10000 Zagreb, Croatia

(Received 24 February, revised 13 March, accepted 13 March 2014)

Abstract: For some synthesized coumarin derivatives, ^{1}H- and ^{13}C-NMR isotropic chemical shifts and some other molecular properties were calculated using the density functional theory. The calculations yielded reliable results that were in good correlation with experimental data. This is a good basis for collaboration between experimentalists and quantum chemists.

Keywords: NMR spectra; Spartan 10 software; quantum chemistry; chemical shifts.

INTRODUCTION

NMR spectroscopy is one of the key analytical methods in modern organic and synthetic chemistry. It is widely used for structure elucidation and in investigations of the reactivity and reaction mechanisms involving organic molecules. In addition, the irreplaceable role of NMR spectroscopy is commonly recognized in biochemistry, biology and pharmacy for structure determination and in studies of biomolecular dynamics.[1]

After preliminary NMR measurements have been realized, it is then decided whether a direct structure determination using other methods should be performed.[2]

Experimentalists expect additional information from quantum chemical calculations; this is obtained by the calculation of NMR chemical shifts for some structure and comparing them to existing NMR data. If the two sets of NMR data

* Corresponding author. E-mail: selmaspirtovic@yahoo.com
doi: 10.2298/JSC140221023S

correlate well, all the molecular properties that were obtained by the calculations can be assigned to the new compound and accordingly, the experimentalist obtains a detailed description. In this way, the calculation of NMR chemical shifts provides an ideal basis for collaboration between experimentalists and quantum chemists.[2]

In recent years, density functional theory (DFT) calculations have been used extensively for the calculation of a wide variety of molecular properties, such as equilibrium structure, charge distribution, NMR spectra, and to provide reliable results that are in good correlation with experimental data.[3,4]

A series of 3-cinnamoyl-4-hydroxycoumarin derivatives were prepared, as reported in a previous paper.[5] In the present research, ^{13}C-NMR spectra and ^{1}H-NMR spectra of these derivatives were recorded. The Beck three-parameter exchange functional[6] with the Lee, Yang and Parr[7] correlation functional (B3LYP), developed by Truhlar *et al*.[8] were used to perform theoretical calculations on the structure, the ^{1}H- and ^{13}C-NMR spectra and some additional properties of the investigated compounds. Correlation coefficients were used to compare the experimentally observed and theoretically computed shifts for each synthesized compound.

MATERIALS AND METHODS

Investigated compounds

The experimental and theoretical properties of three 3-substituted derivatives of 4-hydroxycoumarin were studied. The structures of the investigated compounds are presented in Fig. 1.

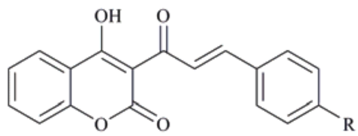

R= Br, OCH_3, Cl

Fig. 1. Structure of the synthesized compounds.

NMR measurements

The one- and two-dimensional homo- and heteronuclear ^{1}H- and ^{13}C-NMR spectra were recorded on a Bruker AV-600 spectrometer, operating at 600.133 MHz for the ^{1}H nucleus and 150.917 MHz for the ^{13}C nucleus. The samples were measured in DMSO-d_6 solutions at 298 and 373 K in 5 mm NMR tubes. The chemical shifts, ppm, are referred to TMS as an internal standard. The following measurement techniques were used: standard ^{1}H-, attached proton test (APT), correlation spectroscopy (COSY), and heteronuclear multiple quantum correlation (HMQC) and heteronuclear multiple bond correlation (HMBC) spectroscopy. The 2D NMR spectra were measured in the pulsed field gradient mode (*z*-gradient).

Theoretical calculations

All the calculations were realized using Spartan 10 software.

The geometries were optimized at the B3LYP level of theory along with standard 1, 2 and 3 G (d) basis set as shown in Fig. 2.

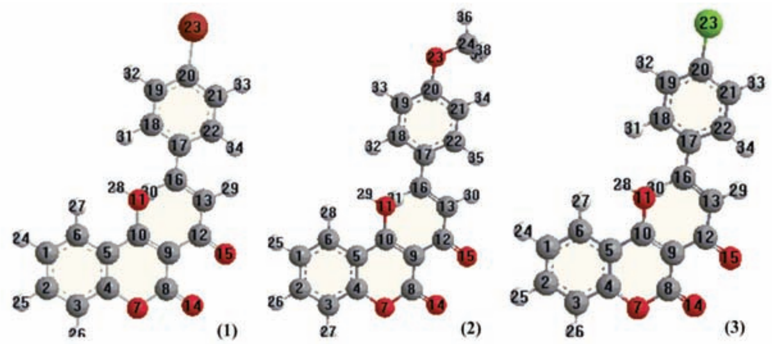

Fig. 2. The optimized geometry of the compounds.

The harmonic vibration frequencies were calculated by this method and the results were compared with the experimental spectra. This method was used for calculating ^{1}H- and ^{13}C- NMR chemical shifts at the B3LYP/6-31*G (d) level for the three synthesized coumarin derivatives.

RESULTS AND DISCUSSION

Spectral data of the prepared compounds are given in the Supplementary material to this paper.

Bond lengths and bond angles

The optimized structural parameters, bond lengths and bond angles for the thermodynamically preferred geometry of compounds **1**–**3** determined at the B3LYP/6-31*G level are presented in Table I in accordance with the atom numbering scheme of the molecules shown in Fig. 2.

From the structural data, it was observed that the various C–C bond distances calculated between the carbon atoms and the C–H and C–O bond length are found to be nearly the same for all three structures. The influence of the substituent on the molecular parameters, particularly on the C–C bond distance of ring carbon atoms, seems to be negligibly small.

The calculated bond angles are very similar to each other in these molecules. An investigation of bond angles O_7–C_8–O_{14}, O_7–C_8–C_9, C_9–C_{12}–C_{15} and C_9–C_{12}–C_{13} showed that these atoms were sp^2 hybridized and that they were completely planar. This data clearly indicates that there is a pronounced tautomer structure between the OH and the C=O group, which is shown in Fig. 3.

Comparison of the experimentally measured and theoretically computed shifts

Chemical shifts calculated using the B3LYP level with the 6-31*G (d) basis sets can be utilized to eliminate the uncertainties in the fundamental assignments of

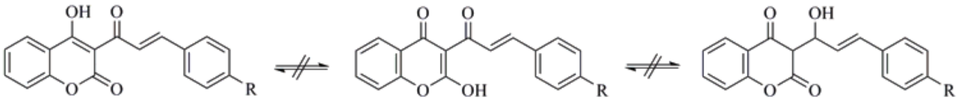

Fig. 3. Tautomerization of the coumarin derivatives.

the spectra. The ^{1}H- and ^{13}C- theoretical and experimental chemical shifts, isotropic shielding tensors and assignments of **1**–**3** are presented in Tables II and III, respectively.

TABLE I. Selected structural parameters calculated for compounds **1–3** by the DFT B3LYP method with 6-31*G basis sets

Bond length, nm				Bond angles, °			
Bond	Compound			Bond	Compound		
	1	**2**	**3**		**1**	**2**	**3**
$O_7–C_4$	0.138	0.136	0.136	$O_7–C_4–C_5$	121.80	121.86	121.40
$C_4–C_5$	0.141	0.141	0.140	$C_4–O_7–C_8$	122.13	122.64	123.48
$C_3–C_4$	0.139	0.140	0.140	$C_4–C_3–H_{26}$	118.88	118.56	119.02
$C_5–C_6$	0.141	0.141	0.141	$C_5–C_6–H_{27}$	120.96	120.57	118.64
$O_7–C_8$	0.140	0.141	0.140	$O_7–C_8–O_{14}$	116.87	116.88	114.96
$C_8–O_{14}$	0.122	0.121	0.121	$O_7–C_8–C_9$	117.00	116.70	117.18
$C_8–C_9$	0.144	0.145	0.146	$C_9–C_{10}–C_5$	120.84	120.89	120.92
$C_9–C_{12}$	0.152	0.152	0.148	$C_9–C_{12}–C_{15}$	119.48	119.79	118.00
$C_{10}–O_{11}$	0.136	0.135	0.131	$C_{10}–O_{11}–H_{28}$	110.19	110.40	104.72
$C_{12}–C_{13}$	0.146	0.147	0.147	$C_9–C_{12}–C_{13}$	119.27	119.79	120.20
$C_{13}–C_{16}$	0.135	0.135	0.135	$C_{13}–C_{16}–H_{29}$	117.63	117.63	118.18
$C_{16}–C_{17}$	0.146	0.146	0.146	$C_{17}–C_{16}–H_{30}$	114.94	114.75	114.90
$C_{17}–C_{18}$	0.141	0.140	0.141	$C_{17}–C_{18}–H_{31}$	119.43	119.03	120.10
$C_{17}–C_{22}$	0.141	0.141	0.141	$C_{17}–C_{22}–H_{34}$	120.18	119.88	119.16
$C_{22}–C_{21}$	0.139	0.138	0.139	$C_{20}–C_{19}–H_{32}$	120.33	121.11	120.26
$C_{20}–C_{19}$	0.140	0.140	0.140	$C_{21}–C_{20}–C_{19}$	121.36	119.56	121.01

TABLE II. The experimental and calculated ^{1}H-isotropic chemical shifts, ppm, with respect to DMSO-d_6 for compounds **1–3**

Assignment	**1**		**2**		**3**	
	Calcd.	Exp.	Calcd.	Exp.	Calcd.	Exp.
H_{24}	7.36	7.40	–	–	7.12	7.40
H_{25}	7.99	7.79	7.07	7.38	7.50	7.78
H_{26}	7.07	7.36	7.40	7.76	7.00	7.35
H_{27}	8.32	8.02	7.10	7.33	8.00	8.01
H_{28}	–	–	7.80	8.00	–	–
H_{29}	8.41	8.22	–	–	8.05	8.21
H_{30}	7.93	7.92	8.30	8.14	7.98	7.93
$H_{31,34}$ for compound **2** H_{31}	7.67	7.65	7.68	7.98	7.46	7.71
$H_{32,33}$ for compound **2** $H_{32,35}$	7.56	7.65	7.70	7.68	7.11	7.49
$H_{33,34}$	–	–	6.80	7.03	–	–
$H_{36,37,38}$	–	–	3.7	3.84	–	–

TABLE III. The experimental and calculated ^{13}C-isotropic chemical shifts, ppm, with respect to DMSO-d_6 for compounds **1–3**

Assignment	**1**		**2**		**3**	
	Calcd.	Exp.	Calcd.	Exp.	Calcd.	Exp.
C_1	129.20	124.00	121.7	123.9	122.68	124.00
C_2	134.21	135.90	131.3	135.7	134.43	135.00
C_3	119.53	116.20	118.0	116.1	116.34	116.20
C_4	158.60	153.80	156.4	153.7	157.17	153.80
C_5	115.70	115.40	115.7	115.7	116.80	115.30
C_6	130.60	124.80	118.4	124.7	127.20	124.80
C_8	167.60	158.90	160.9	159.0	161.80	158.90
C_9	107.60	100.50	112.1	100.0	104.90	100.50
C_{10}	177.20	179.60	179.8	180.1	178.00	179.60
C_{12}	199.30	190.80	192.2	190.4	199.00	190.80
C_{13}	127.40	123.20	125.3	119.3	126.40	123.00
C_{16}	146.00	144.00	146.4	146.2	146.56	143.90
C_{17}	139.10	132.00	127.6	126.7	133.30	132.80
C_{18}, C_{22}	130.20	130.00	130.5	130.5	130.40	129.80
C_{19}, C_{21}	132.00	131.60	114.0	114.4	129.00	128.60
C_{20}	126.50	124.20	160.7	162.0	137.60	135.50
C_{24}	–	–	54.3	55.0	–	–

The aromatic ring carbons gave resonances in the region from 100–150 ppm in the ^{13}C-NMR spectra and from 6.0–8.5 ppm in the ^{1}H-NMR spectra of **1**–**3**.

At the higher temperature, the hydrogen of the hydroxy group on the coumarin moiety (OH at C_4 for compounds **1**–**3**) was not visible in the ^{1}H-NMR spectra (Table II), because of fast hydrogen/deuterium exchange.

It is also interesting to note that this hydrogen was also not visible on the theoretical spectra obtained from the software. The software does not estimate shifts for hydrogen atoms attached to heteroatoms because it also takes into consideration the effects of the solvent.

Due to the influence of the electronegative atom, the values of the chemical shift of C_2, C_{17}, C_{18} and C_{22} in compounds differed significantly in the shift positions in range 126.7–135.9 ppm and the corresponding values of chemical shifts related to C_2, C_{17}, C_{18} and C_{22} were 134.21, 139.10 and 130.20 ppm for compound **1**, 131.30, 127.60 and 130.50 ppm for compound **2** and 134.43, 133.30 and 130.40 ppm for compound **3**, respectively. The higher chemical shift of C_{20} is due to the attachment of the electron withdrawing substituent (Br, OCH_3 or Cl) at C_{20}. The downfield signals at 7.67 and 7.56 ppm for compound **1**, 7.68 and 7.70 ppm for compound **2** and 7.46 and 7.11 ppm for compound **3** are assigned to protons $H_{31,34}$ and $H_{32,33}$ for **1** and **3**, and H_{31} and $H_{32,35}$ for **2**, respectively. This strongly indicates the electron withdrawing nature of Br, methoxy and Cl in their neighborhood. The electron withdrawing methoxy group increased the deshielding of the olefinic proton H_{31} and aromatic protons H_{32}–H_{35} more than Br and Cl.

A downfield shift was observed for C_9 compared with C_8, C_{10} and C_{12} for all three compounds, as given in Table III. This was due to the tautomerization between C_8–C_9–C_{10}–C_{12}.

The calculated and experimental chemical shift values given in Tables II and III show good correspondence. The correlation factors of the linear regression used to compare the experimentally measured and theoretically computed NMR shifts for each compound (**1**–**3**) are presented in Table IV.

TABLE IV. The correlation factors of compared chemical shifts for compounds **1**–**3**

Compound	R^2 for ^{1}H-NMR	R^2 for ^{13}C-NMR
1	0.939	0.979
2	0.984	0.983
3	0.942	0.990

CONCLUSIONS

Selected structural parameters of the optimized geometries of the coumarin compounds were obtained by DFT calculations. The vibration frequencies of the fundamental modes of the compounds was precisely assigned and analyzed, and the theoretical results were compared with the experimental vibrations. The ^{1}H- and ^{13}C-NMR chemical shifts were calculated and the assignments were compared with the experimental values. The conducted research provided complete vibration assignments, structural information and NMR chemical shifts of these compounds.

SUPPLEMENTARY MATERIAL

Spectral data of the prepared compounds are available electronically from http:// //www.shd.org.rs/JSCS/, or from the corresponding author on request.

ИЗВОД

ТЕОРИЈА ФУНКЦИОНАЛА ГУСТИНЕ: ^{1}H- И ^{13}C-NMR СПЕКТРИ ДЕРИВАТА КУМАРИНА

SELMA ŠPIRTOVIĆ-HALILOVIĆ[1], MIRSADA SALIHOVIĆ[1], SNEŽANA TRIFUNOVIĆ[2], SUNČICA ROCA[3], ELMA VELJOVIĆ[1], AMAR OSMANOVIĆ[1], MARIJANA VINKOVIĆ[3] и DAVORKA ZAVRŠNIK[1]

[1]*Department of Pharmaceutical Chemistry, Faculty of Pharmacy, University of Sarajevo, Zmaja od Bosne 8, 71000 Sarajevo, Bosnia and Herzegovina,* [2]*Department of Organic Chemistry, Faculty of Pharmacy, University of Sarajevo, Zmaja od Bosne 8, 71000 Sarajevo, Bosnia and Herzegovina,* [3]*Хемијски факултет, Универзитет у Београду, Студентски трг 12–16, 11000 Београд и* [4]*NMR Centre, Ruđer Bošković Institute, Bijenička cesta 54, 10000 Zagreb, Croatia*

За неке синтетизоване деривате кумарина, ^{1}H- и ^{13}C-NMR изотропна хемијска померања и нека друга молекулска својства израчуната су помоћу теорије функционала густине. Нађено је да су резултати поуздани и у доброј сагласности са експерименталним подацима. Ово представља добру основу за сарадњу између експериментатора и квантних хемичара.

(Примљено 24. фебруара, ревидирано 13. марта, прихваћено 13. марта 2014)

REFERENCES

1. P. A. Belaykov, V. P. Ananikov, *Russ. Chem. Bull.* **60** (2011) 783
2. D. Cremer, L. Olsson, F. Reichel, E. Kraka, *Israel J. Chem*. **33** (1993) 369
3. W. Koch, M. C. Holthausen, *A Chemist's Guide to Density Functional Theory*, Wiley–
–VCH, Weinheim, 2001
4. D. Vikić-Topić, Lj. Pejov, *J. Chem. Inf. Comput. Sci.* **41** (2001) 1478
5. D. Završnik, S. Špirtović-Halilović, Dž. Softić, *Period. Biol.* **113** (2011) 93
6. A. D. Becke, *J. Chem. Phys*. **98** (1993) 5648
7. C. Lee, W. Yang, R. G. Parr, *Phys. Rev*. **37** (1988) 785
8. Y. Zhao, N. Gonzalez-Garcia, D. G. Truhlar, *J. Phys. Chem*. **109** (2005) 2012.

Journal of the Serbian Chemical Society
JSCS@tmf.bg.ac.rs • www.shd.org.rs/JSCS
J. Serb. Chem. Soc. 79 (11) S156–S157 (2014)
Supplementary material

SUPPLEMENTARY MATERIAL TO

Density functional theory: ^{1}H- and ^{13}C-NMR spectra of some coumarin derivatives

SELMA ŠPIRTOVIĆ-HALILOVIĆ[1]*, MIRSADA SALIHOVIĆ[2], SNEŽANA TRIFUNOVIĆ[3], SUNČICA ROCA[4], ELMA VELJOVIĆ[1], AMAR OSMANOVIĆ[1], MARIJANA VINKOVIĆ[4] and DAVORKA ZAVRŠNIK[1]

[1]*Department of Pharmaceutical Chemistry, Faculty of Pharmacy, University of Sarajevo, Zmaja od Bosne 8, 71000 Sarajevo, Bosnia and Herzegovina,* [2]*Department of Organic Chemistry, Faculty of Pharmacy, University of Sarajevo, Zmaja od Bosne 8, 71000 Sarajevo, Bosnia and Herzegovina,* [3]*Faculty of Chemistry, University of Belgrade, Studentski trg 12–16, 11000 Belgrade, Serbia and* [4]*NMR Centre, Ruđer Bošković Institute, Bijenička cesta 54, 10000 Zagreb, Croatia*

J. Serb. Chem. Soc. 79 (11) (2014) 1405–1411

SPECTRAL DATA OF THE PREPARED COMPOUNDS

*(*E*)-3-(3-(4-Bromophenyl)acryloyl)-4-hydroxy-2*H*-chromen-2-one* (**1**). ^{1}H-NMR (600.133 MHz, DMSO-d_6, δ / ppm): 7.40 (1H, *dd*, ^{3}J = 7.57 Hz, H_{24}), 7.79 (1H, *dd*, ^{3}J = 8.40 Hz, ^{4}J = 1.41 Hz, H_{25}), 7.36 (1H, *d*, ^{3}J = 8.40 Hz, H_{26}), 8.02 (1H, *d*, ^{3}J = 7.57 Hz, H_{27}), 8.22 (1H, *d*, ^{3}J = 15.78 Hz, H_{29}), 7.92 (1H, *d*, ^{3}J = 15.78 Hz, H_{30}), 7.65 (2H, *s*, H_{31}, H_{34}), 7.65 (2H, *s*, H_{32}, H_{33}); ^{13}C-NMR (150.917 MHz, DMSO-d_6, δ / ppm): 100.5 (C_9), 115.4 (C_5), 116.2 (C_3), 123.2 (C_{13}), 124.0 (C_1), 124.2 (C_{20}), 124.8 (C_6), 130.0 (C_{18}, C_{22}), 131.6 (C_{19}, C_{21}), 132.0 (C_{17}), 135.9 (C_2), 144.0 (C_{16}), 153.8 (C_4), 158.9 (C_8), 179.6 (C_{10}), 190.8 (C_{12}).

*(*E*)-4-Hydroxy-3-(3-(4-methoxyphenyl)acryloyl)-2*H*-chromen-2-one* (**2**). ^{1}H-NMR (600.133 MHz, DMSO-d_6, δ / ppm): 7.38 (1H, *dd*, ^{3}J = 7.95 Hz, ^{4}J = 0.81 Hz, H_{25}), 7.76 (1H, *ddd*, ^{3}J = 8.43 Hz, ^{3}J = 7.32 Hz, ^{4}J = 1.54 Hz, H_{26}), 7.33 (1H, *d*, ^{3}J = 8.43 Hz, H_{27}), 8.00 (1H, *d*, ^{3}J = 7.95 Hz, H_{28}), 8.14 (1H, *d*, ^{3}J = 15.81 Hz, H_{30}), 7.98 (1H, *d*, ^{3}J = 15.81 Hz, H_{31}), 7.68 (2H, *d*, ^{3}J = 8.70 Hz, H_{32}, H_{35}), 7.03 (2H, *d*, ^{3}J = 8.43 Hz, H_{33}, H_{34}), 3.84 (3H, *s*, H_{36}, H_{37}, H_{38}); ^{13}C-NMR (150.917 MHz, DMSO-d_6, δ / ppm): 55.0 (C_{24}), 100.0 (C_9), 114.4 (C_{19}, C_{21}), 115.7 (C_5), 116.1 (C_3), 119.3 (C_{13}), 123.9 (C_1), 124.7 (C_6), 126.7 (C_{17}), 130.5 (C_{18}, C_{22}), 135.7 (C_2), 146.2 (C_{16}), 153.7 (C_4), 159.0 (C_8), 162.0 (C_{20}), 180.1 (C_{10}), 190.4 (C_{12}).

* Corresponding author. E-mail: selmaspirtovic@yahoo.com

*(*E*)-3-(3-(4-Chlorophenyl)acryloyl)-4-hydroxy-2*H*-chromen-2-one (**3**).* ^{1}H-NMR (600.133 MHz, DMSO-d_6, δ / ppm): 7.40 (1H, *dd*, ^{3}J = 7.86 Hz, ^{4}J = 0.57 Hz, H_{24}), 7.78 (1H, *ddd*, ^{3}J = 8.47 Hz, ^{3}J = 7.41 Hz, ^{4}J = 1.56 Hz, H_{25}), 7.35 (1H, *d*, ^{3}J = 8.47 Hz, H_{26}), 8.01 (1H, *dd*, ^{3}J = 7.86 Hz, ^{4}J = 1.56 Hz, H_{27}), 8.21 (1H, *d*, ^{3}J = 15.81 Hz, H_{29}), 7.93 (1H, *d*, ^{3}J = 15.81 Hz, H_{30}), 7.71 (2H, *d*, ^{3}J = = 8.46 Hz, H_{31}, H_{34}), 7.49 (2H, *d*, ^{3}J = 8.46 Hz, H_{32}, H_{33}); ^{13}C-NMR (150.917 MHz, DMSO-d_6, δ / ppm): 100.5 (C_9), 115.3 (C_5), 116.2 (C_3), 123.0 (C_{13}), 124.0 (C_1), 124.8 (C_6), 128.6 (C_{19}, C_{21}), 129.8 (C_{18}, C_{22}), 132.8 (C_{17}), 135.0 (C_2), 135.5 (C_{20}), 143.9 (C_{16}), 153.8 (C_4), 158.9 (C_8), 179.6 (C_{10}), 190.8 (C_{12}).

Journal of the Serbian Chemical Society
JSCS-info@shd.org.rs • www.shd.org.rs/JSCS
J. Serb. Chem. Soc. *79* (11) 1413–1420 (2014)
JSCS–4675
UDC 546.45'11+546.11'33'34–128.4:
543.422.4:539.196:537.872'12
Original scientific paper

The formation of hydride bonds in cationic complexes of nBeH$_2$···mX with n = 1 or 2, m = 1 or 2 and X = Li$^+$ or Na$^+$

BOAZ G. OLIVEIRA*

Institute of Environmental Sciences and Sustainable Development (ICADS), Federal University of Bahia, 47801-100, Barreiras – BA, Brazil

(Received 24 March, accepted 17 May 2014)

Abstract: The optimized geometries and topological parameters of the $BeH_2\cdots Na^+$, $BeH_2\cdots Li^+$, $2BeH_2\cdots Na^+$, $BeH_2\cdots 2Na^+$, $2BeH_2\cdots Li^+$ and $BeH_2\cdots 2Li^+$ cationic complexes were obtained through BHandHLYP/6-31G(d,p) calculations. Besides the characterization of one or two hydride bonds formed simultaneously on the same hydride center, the analysis of the infrared spectra revealed the existence of red-shifts and blue-shifts on the BeH bonds, the effects of which are not in line with the intermolecular interaction strength determined by means of the supermolecule approach. Quantum theory of atoms in molecules (QTAIM) calculations were developed to measure the charge density concentration on the $H\cdots Na^+$ and $H\cdots Li^+$ hydride bonds. Moreover, the covalent character of these interactions, interpreted based on the ratio between the kinetic and potential electronic energies, was also examined.

Keywords: hydride bonds; infrared; QTAIM.

INTRODUCTION

Since the pioneering insights of Moore, Winmill, Lewis and Pauling, and surely without forgetting the contributions elaborated by Pimentel and McClellan,[1] over all these years, the hydrogen bond was acclaimed as the matriarchal interaction throughout the world of chemistry.[2–7] Some time ago, however, Crabtree *et al*.[8] discovered another type of interaction called the dihydrogen bond in which two hydrogen atoms interact mutually, although one of them is often attributed to a hydride bound with an alkaline earth metal. In some cases, the dihydrogen bond concept is interpreted as an inverse hydrogen bond, although at first sight this interaction might be anomalous once the contact is doubly electropositive.[9,10] In addition, the chemical literature recognizes the existence of this vanguard group of new intermolecular interactions in nature[11] as being formed

* E-mail: boazgaldino@gmail.com
doi: 10.2298/JSC140213054O

by halogen bonds,[12] halogen–hydride bonds,[13] picanogen bonds,[14] or even beryllium bonds.[15]

Nevertheless, one of the most innovative investigations with involvement of alkaline earth metals and hydride compounds is the formation of intermolecular complexes in the configuration of cations,[16] namely as $BeH_2\cdots Li^+$, $BeH_2\cdots Na^+$ and $BeH_2\cdots Mg^{2+}$. A comparison with similar interactions must be worthwhile,[17] although knowledge of the vibration stretch modes followed by their absorption intensities in the infrared spectrum is always treated as one of the states of art upon the formation of intermolecular interactions, such as those in the $C_2H_5^+\cdots\pi$, $BeH_2\cdots HCF_3$ and $LiH\cdots HCF_3$ complexes.[18,19] In this scenario, there are two forms of analyses, namely: the identification of new vibration modes commonly called intermolecular frequency interactions ($H\cdots Na^+$ and $H\cdots Li^+$) or the frequencies of proton donors (Be–H) shifted to upward or downward values followed by decreasing, or sometimes an increasing, absorption intensities.[20–23] Regarding the main purpose of the present study, the formation of cationic systems does not occur in the sense of dihydrogen bonds[7,8] but actually of hydride bonds. Although sodium and lithium cation are not proton donors, they are considered acids whereas beryllium hydride is the basis.

In view of this, this current work was elaborated with the aim of studying the $BeH_2\cdots Na^+$ and $BeH_2\cdots Li^+$ bimolecular complexes, but not only in the light of these bimolecular configurations. Actually, it must be emphasized that trimolecular complexes formed with acids or proton acceptors in excess enlarge the horizons in any intermolecular study once the search for the most stable configuration among three entities is recognized as no easy task.[24] Thus, besides the bimolecular complexes of $BeH_2\cdots Na^+$ and $BeH_2\cdots Li^+$, the trimolecular forms represented by $BeH_2\cdots 2Na^+$ and $2BeH_2\cdots Na^+$, as well as $BeH_2\cdots 2Li^+$ and $2BeH_2\cdots Li^+$, form part of a selected group of systems in which such structures must be governed by the formation of multiple hydride interactions.

COMPUTATIONAL DETAILS

The geometries of the complexes were obtained at the BHandHLYP/6-31G(d,p) level of theory with all calculations executed by the Gaussian 03W[25] program. With the coordinates of the optimized geometries, the QTAIM modeling was developed by the AIMAll 11.05.16 suite of codes.[26]

Additional parameters and the coordinates of the optimized geometries of the $BeH_2\cdots Na^+$, $2BeH_2\cdots Na^+$, $BeH_2\cdots 2Na^+$, $BeH_2\cdots Li^+$, $2BeH_2\cdots Li^+$ and $BeH_2\cdots 2Li^+$ dihydride complexes obtained by calculations at the BhandHLYP/6-31G(d,p) level of theory given in the Supplementary material to this paper.

RESULTS AND DISCUSSION

The optimized geometries of the $BeH_2\cdots Na^+$ (**I**), $2BeH_2\cdots Na^+$ (**II**), $BeH_2\cdots 2Na^+$ (**III**), $BeH_2\cdots Li^+$ (**IV**), $2BeH_2\cdots Li^+$ (**V**) and $BeH_2\cdots 2Li^+$ (**VI**) complexes are grouped and illustrated in Fig. 1, in which the variations on the

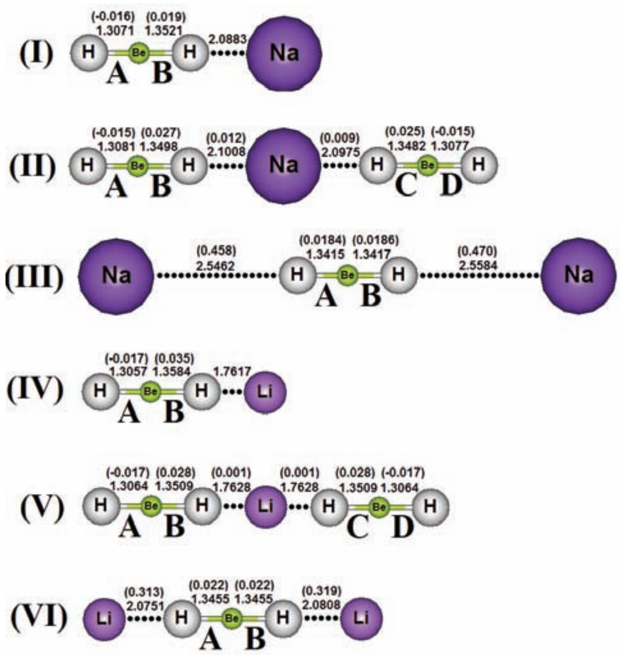

Fig. 1. Optimized geometries of the **I** ($BeH_2\cdots Na^+$), **II** ($BeH_2\cdots Na^+\cdots BeH_2$), **III** ($Na^+\cdots BeH_2\cdots Na^+$), **IV** ($BeH_2\cdots Li^+$), **V** ($BeH_2\cdots Li^+\cdots BeH_2$) and **VI** ($Li^+\cdots BeH_2\cdots Li^+$) complexes at the BHandHLYP/6-31G(d,p) level of theory. The values of the bond length of Be–H (Only in the BeH_2 monomer) is 1.3231 Å computed at the BHandHLYP/6-31G(d,p) level of theory.

bond lengths are also drawn. Due to the absence of experimental data, such as those generated by rotational spectroscopy, the intermolecular distances can be validated by the van der Waals radius of the hydrogen[27] and by the Shanoon crystal radii[28] for the lithium and sodium ions, the values of which are 1.20, 1.24, and 0.92 Å, respectively. By associating these data, the intermolecular distances of 2.44 (radii of H^+ and Na^+) and 2.12 Å (radii of H^+ and Li^+) are referential to examine the single ($H\cdots Na^+$ and $H\cdots Li^+$) and double ($Na^+\cdots H\cdots Na^+$ and $Li^+\cdots H\cdots Li^+$) hydride interactions. By taking into account the values of 2.5462 and 2.5584 Å, it can be seen that only the hydride bonds in **III** are beyond the limit of 2.44 Å. In addition, **VI** is on the intermolecular allowed threshold in that the values of 2.0751 and 2.0808 Å are shorter by 0.0449 and 0.0392 Å in comparison with the referential value of 2.12 Å. In other words, the formation of hydride bonds is valid in **III**. The hydride bond distances of the complexes are shorter than those formed by potassium and calcium when in interaction with beryllium hydride.[29]

On complexation, the structure of the BeH_2 hydride changes distinctly. For this reason, four moieties were assigned, namely A, B, C and D (see Fig. 1). The bond lengths in A and D are reduced regardless of whether a complex is bimolecular (with one BeH_2) or trimolecular (with two BeH_2). On the other hand, the bond length increases not only of B and C, but also of A and B in the complexes **III** and **VI**. Unlike all that has often been documented in the chemical literature that shorter distances followed by high interactions strengths often leads to an enlargement in the bond lengths of proton donors,[30] this systematic tendency is surely not valid here. The determination of the variations in the bond lengths was performed based on analyses of infrared spectra and the obtained values for the vibration modes are listed in Table I.

TABLE I. Values of the main infrared modes (stretch frequency and absorption intensity) of the **I–VI** dihydride-bonded complexes obtained from BHandHLYP/6-31G(d,p) calculations; values at the BHandHLYP/6-31G(d,p) level of theory of the stretch frequencies and absorption intensities of the Be–H oscillator are given in parenthesis; Values at the BHandHLYP/6-31G(d,p) level of theory of υ and I of the Be–H bond (BeH_2 monomer) are 2318.8 cm^{-1} and 240.5 km mol^{-1}, respectively

Mode	Dihydride complex					
	I	**II**	**III**	**IV**	**V**	**VI**
$\nu_{H\cdots 0X1}$ / cm^{-1}	249.0	198.5	48.0	385.8	234.8	159.3
$I_{H\cdots X}$ / km mol^{-1}	10.8	0.002	0.2	61.2	0.0	1.1
$\Delta\nu_{Be–H}$A / cm^{-1}	+25.3	+21.2	–117.2	+36.2	+37.1	–282.9
	(2344.1)	(2340.0)	(2021.1)	(2120.6)	(2355.9)	(2035.9)
$I_{Be–H,c}A/I_{Be–H,m}A$	1.10	2.14	0.0	1.19	2.79	0.0
	(265.2)	(516.0)	(0.03)	(334.5)	(671.6)	(0.01)
$\Delta\nu_{Be–H}$B / cm^{-1}	–226.9	–224.6	–117.2	–198.2	–185.1	–282.9
	(2091.9)	(2094.2)	(2021.1)	(2355.0)	(2133.7)	(2035.9)
$I_{Be–H,c}B/I_{Be–H,m}B$	1.10	1.97	0.0	1.39	2.53	0.0
	(265.6)	(474.6)	(0.03)	(287.2)	(610.1)	(0.01)
$\Delta\nu_{Be–H}$C / cm^{-1}	–	–212.3	–	–	–172.7	–
	–	(2106.5)	–	–	(2146.1)	–
$I_{Be–H,c}C/ I_{Be–H,m}C$	–	0.16	–	–	0.0	–
	–	(38.3)	–	–	(0.0)	–
$\Delta\nu_{Be–H}$D / cm^{-1}	–	+27.4	–	–	+44.9	–
	–	(2346.2)	–	–	(2363.7)	–
$I_{Be–H,c}D/I_{Be–H,m}D$	–	0.24	–	–	0.0	–
	–	(58.3)	–	–	(0.0)	–

The values of the new vibrational modes or hydride bond stretch frequencies are widely varied, *e.g.*, the results of 48.0 and 385.8 $cm^{–1}$ for $\nu_{H\cdots X}$ as well as 0.2 and 61.2 km $mol^{–1}$ for $I_{H\cdots X}$ in **III** and **IV**, respectively. Moreover, if the intermolecular geometry is stabilized either into a global or local minimum in the potential energy surface, the proton donor bond may be strengthened because its frequency is shifted to upward values, and in this case, the blue-shift effect is manifested. No matter if the shift is from red or blue nature,[31] these phenomena validate the bond strength profile of the proton donors. Currently, the interpretations of red shifts and blue shifts in hydrogen-bonded complexes are made if the hyperconjugation or hybridization effects are taken into account,[32] when, under these circumstances, the intermolecular system can be strong or weakly bound. Thus, in agreement with the structural analysis, the reductions in the bond lengths in the subparts of A and D were evidenced by the frequencies shifted to blue, the values of which for $\Delta\nu_{Be–H,A}$ vary from +21.2 to +37.1 cm^{-1}. Moreover, the red shifts of –117.2 and –282.9 cm^{-1} are also in excellent agreement with the increases in the Be–H bond lengths in **III** and **VI**. Regarding B and C, the red shifts are the only infrared effects manifested on their oscillators whereas in D of **II** and **V**, only blue ones are characterized. Concerning the absorption intensities, the values listed in Table I indicate unsystematic profiles. In order to understand better the synergism between the structural changes and frequency shifts in Be–H, the linear relationship between the values of the variations of the bond lengths and red shifts and blue shifts is plotted in Fig. 2.

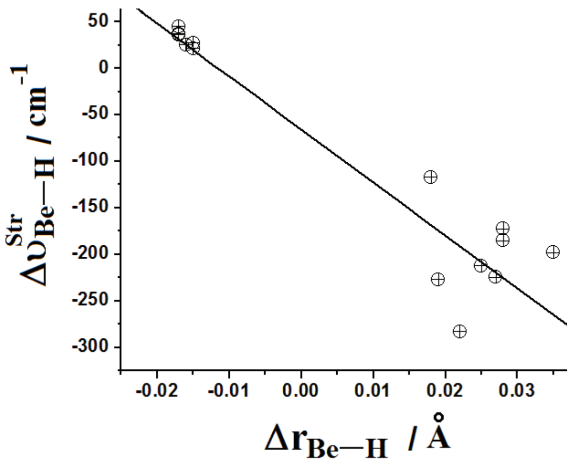

Fig. 2. Relationship between the vibrational displacement in the stretch frequencies (red- or blue-shift) *vs*. the variations on the bond length of the Be–H oscillator at the BHandHLYP/6-31G(d,p) level of theory.

The values of the hydride bond energies[33] with zero-point vibrational energy corrections (*ΔZPV*) and amendments for basis set superposition errors (*BSSE*), as well as those without adjustments are presented in Table II. The shortest bound intermolecular systems, **IV** and **V**, are those whose values of ΔE^C are the highest. On the other hand, the longest bound systems, in this case **III** and **VI**, have values of their interaction energies that are unreal. Not simply by the fact of extremely lengthy distances, but the *BSSE* amounts outweigh these intermolecular energies. These are intermolecular systems the stabilization of which is prejudiced by whether more than two interactions are formed. Although the enhancements on the dipole moment justify the absorption intensities of the hydride bonds of complexes **I** and **IV**, the difference between the ΔE^C values of –51.80 and –55.66 kJ mol^{-1} cannot be appraised by this argument. In comparison, the values of –51.80 and –75.61 kJ mol^{-1} are quite close to –49.12 and –76.44 kJ mol^{-1}, which were obtained by Grabowski *et al.*[16] through MP2/aug-cc-pVQZ calculations. At the MP2(full)/6-31G(3df,3pd) theoretical level, a result of –51.04 kJ mol^{-1} was obtained,[32] which is less stable by 0.76 kJ mol^{-1} in comparison with the value of –51.80 kJ mol^{-1} computed by BHandHLYP/6-31G(d,p). As can be seen, this functional theoretical level seems useful to predict the hydride bond strength or maybe any other intermolecular interaction of interest.

TABLE II. Values of the electronic parameters (dihydride bond energy with *ZPE* and *BSSE* corrections) of the **I–VI** dihydride-bonded complexes obtained from BHandHLYP/6-31G(d,p) calculations

Mode	Dihydride complex					
	I	**II**	**III**	**IV**	**V**	**VI**
ΔE / kJ mol^{-1}	–57.27	–111.11	109.63	–81.73	–156.63	98.01
ΔZPE / kJ mol^{-1}	3.40	7.33	3.48	4.39	10.07	5.85
$BSSE$ / kJ mol^{-1}	2.07	3.83	943.6	1.73	3.52	985.8
ΔE^C / kJ mol^{-1}	–51.80	–49.97	$>10^3$	–75.61	–55.66	$>10^3$
$\Delta\mu$ / Debye*	4.22	–0.0016	0.018	8.03	–0.0038	0.019
$\rho_{H\cdots X}$ / e a_o^{-3}	0.0158	0.0154 (0.0155)^a	0.0068 (0.0067)^a	0.019	0.0189 (0.0189)^a	0.0097 (0.0096)^b
$\nabla^2\rho_{H\cdots X}$ / a_o^{-5}	0.0772	0.0738 (0.0744)^a	0.0189 (0.0182)^a	0.0983	0.0975 (0.0975)^a	0.0368 (0.0361)^b
$G_{H\cdots X}$ / eu	0.0162	0.0155 (0.0157)^a	0.0041 (0.0039)^a	0.0204	0.0203 (0.0203)^a	0.0075 (0.0074)^b
$U_{H\cdots X}$ / eu	–0.0131	–0.0126 (–0.0127)^a	–0.0035 (–0.0033)^a	–0.0163	–0.0163 (–0.0163)^a	–0.0059 (–0.0058)^b
$H_{H\cdots X}$ / eu	0.0031	0.0029 (0.003)^a	0.0006 (0.0006)^a	0.0041	0.004 (–0.004)^a	0.0016 (0.0016)^b
$-G_{H\cdots X}/U_{H\cdots X}$	1.23	1.23 (1.23)^a	1.17 (1.18)^a	1.25	1.24 (1.24)^a	1.27 (1.27)^b

[a]Values related to the Na···H–Be–H(C/D) moiety; [b]values related to the Li···H–Be–H···Li(A/B) moiety

Nevertheless, the interaction strength is one of the main goals in intermolecular studies. Despite the quantification of the interaction strength by means of the supermolecule approach, the prediction of this parameter can be realized by analysis of topological descriptors derived from the quantum theory of atoms in molecules (QTAIM),[34] such as electronic density (ρ), Laplacian ($\nabla^2\rho$), electronic kinetic energy (G) and electronic potential energy (U), and through of them, the interaction strength can be unveiled. The values of the QTAIM parameters are also enumerated in Table I. In addition to the low electronic density, all hydride bonds were identified as closed-interactions due to the positive values of the Laplacian.[35] The QTAIM integrations were able to locate distinct electronic density

* 1 C m = 3×10^{29} Debye

fluxes between $_{Be–H}B\cdots Na^+$ and $Na^+\cdots C_{H–Be}$ of **II**, $Na^+\cdots A_{H–Be}$ and $_{Be–H}B\cdots Na^+$ of **III**, $_{Be–H}B\cdots Li^+$ and $Li^+\cdots C_{H–Be}$ of **V**, and $Li^+\cdots A_{H–Be}$ and $_{Be–H}B\cdots Li^+$ of **VI**.

In advance, the electronic density energy or the sum of the kinetic and potential energy operators is always positive and thereby yields a low intermolecular electronic density flux, *i.e.*, *U* is outweighed by *G*. In terms of interaction strength, the rationalization between *G* and *U* would indicate a covalent character or at least partial if $-G/U < 1$,[36] or even total if $-G/U < 0.5$. Unfortunately, the values depicted in Table I suggest that all **I**–**VI** complexes are non-covalent ones.

CONCLUSIONS

A series of intermolecular complexes formed by hydride bonds were examined herein. Although the structural parameters were in good agreement with the infrared modes, the calculations of the intermolecular energies revealed unusual values, some of which were completely unacceptable. The variation of the dipole moment also fails into rationalize the interaction strength. Finally, the QTAIM method valued the existence of the hydride bonds, and albeit the intermolecular distance was very short, a covalent profile was not found, such as is well-known in other studies.[16,32]

SUPPLEMENTARY MATERIAL

Additional parameters and the coordinates of the optimized geometries of the $BeH_2\cdots Na^+$, $2BeH_2\cdots Na^+$, $BeH_2\cdots 2Na^+$, $BeH_2\cdots Li^+$, $2BeH_2\cdots Li^+$ and $BeH_2\cdots 2Li^+$ dihydride complexes obtained by calculations at the BhandHLYP/6-31G(d,p) level of theory are available electronically from http://www.shd.org.rs/JSCS/, or from the corresponding author on request.

ИЗВОД

ФОРМИРАЊЕ ХИДРИДНИХ ВЕЗА У КАТЈОНСКИМ КОМПЛЕКСИМА nBeH$_2\cdots m$X СА n = 1 ИЛИ 2, m = 1 ИЛИ 2 И X = Li$^+$ ИЛИ Na$^+$

BOAZ G. OLIVEIRA

Institute of Environmental Sciences and Sustainable Development (ICADS), Federal University of Bahia, 47801-100, Barreiras – BA, Brazil

Прорачунима методама BH и HLYP/6-31G(d,p) одређене су оптимизоване геометрије и тополошки параметри за катјонске комплексе $BeH_2\cdots Na^+$, $BeH_2\cdots Li^+$, $2BeH_2\cdots Na^+$, $BeH_2\cdots 2Na^+$, $2BeH_2\cdots Li^+$ и $BeH_2\cdots 2Li^+$. Једна или две хидридне везе су се симултано градиле на истом хидридном центру. Анализа инфрацрвених спектара указује на постојање црвеног и плавог помака код двају BJ веза, што није у складу с предвиђањима на основу модела супермолекула. Помоћу QTAIM прорачуна процењена је густина наелектрисања на $H\cdots Na^+$ и $H\cdots Li^+$ хидридним везама. Разматрана је интерпретација ковалентног карактера ових интеракција на основу односа кинетичке и потенцијалне енергије.

(Примљено 24. марта, прихваћено 17. маја 2014)

REFERENCES

1. P. Goymer, *Nature Chem*. **4** (2012) 863
2. G. R. Desiraju, *Angew. Chem. Int. Ed*. **50** (2011) 52
3. B. G. Oliveira, R. C. M. U. Araújo, A. B. Carvalho, M. N. Ramos, *Spectrochim. Acta, A* **75** (2010) 563
4. B. G. Oliveira, R. C. M. U. Araújo, J. J. Silva, M. N. Ramos, *Struct. Chem*. **21** (2010) 221
5. B. G. Oliveira, R. C. M. U. Araújo, M. N. Ramos, *Struct. Chem*. **19** (2008) 185
6. B. G. Oliveira, R. C. M. U. Araújo, M. N. Ramos, *Struct. Chem.* **19** (2008) 665
7. B. G. Oliveira, *Comput. Theor. Chem.* **998** (2012) 173
8. T. Richardson, S. de Gala, R. H. Crabtree, P. E. M. Siegbahn, *J. Am. Chem. Soc*. **117** (1995) 12875
9. I. Rozas, I. Alkorta, J. Elguero, *J. Phys. Chem. A* **101** (1997) 4236
10. A. Ilnicka, J. Sadlej, *Struct. Chem*. **23** (2012) 1323
11. B. G. Oliveira, *Phys. Chem. Phys. Chem*. **15** (2013) 37
12. B. G. Oliveira, R. C. M. U. Araújo, E. S. Leite, M. N. Ramos, *Int. J. Quantum Chem*. **111** (2011) 111
13. M. Jabłoński, M. Palusiak, *J. Phys. Chem., A* **116** (2012) 2322
14. S. Scheiner, *Theor. Chem. Acc*. **46** (2013) 280
15. M. Yáñez, P. Sanz, O. Mó, I. Alkorta, J. Elguero, *J. Chem. Theory Comput*. **5** (2009) 2763
16. S. J. Grabowski, W. A. Sokalski, J. Leszczynski, *Chem. Phys. Lett*. **422** (2006) 334
17. M. Hô, R. Hernández-Lamoneda, *Int. J. Quantum Chem*. **112** (2012) 3630
18. B. G. Oliveira, M. L. A. A. Vasconcellos, R. R. Olinda, E. B. A. Filho, *Struct. Chem.* **20** (2009) 81
19. B. G. Oliveira, M. N. Ramos, *Int. J. Quantum Chem.* **110** (2010) 307
20. B. G. Oliveira, R. C. M. U. Araújo, F. S. Pereira, E. F. Lima, W. L. V. Silva, A. B. Carvalho, M. N. Ramos, *Quim. Nova* **31** (2008) 1673
21. B. G. Oliveira, R. C. M. U. Araújo, M. N. Ramos, *J. Mol. Struct. (THEOCHEM)* **908** (2009) 79
22. B. G. Oliveira, R. C. M. U. Araújo, A. B. Carvalho, M. N. Ramos, *Struct. Chem.* **20** (2009) 663
23. B. G. Oliveira, R. C. M. U. Araújo, A. B. Carvalho, M. N. Ramos, *Quim. Nova* **30** (2007) 1167
24. B. G. Oliveira, R. C. M. U. Araújo, *J. Mol. Model.* **18** (2012) 2845
25. Gaussian 03, Revision B.04,Gaussian, Inc., Pittsburgh, PA, 2003
26. T. A. Keith, AIMAll Version 11.05.16, 2011
27. A. Bondi, *J. Phys. Chem.* **68** (1964) 441
28. R. D. Shannon, *Acta Crystall., A* **32** (1976) 751
29. B. G. Oliveira, R. C. M. U. Araújo, *Open J. Phys. Chem.* **1** (2010) 131
30. B. G. Oliveira, L. F. C. C. Leite, *J. Mol. Struct. (THEOCHEM)* **915** (2009) 38
31. B. G. Oliveira, M. C. A. Lima, I. R. Pitta, S. L. Galdino, M. Z. Hernandes, *J. Mol. Model.* **16** (2010) 119
32. S. J. Grabowski, *J. Mol. Model.* **19** (2013) 4713
33. F. B. van Duijneveldt, J. G. C. M. Duijneveldt-van de Rijdt, J. H. van Lenthe, *Chem. Rev.* **94** (1994) 1873
34. R. F. W. Bader, *Chem. Rev.* **91** (1991) 893
35. B. G. Oliveira, M. L. A. A. Vasconcellos, *Inorg. Chem. Commun.* **12** (2009) 1142
36. S. J. Grabowski, *Chem. Rev.* **111** (2011) 2597.

J. Serb. Chem. Soc. 79 (11) S158–S159 (2014)

Journal of the Serbian Chemical Society

JSCS@tmf.bg.ac.rs • www.shd.org.rs/JSCS

Supplementary material

SUPPLEMENTARY MATERIAL TO

The formation of hydride bonds in cationic complexes of $nBeH_2\cdots mX$ with n = 1 or 2, m = 1 or 2 and X = Li^+ or Na^+

BOAZ G. OLIVEIRA*

Institute of Environmental Sciences and Sustainable Development (ICADS), Federal University of Bahia, 47801-100, Barreiras – BA, Brazil

J. Serb. Chem. Soc. 79 (11) (2014) 1413–1420

ADDITIONAL PARAMETERS AN D THE COORDINATES OF THE OPTIMIZED GEOMETRIES OF THE $BEH_2\cdots NA^+$, $2BEH_2\cdots NA^+$, $BEH_2\cdots 2NA^+$, $BEH_2\cdots LI^+$, $2BEH_2\cdots LI^+$ AND $BEH_2\cdots 2LI^+$ DIHYDRIDE COMPLEXES OBTAINED BY CALCULATIONS AT THE BHANDHLYP/6-31G(D,P) LEVEL OF THEORY

I		**II**		**III**	
Be	0.000000 0.000000 –2.228812	Be	0.000000 0.000000 3.446979	Be	0.000000 0.023301 0.000000
H	0.000000 0.000000 –3.535955	H	0.000000 0.000000 4.754689	H	1.312989 –0.253010 0.000000
H	0.000000 0.000000 –0.876694	H	0.000000 0.000000 2.098770	H	–1.316371 0.282492 0.000000
Na	0.000000 0.000000 1.21162	Na	0.000000 0.000000 0.001256	Na	–3.809335 0.800534 0.000000
		Be	0.000000 0.000000 –3.449485	Na	3.809642 –0.811688 0.000000
		H	0.000000 0.000000 –4.757655		
		H	0.000000 0.000000 –2.099599		
Energy = –177.9874194 Hartree		Energy = –193.9091853 Hartree		Energy = –339.98752 Hartree	
ZPE = 38849.9 J mol^{-1}		ZPE = 78231.9 J mol^{-1}		ZPE = 38931.2 J mol^{-1}	
Dipole = 4.2231 Debye**		Dipole = 0.0022 Debye		Dipole = 0.0197 Debye	
Imaginary frequency = 0		Imaginary frequency = 0		Imaginary frequency = 1	

* E-mail: boazgaldino@gmail.com

** 1 C m = 3×10^{29} Debye

IV				V				VI			
Be	0.000000	0.000000	1.045934	Be	0.000000	0.000000	3.113729	Be	0.000000	0.002194	0.000000
H	0.000000	0.000000	2.351700	H	0.000000	0.000000	4.420169	H	1.021994	–0.873035	0.000000
H	0.000000	0.000000	–0.312529	H	0.000000	0.000000	1.762821	H	–1.022169	0.877178	0.000000
Li	0.000000	0.000000	–2.074303	Be	0.000000	0.000000	–3.113728	Li	–2.602736	2.221883	0.000000
				H	0.000000	0.000000	–4.420169	Li	2.602794	–2.226190	0.000000
				H	0.000000	0.000000	–1.762820				
				Li	0.000000	0.000000	–0.000001				
Energy = –23.2126542 Hartree				Energy = –39.1426661 Hartree				Energy = –30.4242061 Hartree			
ZPE = 39836.4 J mol-1				ZPE = 80967.2 J mol-1				ZPE = 41292.0 J mol-1			
Dipole = 8.0368 Debye				Dipole = 0.0000 Debye				Dipole = 0.0211 Debye			
Imaginary frequency = 0				Imaginary frequency = 0				Imaginary frequency = 0			

Journal of the Serbian Chemical Society
JSCS-info@shd.org.rs • www.shd.org.rs/JSCS

J. Serb. Chem. Soc. 79 (11) 1421–1432 (2014)
JSCS–4676

UDC 547.536.21–36+547.458.81+
546.33'226:543.555:541.64
Original scientific paper

A conductometric investigation of hydroxypropylmethyl cellulose/sodium dodecyl sulfate/nonionic surfactant systems

LIDIJA B. PETROVIĆ*#, VERICA J. SOVILJ, JADRANKA L. MILANOVIĆ# and JAROSLAV M. KATONA#

Faculty of Technology, University of Novi Sad, Bul. cara Lazara 1, 21000 Novi Sad, Serbia

(Received 21 March, revised 30 May, accepted 2 June 2014)

Abstract: Surfactant mixtures are very often used in various cosmetic and pharmaceutical products because they commonly act in synergism and provide more favorable properties than a single surfactant. Simultaneously, the presence of polymers in mixtures of surfactants may lead to molecular interactions and thereby affecting product stability and activity. For these reasons, it is very important to determine the influence of surfactant interactions on micellization and mixed micellization, as well as polymer–surfactant mixed micelles interactions. In this study, the self-aggregation of nonionic surfactants, polysorbate 20 (Tween 20), polyoxyethylene octylphenyl ether (Triton X100) and polyoxyethylene–polyoxypropylene block copolymer (Pluronic F68), with an ionic surfactant, sodium dodecyl sulfate, was examined in aqueous solution at 40 °C using a conductometric titration method. It was found that the concentration region for mixed micelle formation depends on the characteristics of the nonionic surfactant and its concentration. The formation of mixed micelles of surfactants in the presence of a nonionic polymer, hydroxypropylmethyl cellulose, and their binding to the hydrophobic sites of the polymer were also investigated. An analysis of obtained results indicated to different kinds of interactions in the investigated systems, which are crucial for their application.

Keywords: nonionic surfactants; sodium dodecyl sulfate; mixed micelles; surfactant/polymer interactions.

INTRODUCTION

Surfactant mixtures are commonly used in surfactant-based formulations because they often behave in synergism and provide more favorable properties than single-surfactant systems. A significant amount of work has been devoted to the investigation of the physicochemical properties of mixed micelles containing two or more surfactants of variable structures in solutions. Their extensive use

* Corresponding author. E-mail: lidijap@uns.ac.rs
# Serbian Chemical Society member.
doi: 10.2298/JSC140321059P

has currently been promoted by their much more favorable practical applications than single compound system.[1–3] In this respect, industrial, pharmaceutical, chemical, and biochemical fields are of great importance. Thus, in pharmaceutical products, mixed micelles were found to enhance the absorption of various drugs in the human body.[4–6] Due to their synergistic behavior at the critical micellar concentration (*CMC*), cosmetic industries employ mixed micelles in low concentrations in order to avoid potential skin irritation.[7,8] According to the great application potentials and economical consideration of mixed micelles, it is necessary to search for the most suitable surfactant combinations with desired properties, such as surface activity and solubility.

From a theoretical point of view, mixed surfactant systems have been the subject of a great number of investigations and have attracted much interest in recent years. In an aqueous medium, pure and mixed surfactants can form micelles after reaching the *CMC*, which can be assessed by various methods to understand the self-organizing behavior of surfactants. Similar to the behavior of the individual surfactants on self-aggregation, mixed system undergo significant changes in their physicochemical properties that can be monitored using suitable experimental methods, such as conductometry, tensiometry, calorimetry, fluorometry, NMR spectroscopy,[9–15] *etc*.

In mixed micellar systems of ionic, nonionic, and zwitterionic surfactants, three types of interactions may occur: favorable (ionic–nonionic, ionic–zwitterionic and cationic–anionic), unfavorable and ideal mixing (nonionic mixtures). Ionic–nonionic surfactant mixtures exhibit highly non-ideal behavior on mixing and can change the interfacial and colloidal properties of the system. A mixture of two different surfactants can be characterized by the presence of two kinds of micelles, each essentially containing a pure surfactant, or mixed micelles formed by both surfactants. Compared to pure surfactant micelles, the formation of mixed micelles is accompanied by a series of more complex thermodynamic and structural changes.[9–12]

Polymers and surfactants are very commonly included in many industrial products, and their mixtures can exhibit molecular interactions affecting the properties of the product. In this respect, the mechanism of interaction between a water-soluble polymer, hydroxypropylmethyl cellulose (HPMC), and an anionic surfactant, sodium dodecyl sulfate (SDS), was investigated in detail.[16–18] The presence of a nonionic surfactant in an aqueous HPMC/SDS solution makes the system more complex, considering that various interactions between three different species could occur.

In the present study, conductometric measurements were performed on mixed anionic–nonionic micellar solutions. The anionic surfactant was sodium dodecyl sulfate, SDS, and the nonionic surfactants were Tween 20, Triton X100 and Pluronic F68 (polysorbate 20, polyoxyethylene octylphenyl ether and polyoxyethylene–polyoxypropylene block copolymer, respectively). The micellization behavior of Tween 20/SDS mixtures was previously studied by Gosh and Moulic[12] at 20 °C and by Munoz *et al*. at 25 °C.[14] With regard to the Triton X100/SDS and Pluronic F68/SDS binary mixtures, to the best of our knowledge, no previous information has been provided in the literature concerning these binary systems. It is also interesting to note that no studies have been reported regarding the interaction and micellization behavior of nonionic surfactant/SDS systems in the presence of a nonionic polymer, HPMC.

EXPERIMENTAL

Chemicals

SDS, purity >99 %, was obtained from Merck, Germany. Tween 20 (M = 1200 g mol^{-1}), Triton X100 (M = 625 g mol^{-1}) and Pluronic F68, [$EO_{75}PO_{30}EO_{75}$] (M = 8400 g mol^{-1}), were obtained from Sigma, USA. The *CMC* values of Tween 20, Triton X100 and Pluronic F68, determined at 40 °C by tensiometry, were 0.0915, 0.786 and 0.202 mmol dm^{-3}, respectively.

Pharmaceutical grade HPMC, trade name Methocel K100M, was obtained as a gift from Colorcon Ltd., UK. The viscosity average molecular mass, $\bar{M}_v$, measured at 20 °C was 155.000 g mol^{-1}.[20] and the critical overlap concentration, c^*, determined at 40 °C was 6.25 10^{-3} mmol dm^{-3}.

All samples were used without any further purification.

Preparations of the binary mixtures

Stock solutions of surfactants: 0.277 mmol dm^{-3} SDS, 1.67 mmol dm^{-3} Tween 20, 6.4 mmol dm^{-3} Triton X100 and 2.38 mmol dm^{-3} Pluronic F68 were prepared by dissolving in water with gentle stirring. Stock solution of 0.13 mmol dm^{-3} HPMC was prepared by dispersing the required mass in water at 80 °C under gentle stirring.[17] All solutions were prepared in double distilled water having a specific conductance 2–4 μS cm^{-1} at 40 °C.

Binary mixtures of nonionic surfactants and SDS were prepared by mixing the required volumes of stock solutions. Before further use, the mixtures were left for 24 h at room temperature.

Binary mixtures of HPMC, below (3.22 10^{-3} mmol dm^{-3}) and above (19.35 10^{-3} mmol dm^{-3}) critical overlap concentration, c^*, and the nonionic surfactants were prepared by mixing the required masses of HPMC stock solution with suitably diluted stock solutions of surfactants. Before further use, the mixtures were left for 24 h at room temperature.

Conductometry

Conductivity measurements were realized at 40 °C, in a jacked beaker, by adding 0.2 cm^3 portions of titrant to 50 cm^3 of analyte. After the addition of each portion, the solution was stirred until a steady conductance value was achieved. Specific conductance was measured using conductivity meter INOLAB Level 1, WTW, Germany and conductivity cell with the cell constant of 1.00 cm^{-1}.

The temperature was maintained using a Phoenix II C25P thermostat, Thermo HAAKE, Germany.

RESULTS AND DISCUSSION

Nonionic surfactant/SDS interaction

Conductometric titration is one of the most often used techniques to determine the critical micelle concentration (*CMC*) of ionic surfactants, as well as to examine their interaction with nonionic surfactants and the formation of mixed micelles in dilute solutions.[9–12] The results of the determination of the critical micelle concentration of SDS and an investigation of the nonionic surfactant/SDS interactions are presented in Fig. 1.

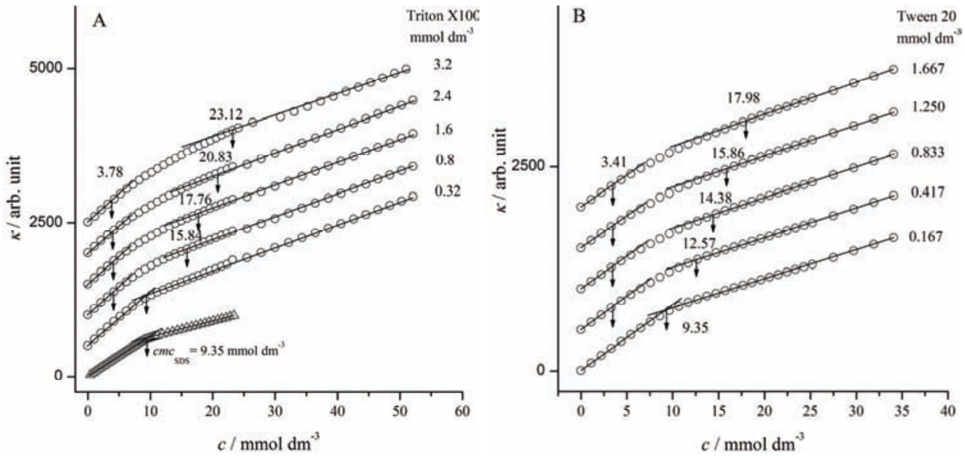

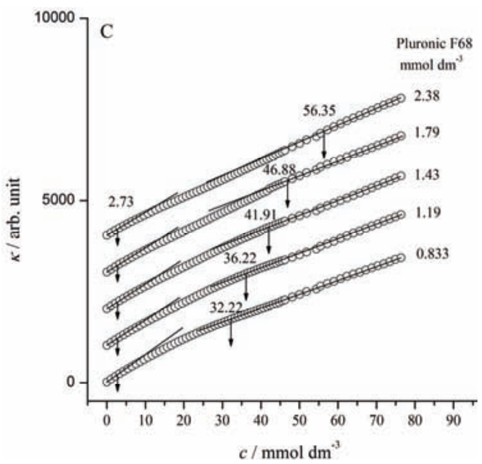

Fig. 1. Plots of conductivity (relative scale units) *vs*. SDS concentration for various concentrations of Triton X100 (A), Tween 20 (B) and Pluronic F68 (C) in water solution.

The addition of SDS to the water caused a linear increase in the specific conductance up to the surfactant concentration at which micelle formation began, *i.e.*, up to the *CMC*. After the *CMC* was attained, the conductance further increased linearly, but with a lower slope than before the *CMC* and the break in the conductance–concentration titration curve gives the *CMC* of the surfactant. For

SDS, the *CMC* determined by conductometric titration at 40 °C was 9.35 mmol dm^{-3} (Fig. 1A). In the presence of the nonionic surfactant, the relationship between the conductance and the SDS concentration (Fig. 1), as with most ionic/ /nonionic surfactant mixtures, showed two break points. The first was when the formation of mixed associates, *i.e.*, micelles, began and the second was when the formation of mixed micelles ended. Between these break points, there was a region of nonlinearity indicating the incorporation of SDS molecules into the mixed micelles and their structural changes with increasing SDS concentration, *i.e.*, mixed micellization. For solutions of Triton X100 and Tween 20, at concentrations of 0.32 and 0.167 mmol dm^{-3}, respectively, the conductometric curves had only one break point that corresponded to the *CMC* of SDS. This indicated that at concentration of the nonionic surfactants close to their *CMC* value, due to the weak interaction with the SDS molecules, there was no mixed micelle formation.

At concentrations of nonionic surfactants well above the *CMC*, the formation of the mixed micelles started at SDS concentration lower than the *CMC* (9.35 mmol dm^{-3}) and it depended on the characteristics of the nonionic surfactant (Fig. 1A–C). Simultaneously, the end of process depended not only on surfactant type, but on its concentration as well. After reaching the second break point, the mixed micellization was finished, the conductivity increased linearly again, but with a higher slope than for SDS without nonionic surfactant after reaching the *CMC*. Namely, further addition of SDS caused only the formation of free SDS micelles that, together with the charged mixed micelles, contributed to the specific conductance.[19]

The amount of SDS molecules that were incorporated in the mixed associates at the end of micellization is presented in Fig. 2.

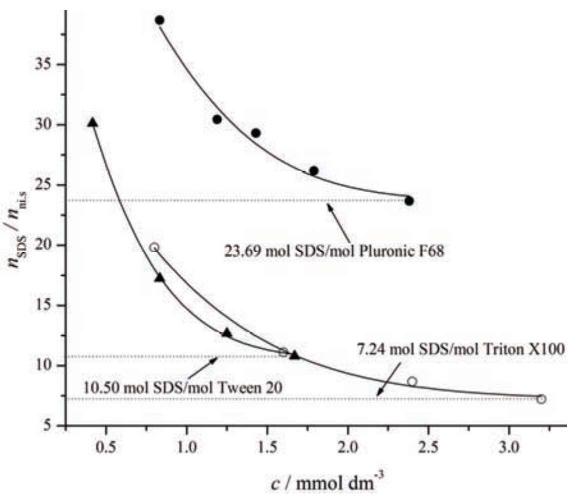

Fig. 2. Dependence of the SDS/ /nonionic surfactant mole ratios ($n_{SDS}/n_{ni.s}$) at the end of mixed micellization on the nonionic surfactant concentration.

As can be seen, the mixed micelles of Pluronic F68 contained the highest mole partition of SDS molecules, 23.6 mol mol^{-1}, and the mixed micelles of Triton X100 the lowest one, 7.24 mol mol^{-1}. These findings could be attributed to the differences in the structures of the nonionic surfactants that affected the packing of SDS molecules into mixed micelles.[20] As reported before,[21,22] a strong attractive interaction of SDS with the ethylene oxide–propylene oxide–ethylene oxide triblock copolymer exists in the micelles and therefore the highest molar ratio of SDS could be expected. With regards to Triton X100, the presence of a phenolic group in the hydrophobic chain of the molecule causes steric hindrance that leads to poor packing of the SDS molecules in the mixed micelles.[13] The concentration of nonionic surfactant, as mentioned before, affects the structure of the mixed micelles; thus, an increase in the concentration causes a decrease in mole share of SDS molecules present in the mixed micelles, *i.e.*, the structure of the micelles.

Interactions of HPMC/nonionic surfactant mixtures with SDS

In our previous work, interactions between HPMC and SDS in aqueous solution, at 30 °C, had been investigated in detail using various experimental techniques.[16,17] Characteristic points, *i.e.*, SDS concentration at which interaction begins, the critical aggregation concentration, *CAC*, and ends, the polymer saturation point, *PSP*, were determined and it appeared that the *CAC* did not depend on the HPMC concentration, whereas the *PSP* was linearly dependent on the HPMC concentration. In order to define the region of interaction between HPMC and SDS at 40 °C, conductometric titrations of HPMC solutions at concentrations below (3.22×10^{-3} mmol dm^{-3}) and above (19.35×10^{-3} mmol dm^{-3}) the critical overlap concentration, c^*, were performed. The obtained results presented in Fig. 3 are in good agreement with those of a previous studies.[16,17]

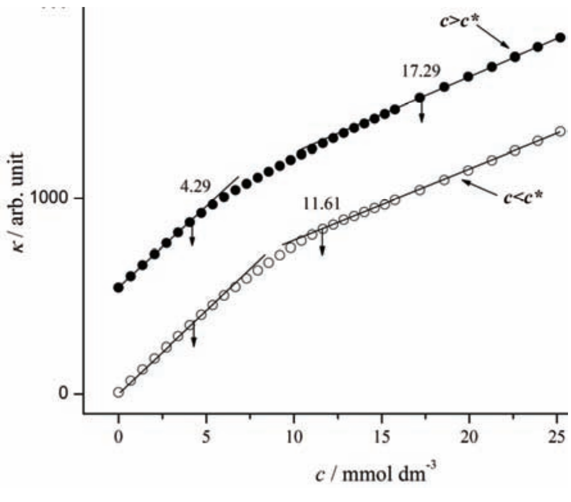

Fig. 3. Dependence of specific conductance (relative scale units) on the SDS concentration for HPMC solutions of concentrations less than 3.22×10^{-3} mmol dm^{-3} and higher than 19.35×10^{-3} mmol dm^{-3}; the critical overlap concentration was 6.25×10^{-3} mmol dm^{-3}.

Namely, the interaction region, observed as a nonlinear conductance–concentration dependence, was much wider for HPMC concentrations higher than c^*. Under such conditions, the hydrophobic substituents of the HPMC molecules are close and interaction with SDS is intermolecular in nature. With increasing SDS concentration, micellar structures are formed around each individual substituent until saturation of all available sites on the polymer molecules.

Considering that HPMC/SDS interactions in solution are influenced by various factors (temperature, the molecular characteristics and concentration of HPMC, ionic strength,[23] *etc.*) and that they could induce changes in the properties of mixed systems, it was interesting to examine the interactions of these two species in the presence of a nonionic surfactant. For these reasons, conductometric titrations of binary mixtures of HPMC and nonionic surfactants with SDS were performed. The concentrations of HPMC in the mixtures were below 3.22×10^{-3} mmol dm^{-3} and above 19.35×10^{-3} mmol dm^{-3}, the critical overlap concentration. Concentrations of Triton X100, Tween 20 and Pluronic F68 in the binary mixtures were 1.6, 8.33 and 1.19 mmol dm^{-3}, respectively. The results of these investigations are presented in Fig. 4.

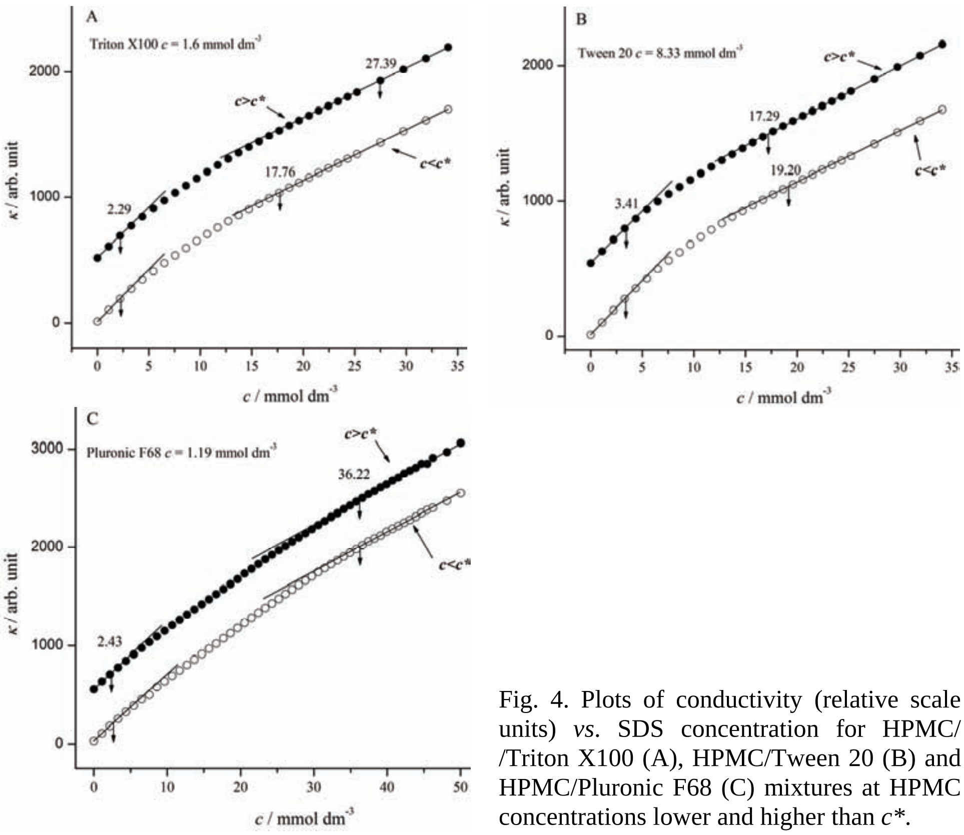

Fig. 4. Plots of conductivity (relative scale units) *vs*. SDS concentration for HPMC/ /Triton X100 (A), HPMC/Tween 20 (B) and HPMC/Pluronic F68 (C) mixtures at HPMC concentrations lower and higher than c^*.

The addition of SDS to the mixture of HPMC and Triton X100 below c^* of HPMC (Fig. 4A) caused changes in the slope of the conductance–concentration curve at characteristic SDS concentrations (2.29 and 17.76 mmol dm^{-3}), which are the same as for the Triton X100/SDS system presented in Fig. 1A. This means that in such a system mixed micellization was a more favorable process than HPMC/SDS interaction. After mixed micellization was finished, the conductometric curve became linear again, indicating that only free micelles of SDS molecules were being formed, *i.e.*, there was no interaction with HPMC. When the HPMC concentration in a binary mixture is above c^*, the second break point is much higher (27.39 mmol dm^{-3}) meaning that after the formation of mixed micelles, the SDS molecules started to form micellar aggregates around the hydrophobic substituents of the adjacent polymer chains, *i.e.*, HPMC/SDS interaction occurred.[17] Such behavior could be explained by the fact that in semi-dilute conditions, at $c>c^*$, the hydrophobic substituents of the HPMC molecules were very close, expressing more hydrophobicity and hence, HPMC/SDS interaction could occur.

Interactions in binary mixtures of HPMC and Tween 20 with SDS, determined by conductometry, are presented in Fig. 4B. It could be observed that, at HPMC concentration below c^*, the nonlinearity region in conductometric curve is wider than for Tween 20/SDS system (Fig. 1B), implying that HPMC/SDS hydrophobic interaction occurs as well. However, when the HPMC concentration in the mixtures was higher than c^*, it seems that after the formation of mixed micelles, binding of SDS to hydrophobic sites of HPMC was disabled. Namely, Tween 20 has a highly branched, voluminous polar head and is thus expected that mixed micelles would be voluminous as well. Their presence in the neighborhood of the binding sites on the HPMC molecules, between neighboring polymer chains, probably resulted in steric hindrance and disabled the hydrophobic binding of SDS.

The addition of SDS to mixtures of HPMC and Pluronic F68 caused mixed micelle formation at HPMC concentration below and above c^*. Namely, the conductometric titration curves, presented in Fig. 4C, had exactly the same form as the one presented in Fig. 1C for the same Pluronic F68 concentration. After the mixed micelles had formed, further addition of SDS to the mixtures led to the formation of free SDS micelles only. As it can be seen, regardless of the HPMC concentration in the mixture, HPMC/SDS hydrophobic interaction failed. Such a behavior could be attributed to the shape of the formed Pluronic F68/SDS mixed micelles that sterically hindered hydrophobic SDS binding to the HPMC molecules.[24]

Interactions of HPMC with nonionic surfactant/SDS mixed micelles

In order to examine the interactions of HPMC with nonionic surfactant/SDS mixtures, conductometric titrations of HPMC solutions at $c<c^*$ and $c>c^*$ with binary mixtures of the surfactants were performed. HPMC solutions were titrated with Triton X100/SDS, Tween 20/SDS and Pluronic F68/SDS mixtures at the mole ratios 1/1.7, 1/10.5 and 1/23.69 mol mol^{-1}, respectively. The nonionic surfactant/SDS mole ratios were chosen to include the amount of SDS molecules in the mixed micelles at the end of micellization (Fig. 2). Micellization of the nonionic surfactant/SDS mixtures in water were also determined, and the results are presented in Fig. 5.

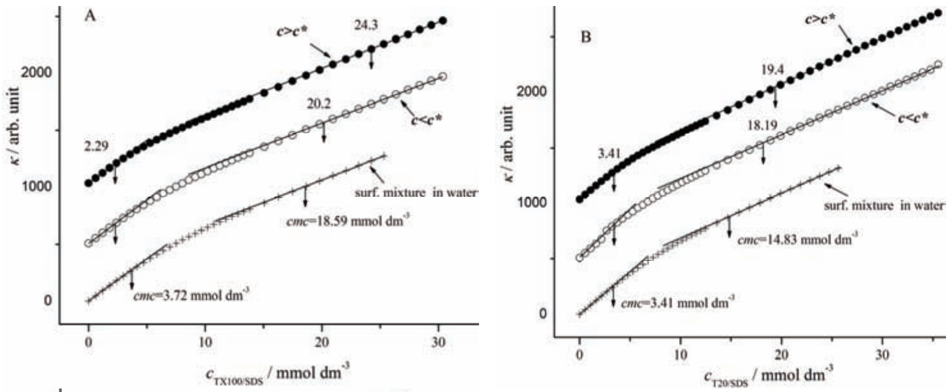

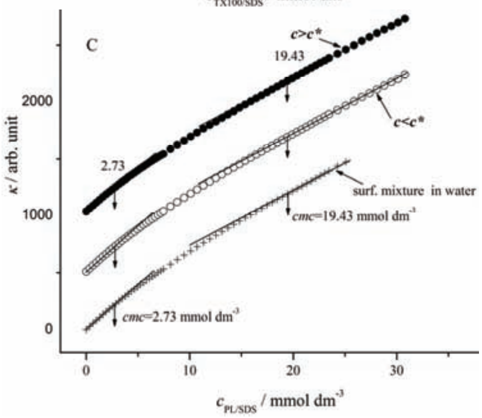

Fig. 5. Plots of conductivity (relative scale units) *vs.* nonionic surfactant/SDS concentration for HPMC concentrations in water solution lower and higher than c^*; A) TX100/ /SDS–Triton X100/SDS mixture of molar ratio 1/7.24, B) T20/SDS–Tween 20/SDS mixture of molar ratio 1/10.5 and C) PL/ /SDS–Pluronic F68/SDS mixture of molar ratio 1/23.69.

For all nonionic surfactant/SDS binary mixtures, the conductance *vs.* concentration curves showed two break points, *i.e.*, two *CMC* values. The existence of two break points for some surfactant mixtures was previously reported, which indicated the formation of two different kinds of mixed micellar aggregates, *i.e.* non-ideal behavior on mixing.[10,14] The first break point at low surfactant concentrations corresponded to mixed micelles with a high degree of ionization, shown by the slight change in the slope of the conductance–concentration curve. The second break point at higher surfactant concentration shows the existence of another type of micelle with a lower degree of ionization. Such a behavior is in agreement with the results presented in Fig. 2, indicating that the mixed micelles had the lowest molar content of SDS at the end of micellization.

Changes in the conductance of HPMC solutions at $c<c^*$ and $c>c^*$ with the addition of Triton X100/SDS binary mixtures showed two break points (Fig. 5A), which are related to the start and the end of the formation of HPMC/surfactant mixture interactions. The region of nonlinearity started at a mixture concentration of 2.29 mmol dm^{-3} (lower than the first *CMC*), indicating binding of surfactants molecules to the hydrophobic sites of polymer, which is more favorable than the formation of mixed micelles. This binding continues until saturation of all the available sites on the HPMC molecules, which is determined by the second break point (20.2 mmol dm^{-3} for $c<c^*$). Further addition of the surfactant mixture caused the formation of free micelles only, observed as the linear increase in conductance with the same slope as for the surfactant mixture in water after reaching second *CMC*. As expected, the interaction region is pronounced at HPMC concentrations higher than c^*.

The interaction of HPMC and Tween 20/SDS mixture was less pronounced (Fig. 5B). Namely, for both HPMC concentrations, the regions of nonlinearity in conductance–concentration titration curves were slightly wider compared to the region of the formation of mixed micelles. The micellization and/or interaction started at same concentration (3.41 mmol dm^{-3}) and it is possible that they occurred simultaneously. At both HPMC concentrations, the second break point, *i.e.*, the end of nonlinear region, was shifted toward higher concentrations of Tween 20/SDS mixtures, indicating that interactions occurred to a certain degree.

Concerning the Pluronic F68/SDS mixture, there was no interaction with HPMC, regardless of its concentration (Fig. 5C). Namely, the conductometric curves show two break points at the same concentrations as for the pure surfactant mixture in water. It is clear that formation of mixed Pluronic F68/SDS micelles was more favorable than its interaction with HPMC.

CONCLUSIONS

The conductometric titration method was a useful and relatively simple technique for investigations of nonionic/ionic surfactant mixed micellization and mixed micelles interactions with the nonionic polymer HPMC. The formations of mixed micelles of Triton X100, Tween 20 or Pluronic F68 with SDS were energetically more favorable than the formation of single surfactant micelles and the formation depended on the characteristics of the surfactant. The mixed micellar systems underwent significant changes in structural organization during aggregation and the concentration of the nonionic surfactant affected their structure, *i.e.*, the molar share of SDS molecules present in mixed micelles decreased with increasing concentration.

In the HPMC/nonionic surfactant mixtures, the surfactant molecules were in the neighborhood of the HPMC hydrophobic sites and the introduction of SDS caused mixed micelle formation. After formation of the micelles, further addition of SDS could lead to interaction with HPMC depending on the HPMC concentration and on the size and shape of the formed mixed micelles. These parameters also affected the interaction of HPMC with nonionic surfactant/SDS mixed micelles.

Acknowledgement. This work has been supported by the Ministry of Education, Science and Technological Development of the Republic of Serbia, Project Grant No III 46010.

И З В О Д

КОНДУКТОМЕТРИЈСКО ИСПИТИВАЊЕ СИСТЕМА ХИДРОКСИПРОПИЛМЕТИЛ-ЦЕЛУЛОЗА/НАТРИЈУМ-ДОДЕЦИЛСУЛФАТ/НЕЈОНСКИ СУРФАКТАНТ

ЛИДИЈА Б. ПЕТРОВИЋ, ВЕРИЦА Ј. СОВИЉ, ЈАДРАНКА Л. МИЛАНОВИЋ и ЈАРОСЛАВ М. КАТОНА

Технолошки факултет, Универзитет у Новом Саду, Бул. цара Лазара 1, 21000 Нови Сад

Смеше сурфактаната се веома често користе у различитим формулацијама козметичих и фармацеутских производа јер делују синергистички, обебеђујући боља својства производа. Истовремено, присуство полимера у смеши са сурфактанатима може да доведе до молекулских интеракција, а самим тим и до промена стабилности и активности готовог производа. Из ових разлога веома је значајно испитати утицај интеракције појединих компонентата смеша сурфактаната на процесе формирања мицела и мешаних мицела, као и интеракције мешаних мицела са молекулима полимера. У раду је испитано формирање мешаних мицела нејонских сурфактаната, полисорбата 20 (Tween 20), полиоксиетиленоктилфенил етра (Triton X100) и полиоксиетилен–полиоксипропилен блок колполимера (Pluronic F68), и јонског сурфактанта, натријум-додецилсулфата, у води применом кондуктометријске титрације на 40 °C. Утврђено је да област формирања мицела зависи од својстава и концентрације нејонског сурфактанта. Формирање мешаних мицела у присуству нејонског полимера, хидроксипропилметил целулозе, и њихово везивање за хидрофобне центре на молекулима полимера је такође испитано. Анализа добијених резултата указује на присутво различитих интеракција у испитиваним системима, које су од пресудног значаја за њихову примену.

(Примљено 21. марта, ревидирано 30. маја, прихваћено 2. јуна 2014)

REFERENCES

1. T. W. Dawey, W. A. Ducker, A. R. Hayman, *Langmuir* **16** (2000) 2430
2. M. L. Castaldi, O. Ortona, L. Paduano, V. Vitagliano, *Langmuir* **14** (1998) 5994
3. S. B. Sulthana, P. V. C. Rao, S. G. T. Bhat, A. K. Rakshit, *J. Phys. Chem.* **102** (1998) 9653
4. A. B. E. Attia, Z. Y. Ong, J. L. Hedrick, P. P. Lee, P. L. R. Ee, P. T. Hammond, Y. Y. Yang, *Curr. Opin. Colloid Interf. Sci.* **16** (2011) 182
5. C. Rupp, H. Steckel, B. W. Müller, *Int. J. Pharm.* **395** (2010) 272
6. G. Dongowski, B. Fritzsc, J. Giessler, A. Hartl, O. Kuhlmann, R. H. H. Neubert, *Eur. J. Pharm. Biopharm.* **60** (2005) 147
7. C. Prottey, T. Ferguson, *J. Soc. Cosmet. Chem.* **26** (1975) 29

8. L. D. Rhein, F. A. Simion, R. L. Hill, R. H. Cagan, J. Mattai, H. I. Maibach, *Dermatologica* **180** (1990) 186
9. K. S. Sharma, S. R. Patil, A. K. Rakshit, K. Glenn, M. Doiron, R. M. Palepu, P. A. Hassan, *J. Phys. Chem.* **108** (2004) 12804
10. M. Prasad, S. P. Moulic, R. Palepu, *J. Colloid Interf. Sci*. **284** (2005) 658
11. C. Das, T. Chakraborthy, S. Gosh, B. Das, *Colloid Polym. Sci.* **286** (2008) 1143
12. S. Gosh, S. P. Moulik, *J. Colloid Interf. Sci*. **208** (1998) 357
13. M. S. Bakshi, S. Sachar, K. Singh, A. Shaheen, *J. Colloid Interf. Sci*. **286** (2005) 369
14. M. Munoz, A. Rodriguez, M. del Mar Graziani, M. L. Moya, *Langmuir* **20** (2004) 10858
15. X. Cui, Y, Jiang, C. Yang, X. Lu, H. Chen, S. Mao, M. Liu, H. Yuan, P. Luo, Y. Du, *J. Phys. Chem., B* **114** (2010) 7808
16. V. J. Sovilj, L. B. Petrovic, *Colloid Polym. Sci.* **284** (2005) 334
17. V. J. Sovilj, L. B. Petrovic, *Carbohyd. Polym.* **64** (2006) 41
18. L. B. Petrovic, V. J. Sovilj, J. M. Katona, J. L. Milanovic, *J. Colloid Interf. Sci*. **342** (2010) 333
19. N. V. Sastry, H. Hoffmann, *Colloids Surfaces, A* **250** (2004) 247
20. N. Homendra, C. H. Devi, *J. Surface Sci. Technol.* **22** (2006) 119
21. J. B. Vieira, R. K. Thomas, Z. X. Li, J. Penfold, *Langmuir* **21** (2005) 4441
22. J. James, S. Vellaichami, R. S. G. Krishnan, S. Samikannu, A. B. Mandel, *Chem. Phys.* **312** (2005) 275
23. A. Tomsik, J. Katona, S. Njaradi, L. Petrovic, B. Marčeta, J. Milanovic, in *Proceedings of 27^th^ Conference of ECIS*, 2013, Sofia, Bulgaria, 2013, p. C1P:15
24. E. Hecht, H. Hoffmann, *Langmuir* **10** (1994) 86.

Journal of the Serbian Chemical Society
Version Electronic
JSCS-info@shd.org.rs • www.shd.org.rs/JSCS

J. Serb. Chem. Soc. *79* (11) 1433–1443 (2014)
JSCS–4677

UDC 546.47–31+542.913:544.526.5+
542.92:667.281
Original scientific paper

Hydro- and solvothermally-prepared ZnO and its catalytic effect on the photodegradation of Reactive Orange 16 dye

BOJANA SIMOVIĆ[1*#], ALEKSANDAR GOLUBOVIĆ[2#], IVANA VELJKOVIĆ[3], DEJAN POLETI[4#], JELENA ZDRAVKOVIĆ[5#], DUŠAN MIJIN[4#] and ANĐELIKA BJELAJAC[5#]

[1]Institute for Multidisciplinary Research, University of Belgrade, Kneza Višeslava 1, 11030 Belgrade, Serbia, [2]Institute of Physics, University of Belgrade, Pregrevica 118, 11080 Belgrade-Zemun, Serbia, [3]The Netherlands Organization for Applied Scientific Research – TNO, De Rondom 1, Eindhoven, The Netherlands, [4]Department of General and Inorganic Chemistry, Faculty of Technology and Metallurgy, University of Belgrade, Karnegijeva 4, 11120 Belgrade, Serbia and [5]Innovation Centre – Faculty of Technology and Metallurgy, University of Belgrade, Karnegijeva 4, 11120 Belgrade, Serbia

(Received 20 May, revised 14 July, accepted 17 July 2014)

Abstract: In this work, zinc oxide powders were obtained by two different techniques: hydro- and solvothermal synthesis starting from $Zn(NO_3)_2$ and $Zn(CH_3COO)_2$, respectively. The influence of synthetic procedure on the structural, microstructural, thermal and photocatalytic properties of the prepared ZnO powders was investigated. Both ZnO samples were further annealed under moderate conditions (300 °C) to avoid grain growth and to remove traces of impurities. In all four cases, single-phase hexagonal ZnO was confirmed by X-ray powder diffraction. The morphologies of prepared ZnO powders were different and they varied from rounded nanograins to microrods. All prepared samples showed higher photocatalytic efficiency in the degradation of the textile azo dye Reactive Orange 16 (RO16) than commercial ZnO. In addition, the non-annealed samples had better photocatalytic properties than the commercial Degussa P25 TiO_2 powder.

Keywords: synthesis; ZnO powders; Reactive Orange 16; photocatalysis.

INTRODUCTION

Zinc oxide, ZnO, can be used in a large number of areas, since it is an inexpensive, chemically stable, easy to prepare and non-toxic material. ZnO has the ability to form a wide range of nanostructures: nanowires, nanorings, nanohoneycombs, nanorods, nanofibers, nanospheres, *etc*. Such ZnO nanopowders have

* Corresponding author. E-mail: bsimovic@tmf.bg.ac.rs
[#] Serbian Chemical Society member.
doi: 10.2298/JSC140520077S

initiated numerous studies,[1,2] and one of the many potential ZnO applications is in the ecological field.

Today most of water resources are polluted, and the contamination is constantly increasing due to rapid population growth, industrialization and urbanization. The wastewaters of the textile industries are the most polluting of all industrial sectors. Advanced oxidation processes are of interest for the effective oxidation of diverse organics and dyes. Among them, heterogeneous photocatalysis has become an important technology for the total mineralization of various organic pollutants, including reactive organic dyes.[3]

Most of the photocatalytic studies applied synthetic or commercial TiO_2 as the catalyst. However, the well-known employment of TiO_2 is not economic for large-scale water treatment and therefore attention has been drawn to the search for appropriate alternatives. Between many other semiconductors, ZnO appears to be a highly promising photocatalyst because it is one of the most important wide-band-gap materials with a direct band gap energy of 3.3 eV at room temperature, which corresponds to emission in the UV region.[1] In the last decades, the preparation fine ZnO nanopowders has attracted great interest. The great advantage of ZnO is that it absorbs a larger part of the solar spectrum than TiO_2. For this reason, ZnO is very suitable for photocatalytic degradation in the presence of both UV[4] and visible light.[5] For example, the photodegradation of Acid Brown 14 was studied by Sakthivel *et al*.[5] using ZnO irradiated with solar light. It is found that the photodegradation efficiency decreased with increasing initial dye concentration and optimum catalyst loading was 250 mg in 100 mL. Akyol *et al*.[6] studied the photocatalytic decolorization of Remazol Red by ZnO under UV light. Pandurangan *et al*.[7] realized the photodegradation of Basic Yellow Auramine O using ZnO exposed to solar radiation.

Studies that compared the efficiency of different catalysts for a particular dye under identical conditions are scarce.[5,6,8,9] For example, Daneshvar *et al*.[8] reported that ZnO is a suitable alternative to TiO_2 for the degradation of Acid red 14 azo dye. It was also found that the photodegradation mechanism of the dye by ZnO was similar to that by TiO_2.[8,9]

To the best of our knowledge, there are only three studies in which the photodegradation of RO16 dye by ZnO was attempted. In the first case, a ZnO suspension,[10] in the second one ZnO plates,[11] and in the third one ZnO coated thin film[12] were used. However, although many details were clarified, in all cases commercial ZnO was used as a catalyst, but only once[11] was it ball milled before the preparation of the corresponding plates.

In this work, hydro- and solvothermally prepared ZnO powders were compared with commercial ZnO and Degussa P25 TiO_2 for their efficiency in the photodegradation of RO16 azo dye in aqueous solution, using imitated sunlight illumination.

EXPERIMENTAL

Materials

All the reagents: poly(vinyl pyrrolidone), zinc acetate dihydrate, zinc nitrate hexahydrate (all Sigma Aldrich), ethylene glycol (Carlo Erba) and sodium hydroxide (*p.a.*) were of analytical grade and used without further purification. The textile dye, C.I. Reactive Orange 16, was obtained from Bezema as a gift.

Solvothermal method (ST-ZnO)

To prepare the precursor, 1.80 g of poly(vinyl pyrrolidone) (PVP) was dissolved in 75 mL of ethylene glycol (EG) and then 3.60 g of solid $Zn(CH_3COO)_2\cdot 2H_2O$ was slowly added into the solution. The resulting mixture was stirred for several minutes, followed by the addition of 1.80 g of solid NaOH. An aliquot of 65 mL of the mixture was treated solvothermally using a Teflon®-lined stainless steel autoclave (V = 75 mL) at 120 °C for 18 h under autogenous pressure. After spontaneous cooling to room temperature, the white precipitate at the bottom of the autoclave was washed with distilled water and alcohol, and dried at 100 °C for 3 h. One part of the product was additionally heated at 300 °C for 2 h in order to investigate the influence of annealing (sample ST-ZnO-a). The mass loss during annealing was 1.9 mas. %.

Hydrothermal method (HT-ZnO)

To prepare the precursor, 50 mL of $Zn(NO_3)_2\cdot 6H_2O$ (0.5 mol dm^{-3}) was added dropwise into 50 mL of NaOH solution (0.5 mol dm^{-3}) during 30 min under intensive stirring. The precursor mixture was further treated in the same way as described above. The mass loss during annealing was 2.7 mas. %. The annealed product was labeled as HT-ZnO-a.

Characterization techniques

X-Ray diffraction (XRD) patterns were collected over the range 20° < 2θ < 90° on an Ital Structures APD2000 X-ray diffractometer using Cu$K\alpha$ radiation (λ = 1.5418 Å). Thermogravimetric analysis (TG) was realized using an SDT Q600 instrument (TA Instruments) up to 700 °C under a dynamic air atmosphere (heating rate: 20 °C min^{-1}, flow rate: 100 mL min^{-1}). The presence of impurities was checked by Fourier transform infrared (FTIR) spectroscopy on a Bomem MB-100, Hartmann Braun FTIR spectrophotometer (range: 4000–400 cm^{-1}) using the KBr pellet technique. The size and morphology of the prepared particles were characterized using field emission scanning electron microscopy (FESEM, Tescan Mira X3).

Irradiation experiments

Photodegradation was performed using an open double-wall flask (volume 100 mL) in a dark chamber equipped with an Osram Ultra-Vitalux 300 W lamp, which produces radiation similar to the radiation of natural sunlight. The lamp was placed 50 cm away from the surface of the dye solution. Constant mixing of the solution was insured using a magnetic stirrer, while constant temperature was maintained by circulating the water through the wall of the reactor. The photodegradation of RO16 dye was studied by mixing 25 mL of an aqueous solution containing dye (50 mg dm^{-3}) and the prepared ZnO samples (50 mg) as a catalyst. The solution was then stirred to keep the suspension homogenous and left in the dark for 90 min to achieve adsorption equilibrium. Subsequently, the lamp was switched on and after 30 and 60 min of irradiation, the solution (3 mL) was sampled. The residual concentration of dye was determined using a UV–Vis spectrophotometer (Shimadzu 1700) after centrifugation of the solution. The absorption spectra and rate of photodegradation were observed in terms of the absorbance change at the peak maximum of the dye (λ_{max} = 492.5 nm). The commercial ZnO (Orka) and Degussa P25 TiO_2 powders were treated in the same way for comparison.

RESULTS AND DISCUSSION

X-Ray powder diffraction, TG and FTIR analysis

The XRD patterns of all prepared samples (Fig. 1) are readily indexed to the hexagonal ZnO phase (wurtzite type structure, JCPDS card 80-0075, *a* = 3.2539 Å, *c* = 5.2098 Å). No impurities could be detected, meaning that single-phase ZnO powders were obtained using both synthetic routes. The average crystallite sizes of ZnO powders were calculated using the Scherrer formula.[13] The solvothermally prepared samples had a much smaller crystallite size (Table I) compared to the hydrothermally prepared ones and the commercial ZnO. This could be attributed to the already recognized role of PVP in controlling the size and shape of ZnO grains.[14] The slight increase in the unit cell parameters and crystallite sizes after annealing at 300 °C were observed in both cases. Very likely, these small changes in lattice parameters could be related to the changes in the particle sizes.[15]

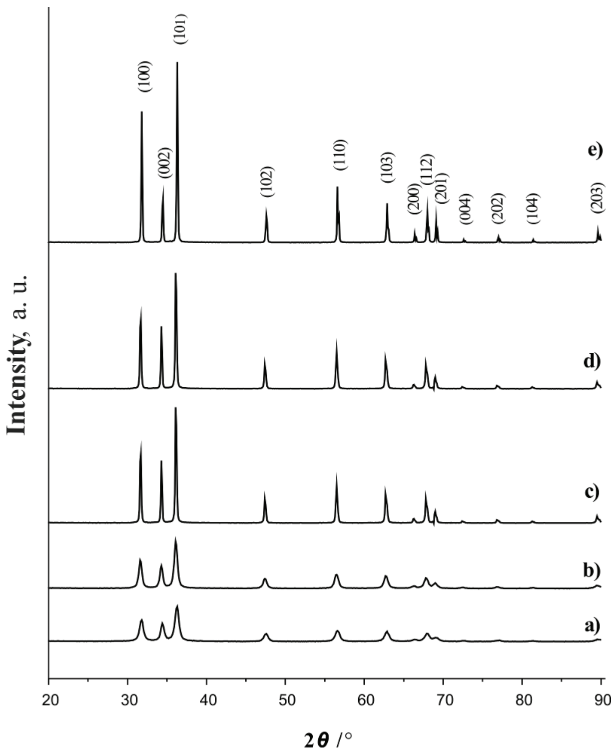

Fig. 1. XRD patterns of: a) ST-ZnO, b) ST-ZnO-a, c) HT-ZnO, d) HT-ZnO-a and e) commercial ZnO.

TABLE I. Structural and microstructural properties of the prepared ZnO materials; <*D*> calculated by the Scherrer formula using 13 well-defined ZnO diffraction maxima

Sample	Unit cell parameters and volume a, c / Å, V / Å^3	The average crystallite size, <*D*> / nm
ST-ZnO	a = 3.2550(1), c =5.2107(2), V = 47.812(3)	16.7(1)
ST-ZnO-a	a = 3.2571(1), c = 5.2215(2), V = 47.971(3)	21.1(3)
HT-ZnO	a = 3.2452(1), c = 5.1980(4), V = 47.407(3)	71.7(5)
HT-ZnO-a	a = 3.2556(1), c = 5.2143(2), V = 47.861(3)	75.0(5)
Commercial ZnO	a = 3.2491(1), c = 5.2028(2), V = 47.570(3)	94.6(1)

The TG curves are shown in Fig. 2. The annealed HT-ZnO-a sample (Fig. 2, curve e) and commercial ZnO (Fig. 2, curve d) showed almost negligible mass loss (less than 1.0 mas. %), probably due to their slightly hygroscopic nature. The ST-ZnO-a sample (Fig. 2, curve c) showed a little greater mass loss (about 2 mas. %) that could be ascribed to the better H_2O adsorption due to nanosize effects. As expected for the non-annealed samples (Fig. 2, curves a and b), a higher total mass loss (about 3.0 mas. %) was obtained. In the case of the HT-ZnO sample (Fig. 2, curve a), an abrupt loss at about 250 °C very likely corresponds to the decomposition of $Zn(NO_3)_2$.[16]

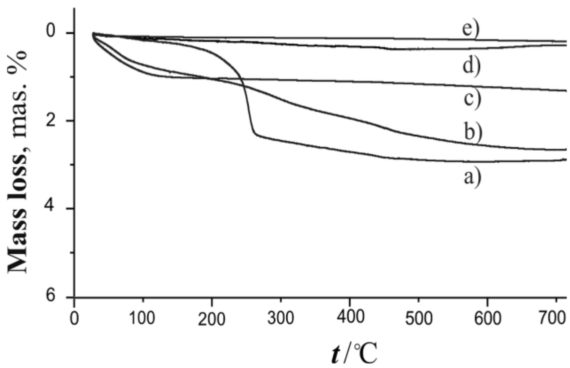

Fig. 2. TG curves of: a) HT-ZnO, b) ST-ZnO, c) ST-ZnO-a, d) commercial ZnO and e) HT-ZnO-a.

The ST-ZnO (Fig 2, curve b) sample is similar to HT-ZnO, but the process has no clearly distinguished steps or thermal effects. Considering this result, the mass loss could be attributed to the simultaneous decomposition of traces of acetate ions and PVP.[17,18]

Considering the FTIR spectra (Fig. 3), the intensive band at around 480 cm^{-1} is characteristic for Zn–O stretching vibrations.[19] The bands at 2850 and 2920 cm^{-1} correspond to the ν(CH_2) vibrations. The bands at around 1640 and 1400 cm^{-1} could be attributed to the asymmetrical and symmetrical stretching of the COO groups, respectively. The appearance of these bands supports the presence of acetate groups, although residual PVP could not be totally excluded. However, these bands also existed in the spectrum of the commercial ZnO and agree with the corresponding literature data,[20] *i.e.*, the commercial and the herein described ZnO have identical FTIR spectra. The broad bands centered at about 3440 cm^{-1} could be attributed to the ν(OH) vibrations that arise from the slightly hygroscopic nature of ZnO and the consequential surface adsorption of ambient water.[20] According to the mass loss during annealing of the ST-ZnO sample, the percentage of hygroscopic H_2O was lower than 2 mas. %.

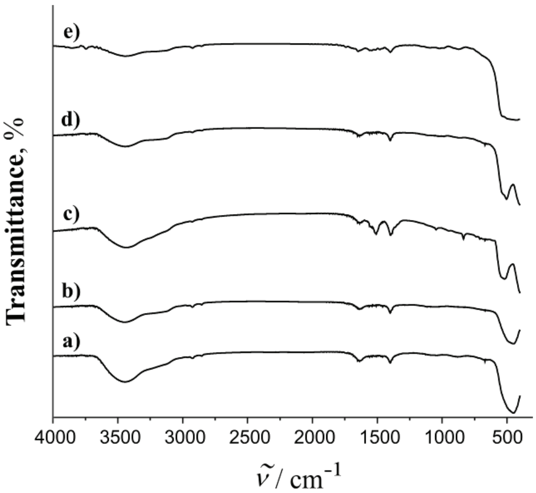

Fig. 3. FTIR spectra of: a) ST-ZnO, b) ST-ZnO-a, c) HT-ZnO, d) HT-ZnO-a and e) commercial ZnO.

The bands due to the N–O stretch at 1515–1560 cm^{-1} in the spectrum of the HT-ZnO sample disappeared after annealing, meaning that the residual nitrate ions were easily decomposed at 300 °C, which confirmed the TG results. Regarding the results of XRD analysis and the mass loss during annealing, the content of impurities in the as-prepared HT-ZnO sample should be less than 3 mas. %.

Morphology of the nanostructures

The morphologies of the prepared ZnO powders were very different. The commercial ZnO (Fig. 4, a) consisted of hexagonal prisms of different sizes, with diameters between 50 and 500 nm and lengths from 100 to 700 nm.

The HT-ZnO and HT-ZnO-a particles shown in Fig. 4, b and c, were very similar in size and morphology. Both samples consisted of hexagonal shaped rods with diameters of up to 800 nm and the lengths up to several micrometers, but HT-ZnO-a had more uniformly distributed dimensions. Identical, sometimes hollowed rods were obtained previously when water was used as the medium.[4] In addition, there was a small amount of web-like nanofibers in HT-ZnO, and a small quantity of nanograins in the HT-ZnO-a sample. Thus, in both cases, a bimodal grain size distribution with a great predominance of rods was observed.

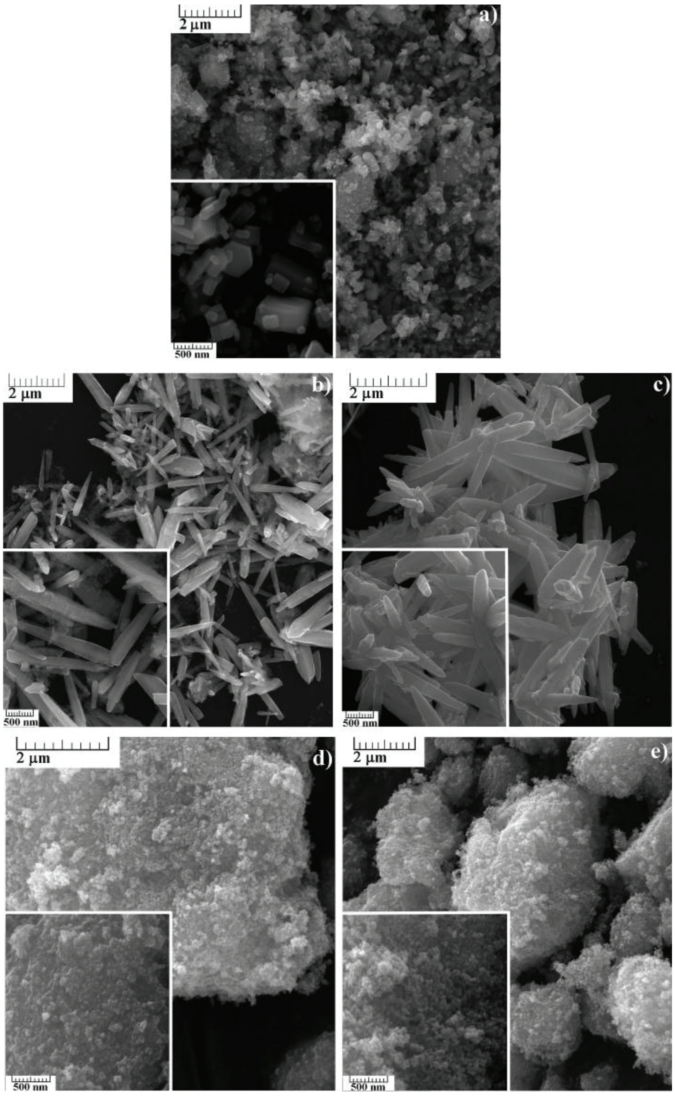

Fig. 4. FESEM images of: a) commercial ZnO, b) HT-ZnO rods, c) HT-ZnO-a rods, d) ST-ZnO nanopowder and e) ST-ZnO-a nanopowder.

The ST-ZnO and ST-ZnO-a particles (Fig. 4, d and e) were also related. Precisely, they consisted of small (<50 nm), rounded nanograins, creating very loosely packed aggregates. PVP played an important role in controlling the size and shape of the ZnO particles during the synthesis. Here, PVP together with EG, limited the growth of the ZnO particles probably along all crystal planes, causing the uniformity in size and approximately spherical shape of the particles.[21]

Photodegradation of RO16 dye

As shown in Fig. 5, all the prepared ZnO materials had a higher efficiency in the photodegradation of RO16 dye than the commercial ZnO. The results also indicated that non-annealed samples of ZnO had a higher photocatalytic efficiency than Degussa P25 TiO_2, which is the standard material in the field of photocatalytic reactions. After 30 min, the effectivenesses of the solvothermally prepared samples and commercial ZnO were approximately the same. However, the efficiency of commercial ZnO markedly decreased after 60 min, whereas the as-prepared samples were more efficient, resulting in almost complete degradation of RO16 dye. In total, the ST-ZnO nanoparticles were slightly more efficient than the HT-ZnO rods, probably due to the smaller size and higher active surface area. In addition, the smaller sizes of the crystallites in the ST-ZnO samples, inherently meaning a higher number of defects, should be taken into account. Nevertheless, none of these factors had a significant influence on the photodegradation process, as shown by very similar efficiencies of all samples.

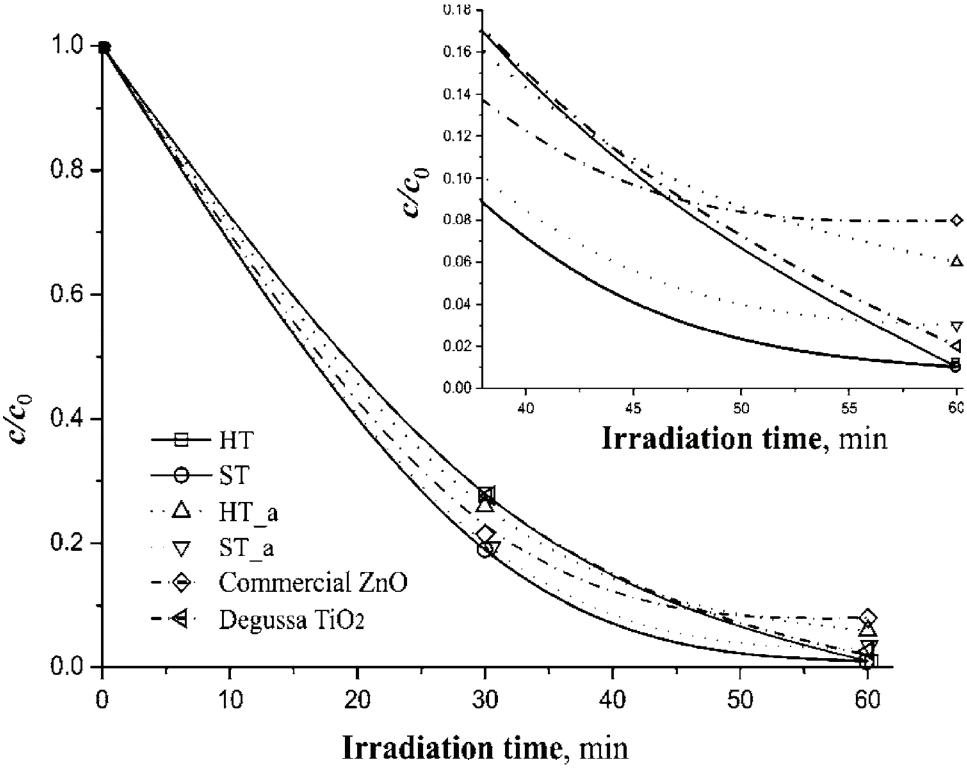

Fig. 5. The rate of photodegradation of RO16. The inset shows the activity between 35 and 60 min.

The order of decreasing activity was ST-ZnO > HT-ZnO > Degussa P25 TiO_2 > ST-ZnO-a > HT-ZnO-a > commercial ZnO. A negligible decrease of photocatalytic activity was observed after annealing; this could be assigned to the increasing of crystallite sizes and changes in porosity.

A comparison with three already mentioned papers[10–12] was difficult, since Dhodapkar *et al*.[10] reported the results of RO16 degradation using natural sunlight, while in the other two studies,[11,12] a UV lamp was used and the ZnO catalyst was in the form of a stationary layer. Moreover, different dye concentrations and doses of the photocatalysts were applied. Generally, it is challenging to compare the efficiency of photocatalysts because the published studies were, as a rule, performed under different conditions, which had to be taken into account.[22,23] For these reasons, in this paper, the efficiency of the photocatalysts prepared under the same conditions was compared in order to select a better procedure for future research.

CONCLUSIONS

Two ZnO powders with diverse morphologies were prepared by the hydrothermal and solvothermal methods. The phase purity of the samples was confirmed by XRD analysis, although a small amount of residual NO_3^- groups was detected by FTIR analysis in the as-prepared HT-ZnO sample. These impurities were easily removed by annealing at 300 °C for 2 h. In summary: a) all prepared ZnO samples had a high efficiency for the photodegradation of RO16 textile dye; b) both non-annealed samples were more active than commercial ZnO, especially when the concentration of the dye was low; c) both non-annealed samples had a slightly higher efficiency than the commercial Degussa P25 TiO_2; d) the solvothermally prepared, non-annealed ZnO particles were found to be the most efficient photocatalysts, exhibiting slightly higher activity than the hydrothermally as-prepared rods; e) application of the surfactant PVP was directly related to small crystallite and particle sizes, and for this reason, it is recommended the use of this polymer in future studies for this application; f) the photocatalytic activity of the ZnO materials depended much neither on the crystallite and particle size nor on the morphology; g) the presence of impurities in the as-prepared samples and their further annealing had only a minor influence on their photocatalytic activity. Therefore, the photocatalytic degradation of textile dyes and textile effluent assisted with ZnO materials might be an economic, environmentally friendly and efficient method for water treatment.

Acknowledgements. This work was funded by the Ministry of Education, Science and Technological Development of the Republic of Serbia under Grants Nos. III45007, ON171032, ON172013 and the SASA Project F-134.

ИЗВОД

ХИДРО- И СОЛВОТЕРМАЛНО ПРИПРЕМЉЕН ZnO И ЊЕГОВ КАТАЛИТИЧКИ УТИЦАЈ НА ФОТОДЕГРАДАЦИЈУ БОЈЕ *REACTIVE ORANGE* 16

БОЈАНА СИМОВИЋ[1], АЛЕКСАНДАР ГОЛУБОВИЋ[2], ИВАНА ВЕЉКОВИЋ[3], ДЕЈАН ПОЛЕТИ[4], ЈЕЛЕНА ЗДРАВКОВИЋ[5], ДУШАН МИЈИН[4] и АНЂЕЛИКА БЈЕЛАЈАЦ[5]

[1]Институт за мултидисциплинарна истраживања, Универзитет у Београду, Кнеза Вишеслава, 11030 Београд, [2]Институт за физику, Универзитет у Београду, Прегревица 118, 11080 Београд-Земун. [3]The Netherlands Organization for Applied Scientific Research – TNO, De Rondom 1, Eindhoven, The Netherlands, [4]Катедра за општу и неорганску хемију, Технолошко–металуршки факултет, Универзитет у Београду, Карнегијева 4, 11120 Београд, и [5]Иновациони центар Технолошко–металуршког факултета, Универзитет у Београду, Карнегијева 4, 11120 Београд

У овом раду, прахови цинк-оксида синтетисани су на два различита начина: хидро- и солвотермалном синтезом полазећи, истим редом, од $Zn(NO_3)_2$ и $Zn(CH_3COO)_2$. Оба тако припремљена узорка су потом жарена на благим условима (300 °C) да би се избегао раст зрна и да би се уклонили трагови нечистоћа. Испитан је утицај начина синтезе на структурна, микроструктурна, термичка и фотокаталитичка својства добијених прахова ZnO. Рендгенском дифракцијом праха потврђено је присуство само једне фазе, хексагоналног ZnO у сва четири узорка. Морфологије добијених прахова ZnO биле су различите и варирале су од нанозрна приближно сферног облика до микроштапића. Сви припремљени узорци показују већу фотокаталитичку ефикасност него фабрички ZnO у деградацији комерцијалне текстилне азо боје *Reactive Orange* 16. Такође, нежарени узорци имају нешто боља фотокаталитичка својства него фабрички TiO_2 прах Degussa P25.

(Примљено 20. маја, ревидирано 14. јула, прихваћено 17. јула 2014)

REFERENCES

1. C. Wang, E. Shen, E. Wang, L. Gao, Z. Kang, C. Tian, Y. Lan, C. Zhang, *Mater. Lett.* **59** (2005) 2867
2. C. Wu, X. Qiao, J. Chen, H. Wang, F. Tan, S. Li, *Mater. Lett.* **60** (2006) 1828
3. R. Andreozzi, V. Caprioa, A. Insola, R. Marotta, *Catal. Today* **53** (1999) 51
4. L. Xu, Y. L. Hu, C. Pelligra, C. H. Chen, L. Jin, H. Huang, S. Sithambaram, M. Aindow, R. Joesten, S. L. Suib, *Chem. Mater.* **21** (2009) 2875
5. S. Sakthivel, B. Neppolian, M. V. Shankar, B. Arabindoo, M. Palanichamy, V. Murugesan, *Sol. Energ. Mat. Sol., C* **77** (2003) 65
6. A. Akoyl, H. C. Yatmaz, M. Bayramoglu, *Appl. Catal., B* **54** (2004) 19
7. A. Pandurangam, P. Kamala, S. Uma, M. Palanichamy, V. Murugesan, *Indian J. Chem. Technol.* **8** (2001) 496
8. N. Daneshvar, D. Salari, A. R. Khataee, *J. Photochem. Photobiol., A* **157** (2003) 111
9. S. K. Asl, S. K. Sadrnezhaad, M. K. Rad, D. Uner, *Turk. J. Chem.* **36** (2012) 121
10. R. S. Dhodapkar, V. Chaturvedi, N. R. Neti, S. N. Kaul, *Ann. Chim.* **93** (2003) 739
11. E. Yassıtepe, H. C. Yatmaz, C. Ozturk, K. Ozturk, C. Duran, *J. Photochem. Photobiol., A* **198** (2008) 1
12. L. S. Roselin, R. Selvin, *Sci. Adv. Mater.* **3** (2011) 251
13. H. P. Klug, L. E. Alexander, *X-Ray Diffraction Procedures*, 2nd Ed., Wiley, New York, 1974, p. 687
14. T. Thilagavathi, *J. Nanomater.* **2013** (2013) 7
15. M. Hosokawa, K. Nogi, M. Naito, T. Yokoyama, *Nanoparticle Technology Handbook*, Elsevier, Amsterdam, 2007, p. 644

16. M. Maneva, N. Petrov, *J. Therm. Anal.* **35** (1989) 2297
17. D. L. Golić, G. Branković, M. P. Nešić, K. Vojisavljević, A. Rečnik, N. Daneu, S. Bernik, M. Šćepanović, D. Poleti, Z. Branković, *Nanotechnology* **22** (2011) 395603
18. C. Song, X. Dong, *Adv. Chem. Eng. Sci*. **2** (2012) 108
19. R. Y. Hong, J. H. Li, L. L. Chen, D. Q. Liu, H. Z. Li, Y. Zheng, J. Ding, *Powder Technol.* **189** (2009) 426
20. G. Xiong, U. Pal, J. G. Serrano, K. B. Ucer, R. T. Williams, *Phys. Stat. Sol., C* **3** (2006) 3577
21. D. Yiamsawas, K. Boonpavanitchakul, W. Kangwansupamonkon, *J. Micros. Soc. Thailand* **23** (2009) 75
22. S. M. Lam, J. C. Sin, A. Z. Abdullah, A. R. Mohamed, *Desalin. Water Treat.* **41** (2012) 131
23. S. Ahmed, M. G. Rasul, W. N. Martens, R. Brown, M. A. Hashib, *Water Air Soil Pollut.* **215** (2011) 3.

Journal of the Serbian Chemical Society
JSCS-info@shd.org.rs • www.shd.org.rs/JSCS

J. Serb. Chem. Soc. 79 (11) 1445–1460 (2014)
JSCS–4678

UDC *Ceratophyllum demersum:546.47/
.49’56’815:536.551:627.222.5.000.57(497.16)
Original scientific paper

Bioaccumulation and translocation of heavy metals by *Ceratophyllum demersum* from the Skadar Lake, Montenegro

VLATKO KASTRATOVIĆ[1*#], SLAĐANA KRIVOKAPIĆ[1], MILJAN BIGOVIĆ[1#], DIJANA ĐUROVIĆ[2#] and NADA BLAGOJEVIĆ[3]

[1]*Faculty of Natural Sciences and Mathematics, University of Montenegro, G. Washington Street, P. O. Box 5455, 81000 Podgorica, Montenegro,* [2]*Institute of Public Health of Montenegro, Ljubljana bb, 81000 Podgorica, Montenegro and* [3]*Faculty of Technology and Metallurgy, University of Montenegro, G. Washington Street, P. O. Box 5455, 81000 Podgorica, Montenegro*

(Received 9 April, revised 11 July, accepted 14 July 2014)

Abstract: Lacustrine systems are very complex water systems in terms of the transport of and interaction with heavy metals. Primarily due to its high variability and current chemical parameters, the tissue of macrophytes is a more plausible bio-indicator of the load level of metals within lake ecosystems than are water or sediment analyses. The macrophyte, *Ceratophyllum demersum*, sampled from the Skadar Lake in Montenegro was used as a bio-indicator. Sediments, water and plants were examined for their contents of ten metals in four different periods of 2011. The concentrations of the metals followed the trend: sediment > leaf *C. demersum* > stem *C. demersum* > water. There were differences in the sequences of the metal content in the plant compared to the sequences of their bioaccumulation ability. These differences suggest a different capacity of macrophytes for different metals. The accumulation of Mn was several times higher than the accumulation of the other analyzed metals. The highest ratio of leaf/stem concentrations was recorded for Mn (2.19) and the lowest was for Pb (1.04). The highest contents of Cd, Co, Cr, Pb, V and Sr were found in the tissues of *C. demersum* at the beginning of the growing season, whereas Ni, Zn, Cu and Mn were found at the end of the vegetative phase.

Keywords: *Ceratophyllum demersum*; Lake Skadar; heavy metals; bioaccumulation; translocation.

INTRODUCTION

Due to their toxicity, resistance to bio-degradation and long duration in the environment while entering the food chain, heavy metals are considered to be

* Corresponding author. E-mail: vlatkok@ac.me
# Serbian Chemical Society member.
doi: 10.2298/JSC140409074K

some of the most serious potential pollutants of aquatic ecosystems.[1] Therefore, the behavior of metals in sediment, their adoption by the plant and further fate of the plant tissues, although extremely complex, is undoubtedly of great importance for research in the environment. There is no single theoretical model by which the metal content of plants could be predicted from its content in a nearby sediment or water. Likewise, no pattern existed by which plants acquired metals and transported them through their tissues.

The application of plant organisms for research of heavy metal pollution in a lake environment has a number of advantages over standard methods for the detection of metals in water by chemical analysis. Thus, metal concentrations in water are often below the detection limit of the employed instrument whereas the concentrations of metals in plants are much higher and allow for the determination of the available biological and cellular metals in aqueous medium.[2–4]

When choosing the type of macrophyte for either biomonitoring or phytoremediation, it is necessary to reach a compromise between certain conditions:[5]

– it is essential that macrophytes constantly accumulate and tolerate large amounts of metal without harmful effects on their growth and development;

– it must be widespread, but being linked to one place, it could be a real representative of a given area;

– it must be easily accessible for the collection, identification and handling;

– its lifetime must be long enough for it to become a bioaccumulation phenomenon;

– there must be sufficient disposable tissue for chemical analysis;

– it must tolerate physical and chemical changes in the environment.

The achieved level of precision and accuracy of instrumental analytical methods today, and the training and experience of the analysts keeps the errors in the determination of the contents of the metals to a minimum. The greatest source of inaccuracies could be the sampling of the materials; hence, it is especially important to ensure that the sampled material is truly representative.

The preparation of the samples for analysis must be consistent with the accepted standards in order that the results are comparable with those from other geographic areas.

Ceratophyllum demersum is a perennial submerged, free-floating aquatic rootless plant, which grows in stagnant or slow-moving waters. The buds grow in the winter at the bottom of lake water and form a new plant in the spring.

C. demersum can be used as a measure of the lake pollution, as its tissue may contain toxic metals, such as Cd and Pb.[6] It could also be used to remove low concentrations of heavy metals from aquatic ecosystems.[7]

There are a small number of studies on the trace metals concentrations in plant species of Lake Skadar, and particularly insufficient data on their concentration in different parts of aquatic macrophytes and their seasonal variations.[8]

In the present study, the content of heavy metals (Cd, Co, Cr, Cu, Mn, Ni, Pb, Zn, Sr and V) in sediment, water and different organs of *C. demersum* collected from Lake Skadar, Montenegro, was investigated during different periods in 2011.

The aim of this study was to determine the ways and means of metal adoption within *C. demersum* tissue, as well as the differences and degree bioaccumulation in dependence on the metal, plant part, location and season.

EXPERIMENTAL

Geographical details about the study area are given in the Supplementary material to this paper.

Sample collection

Samples of *C. demersum* were collected four times by hand from six locations every 60––70 days from early April to late October in 2011 (Fig. S-1 of the Supplementary material). Places of maximum coverage and density were selected for examination of the macrophyte sample. Aiming at repeating the results from each site, 3–4 whole, healthy plants of similar size, shape and weight were sampled at each site separately within an area of about 25 m^2. The plant material was labeled, packed in polyethylene bags and transferred to the laboratory in the shortest possible time. Water and sediment samples were also taken from the same place as the plant material. Sediment sampling was conducted using an Eckman dredge to a depth of 0–20 cm. Stones and coarse plant material were mechanically removed. The sediment samples were placed in plastic boxes, carefully labeled and transferred to the laboratory for further analysis. Water samples were collected from the depth of 0.5–1 m using 1.5 L PET bottles. The samples were stored in a refrigerator (5±2 °C).

Sample analyses

The sampled plant material was first washed with tap water, and then twice with deionized water and gently dried with a paper towel. The samples of the *C. demersum* plants were separated into stem and leaf to determine bioaccumulation diversity of the plant organs. The plant material was then dried at 75 ° C for 48 h. The samples were ground into a fine powder and homogenized in an electrical mill (Büchi-Mixer B-400). The samples were mineralized to avoid the influence of the matrix. 0.5 g of prepared samples were approximately measured with an accuracy of ±0.0001 g and mineralized using a Milestone Microwave Ethos model 1600, with a mixture of HNO_3 and H_2O_2 (3:1). Mineralization was realized in two stages: pretreatment at a power of 300 W for a period of six min, followed by five minutes of microwave digestion at a power of 500 W. After digestion, the solutions were diluted with deionized water to a final volume of 50.0 cm^3.

The plant samples were ready for analysis and dry ashing. The measured plant material (0.5±0.0001 g) was heated in a porcelain crucible on hot plate to ash while care was taken not to ignite the sample. Then it was placed in a muffle furnace and the temperature was gradually increased to 550 °C, at which temperature, the samples were calcined for 5 h. The carbonized plant material was transferred with 2 M HCl to a 50.0 cm^3 volumetric flask. Prior to analysis, the samples were kept in plastic bottles. The analytical accuracy of the measured concentrations of the metals in the plants was tested using a tealeaf reference material (INCT–TL-1). The reproducibility of the results was within 8 % of the certified values.

The sediment samples were dried in air and then in an oven at 75 ° C for 48 h. The dried sediment samples were ground in an agate mortar and sieved through a 1.5 mm sieve. Approximately, 0.5 g (±0.0001 g) of each sample mineralized under pressure and high temperature and microwave digested with a mixture of $HCl:HNO_3$ (3:1). After digestion, the solutions were diluted with 2 M HNO_3 to a final volume of 100 cm^3.[9] The analytical accuracy was determined using a certified standard reference material of the National Institute of Standards and Technology (USA) for trace elements in lake sediment (SRM 2709). The recoveries were within 10 % of the certified values.

Water samples were filtered through a 0.45 μm Millipore filter and stored in plastic 1L bottles to which 2 mL of 70 % super pure nitric acid was added.

All parts of the plant samples, sediments and water were prepared in triplicate and their average value was assessed. Blank solutions were added to the series of samples and measured after every tenth sample determination. The concentrations of the heavy metals (Cd, Cu, Co, Cr, Mn, Ni, Pb, Zn, V and Sr) were determined by the ICP-OES technique using a Spectro Arcos instrument.

Statistical analysis

The Microsoft Excel 2000 package was used for the calculation of the mean, standard deviation and variation coefficient. One-way ANOVA with a value of $p < 0.05$ was performed between the content of each metal in the stems and leaves. If the differences between the mean values were significant at the level of 5 %, the *post hoc* Duncan test was applied to determine the minimum allowable differences between particular result groups. All calculations were performed using the SPSS (version 11.5) software package (SPSS Inc., Chicago, IL, USA).

The ability of plants to absorb and accumulate metals from the aqueous growth media was evaluated using the bio-concentration factor (*BCF*). The *BCF* value is calculated as the ratio of the concentrations of metals in the plant and the associated water:

$$BCF = \frac{\left[\mathrm{Metal}\right]_{\text{part of plant}}}{\left[\mathrm{Metal}\right]_{\text{water}}}$$

Higher BCF values imply greater phyto-accumulation ability of the plant.

The possibility of plants to transport metals from the stems to the leaves was estimated using the translocation ability (*TA*). Translocation ability was calculated as the ratio of the concentrations of metals in leaves and stems:

$$TA = \frac{\left[\mathrm{Metal}\right]_{\text{leaf}}}{\left[\mathrm{Metal}\right]_{\text{stem}}}$$

A higher *TA* value means higher translocation ability.

RESULTS

The minimum and maximum values of the metal content in the lake water during the research period in the studied locations, as well as the mean value with the standard deviation results are presented in Table S-I of the Supplementary material to this paper.

There was no temporal variation in the mean concentrations of metals at the 95 % level of confidence. There were considerable spatial variations in the results, reflected in the high standard deviation. Low concentrations of metals were registered in the water samples. Strontium has the highest concentration, whereas Cd, Co and Pb were below the LOD (lower limit of detection) at all sampling locations. Chromium was below the LOD at one location and Ni at three of the six sampling locations. Low concentrations of metals naturally occur in fresh water. The levels in sediments and organisms are much higher because of their concentration through natural processes. Even in relatively pristine areas, metal contents can vary between different water systems because of variations in the sediment characteristics and organic matter concentration. The amounts of metals in macrophytes (and other organisms) and the "total" metal content in the sediment cannot be estimated based on their content in the surrounding water.

The results of the determination of the average metal content in the sediment are given in Table S-II. Temporal and spatial changes in metal concentrations (ppm d.w.) in the parts of *C. demersum* are given in Table S-III. The seasonal minimum and maximum concentrations in the individual parts of *C. demersum* are given in Table S-IV. The Tables S-II–S-IV can be found in the Supplementary material to this paper. There was no significant seasonal variation in the results of the metal content in the sediments, as opposed to the variations found in the organs of *C. demersum*.

The concentrations of metals in the individual parts of *C. demersum* were significantly different from their concentrations in water and sediment and followed the trend: sediment > leaf *C. demersum* > stem *C. demersum* > water, except for Mn (stem and leaf) and Zn (leaf, October), when a higher concentration was found than in the sediment.

Concentrations of the metals in the stem and in the leaf of *C. demersum* followed the trend: Mn > Zn > Sr > Cu, Ni > Pb > Cr > Co > V > Cd. A similar sequence of metal contents in the tissues of *C. demersum* were reported previously.[10–14]

The concentrations of Co and Cr did not show spatial variation in the results (see Tables S-III and S-IV). Significantly higher values of the concentration of Mn, Ni and Zn were recorded at the locations Raduš, Plavnica and the right estuary of the Morača compared to the other three sites (Table S-III). The concentration of cadmium was significantly higher in the tissues of *C. demersum* sampled from Crnojevića River, Cu from the left estuary of the Morača, Pb from the right estuary of the Morača and V from Crni Žar. Strontium had significantly lower scores from the sites Crni Žar and Crnojevića River (Table S-III).

The bioaccumulation capacity of *C. demersum* was shown through the bioaccumulation factors (Fig. 1), which shows that the concentration of the studied metals in the stem and leaf decreased as follows:

– for the stem ($BCF_{\text{stem/water}}$): Mn > Zn > Ni > Cr > Cu > Co > Pb > Sr > > V > Cd;

– for the leaf ($BCF_{leaf/water}$): Mn > Zn > Ni > Cr > Co > Cu > Pb > V > Sr > > Cd.

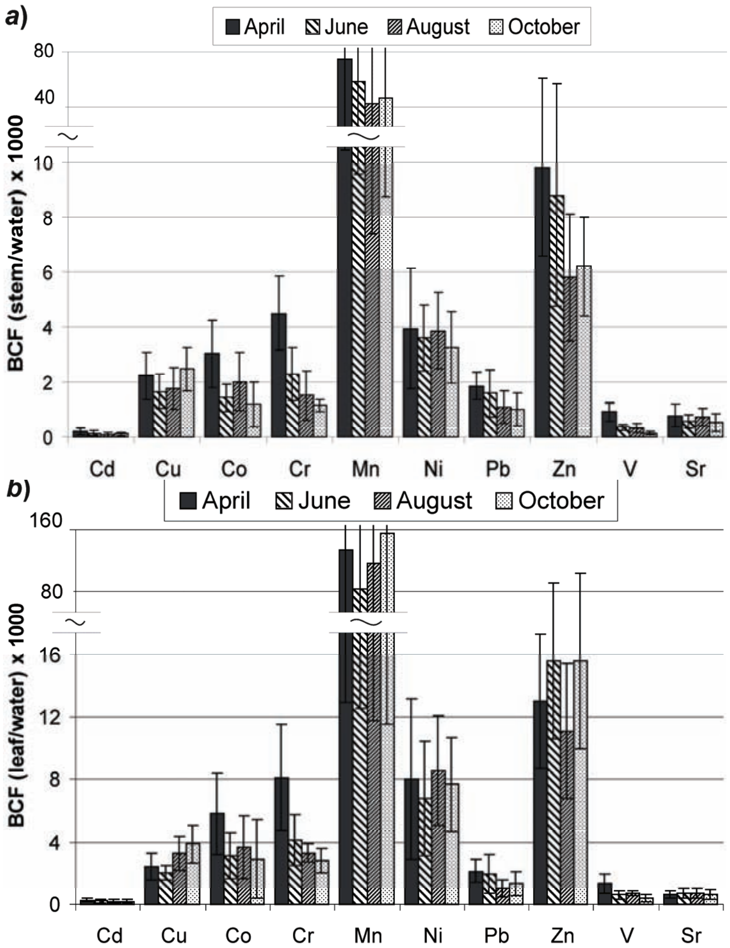

Fig. 1. Seasonal changes of bioconcentration factor (BCF): a) stem and b) leaf of *Ceratophyllum demersum*.

Differences in the sequences of the metal contents in the plant, the sequences of their bioaccumulation capacity and their numerical relationships could be seen to a certain extent. These differences suggest a different bioaccumulation capacity of macrophytes for different metals. The plant accumulates certain metals irrespective of their concentrations in water and sediment, which is obviously a characteristic provided by its capacity for each individual element.

The orders of the intensity of bioaccumulation of the examined metals in the stem and leaf were different. These differences cannot be interpreted solely by differences in metal translocation through the plant because, most probably, the bioaccumulation capacities of the leaves for individual metals directly from the water are different.

The bioaccumulation capacity of *C. demersum* for Mn was several times higher than those for the other metals (Fig. 1).

The contents of all investigated metals in the leaf of *C. demersum* were higher than in the stem at all sites and during all seasons (Tables S-III and S-IV), except Pb (at three locations during the season in August) and Sr (at three locations during the season in April). The largest ratio leaf/stem concentration of 7.14 was recorded for Cd in the sample from the right estuary of the Morača in August, whereas the lowest ratio of 0.42 was found for Pb in the sample from the left estuary of the Morača in August. The seasonal values of the trans-located capabilities are given in Table I, from which it can be seen that the translocation ability decreases in the following order: Mn > Ni > Co > Cr > V > Zn > Cd > Cu > Sr > Pb. It is important to note that with a submersed macrophyte, translocation is not uniquely determined, since in addition to translocation from the stem, the leaf certainly contains metals absorbed directly from the water.

TABLE I. Seasonal changes of translocation ability (*TA*)

Metal	Sample	April	June	August	October
Cd	Leaf/stem	1.43	1.33	1.96	1.09
Cu	Leaf/stem	1.03	1.14	1.82	1.35
Co	Leaf/stem	1.78	2.17	1.64	2.13
Cr	Leaf/stem	1.52	1.78	1.96	2.27
Mn	Leaf/stem	1.47	1.47	2.50	3.33
Ni	Leaf/stem	2.00	1.89	2.22	2.22
Pb	Leaf/stem	1.11	1.03	0.82	1.22
Zn	Leaf/stem	1.19	1.78	1.75	2.38
V	Leaf/stem	1.39	1.59	2.22	2.22
Sr	Leaf/stem	0.86	1.37	1.05	1.26

DISCUSSION

Cadmium

Of the studied metals, cadmium was present in the lowest amount in the tissues of *C. demersum* in the stem from 0.03 to 0.35 ppm (mean annual value of 0.13 ppm) and from 0.05 to 0.42 ppm (mean value 0.21 ppm) in the leaf. The concentration of Cd in the stems and leaves decreased during the season (Tables S-III and S-IV).

Pourkhabbaz *et al.*[13] found higher concentrations of Cd in the leaf of *C. demersum* from the Anzali Wetland, Iran, 0.94–1.26 ppm. Borišev *et al.*[10] did not find Cd in the tissues of *C. demersum* sampled from four sites on the River Jegricka (Serbia), while Bilyk[15] found Cd within the limits of detection in the plant of Vyrlytsa Lake (Ukraine). On the contrary, Babovic *et al*.[12] recorded 9.69 ppm throughout the whole plant from the Fish Pond Ečka, Serbia.

Bio-concentration factor (*BFC*) for Cd was the highest in April, 1.16, which is given as the ratio of the Cd concentration in the whole plant and sediment, as compared to the water >420. Assia *et al*.[16] found a BCF_{Cd} of 600, as the ratio of Cd content in *C. demersum* (Bahr in the El Bakar drain, Egypt) in relation to water. They also found that the value of the *BFC* tended to decline with increasing metal concentration in the water.

Out of 16 tested macrophytes from around Wroclaw, Poland, Samecki-Cymerman and Kempers[17] found the highest concentration of Cd in the tissue of *C. demersum*, 0.65 ppm. Foroughi *et al*.[18] claimed that *C. demersum* collected from the Zayanderood River (Iran) had a greater ability for the removal of Cd (even Pb and Ni) with respect to Fe, Mn and Zn. In their experiments with prolonged plant contact with wastewater, opposing results were obtained for the absorption of some metals.

Copper

The minimum and maximum values of Cu in the stem of *C. demersum* for all seasons were in the range 6.48–24.5 ppm (Tables S-III and S-IV) with an average annual concentration of 14.2 ppm, while in the leaves, the range was 9.85–34.5 ppm (mean value 19.5 ppm). The variations during different seasons in the Cu concentration in the stems and leaves were the smallest compared to the other studied metals (Table S-III). The largest leaf/stem ratio concentration of 1.82 was recorded in August. The maximum value of the bio-concentration factor (for leaf) in relation to water was found in the October sample and it amounted to 3900. In April, the Cu content in the whole plant was similar to that in the sediment. Contrary to this, in August and October, the content was higher in the plant (Tables S-II and S-III). These values mostly refer to accumulation capabilities of *C. demersum* for Cu, and the plant is recommended as bio-indicator of Cu, regardless of its low content in the water.

El Sarraf[19] found two-times higher concentration of Cu in the leaves of *C. demersum* than in the stems. Pourkhabbaz *et al*.[13] also found a higher Cu content in the leaves of *C. demersum* in the range of 19.9–40.0 ppm. Osmolovskaya and Kurylenko[20] detected 10.8 times more copper in *C. demersum* from contaminated compared to uncontaminated areas from five inland ponds within the city of Saint-Petersburg.

Shaltout *et al*.[21] observed the seasonal changes of Cu in tissues of *C. demersum* from the Nile Delta, Egypt. The concentrations increased from winter, when the concentration was the lowest, rose during the spring and reached the maximum in summer, and thereafter decreased. Zuccarini and Campus[22] indicated *C. demersum* as one of the macrophytes with greatest tolerance to Cu. Therefore, they recommended it as a valid bio-indicator for medium to high levels of copper in fresh water.

Cobalt

Highest mean concentration of Co, 5.82 ppm, was observed in April in the leaf of *C. demersum* and it was statistically significantly different from the concentration of Co in the leaf and in the stem in the other months (Table S-III). The mean concentration of Co in the stem was 1.91 (0.69–5.78 ppm) and in the leaf it was 3.88 ppm (1.48–7.63 ppm) (Table S-IV). In addition to the concentration, the highest bio-concentration of Co was recorded in April in the stem and in the leaf, which then declined until October (Fig. 1).

Pajević *et al*.[23] recorded 5–8 ppm Co in *C. demersum* from the littoral zone of Danube–Tisza–Danube canal system, while Bilyk *et al*.[15] found the amount of Co was lower than the detection limit. Samecka-Cymerman and Kempers[17] found a mean value of 7.2 ppm of Co in the tissues of *C. demersum*.

Al-Rekabi[24] observed the monthly changes of the Co concentrations in the tissues of *C. demersum* from southern Iraq; the concentrations increased from January to June, decreased until August and September, then increased again until October and November, when they reached the maximum, and eventually decreased until December. Compared to other seasons, the greatest bio-concentration was observed during the summer season.

Chromium

Significant seasonal variations in concentrations of Cr have been observed (Table S-IV). Highest concentrations were recorded in the stem and in the leaf during April having declined until October. Cr content ranges from 0.89 to 8.81 ppm (average 3.32 ppm) in the stems while in the leaves it ranges from 2.08 to 18.6 ppm (average 6.44). Bio-concentration of Cr in relation to sediment in *C. demersum* is the smallest out of the studied elements. However, there is a noticeable translocation of the average ratio leaf/stem 1.85 (Table I), compared to locations and sampling periods.

The results of Rai *et al.*[25] have showed that *C. demersum*, under laboratory conditions, reduces the level of Cr from water contaminated by effluents from various industrial sources. Reduction varies from the concentration of 4.866 μM to below the 2 μM. Their results indicate the possibility of removing Cr from diluted wastewater by this plant.

Higher concentrations of Cr in the leaves (1.03–2.71 ppm) compared to the stems of *C. demersum* were found by Pourkhabbaz *et al*.[13]

Osmolovskaya and Kurylenko[20] reported that the Cr content was 16.5 times higher in the tissues of *C. demersum* from polluted lake ecosystems compared to unpolluted ones.

Manganese

Manganese was the most abundant metal found in the tissues of *C. demersum* (Tables S-III and S-IV). The mean concentration of Mn in the stem ranged from 275 to 1189 ppm (mean annual value 557 ppm) whereas in the leaf it was 539 to 1984 ppm (mean value 1218 ppm). Spatial and temporal variations in the results were evidenced (Tables S-III and S-IV). The Mn content in the stem declined throughout the study period, while that of the leaf decreased from April to June and then increased, reaching a maximum at the end of the vegetative cycle.

According to a number of authors,[11,15,20,26] together with Fe in the tissues of *C. demersum*, Mn had the highest content of metals and/or maximum bioaccumulation capacity. The Mn concentrations reached values of up to 1000 ppm, the bio-concentration factor reached 2000 and the accumulation of Mn was higher in the leaf of *C. demersum* in relation to the stem.

El-Sarraf[19] claimed that the content of Mn in the leaf was more than two times higher than in the stem. Shaltout *et al*.[21] followed the seasonal variations of Mn in *C. demersum*. The Mn content was the lowest in the winter and then increased during flowering and ripening (spring and summer). According to the authors, unlike Cu and Pb, the Mn concentrations increased in the tissues of *C. demersum* after summer and reached its maximum in autumn, during the maximum vegetative stage.

Nickel

The contents of Ni in the stem of *C. demersum* were significantly different from the contents in the leaf (Table S-III). The Ni concentrations ranged from 3.68 to 14.9 ppm in the stem during the research period (the mean concentration was 7.35 ppm) and in the leaf the Ni content ranged from 6.48 to 28.5 ppm (the mean concentration was 15.5 ppm) (Table S-IV). The contents of Ni in the leaves and stems were relatively uniform throughout the sampling period. After Mn and Zn, nickel showed the highest bioaccumulation ability (Fig. 1) and after Mn, it exhibited the highest translocation ability (Table I), as compared to other investigated metals.

Samecki and Kempers[17] found 36.1 ppm Ni in the tissues of *C. demersum*. Pajević *et al*.[23] determined 5–12 ppm and Babovic *et al*.[12] evidenced 23.6 ppm in the tissues of *C. demersum*.

Al-Rakabi[24] observed the seasonal changes in the concentration of Ni in the tissues of *C. demersum*. The concentration of Ni was constant from January to March, then grew until May and June, declined until July and remained balanced until September, again increasing until October and November, and then decreased until December.

Chorom *et al*.[27] recorded decreases in the biomass of *C. demersum* when grown under laboratory conditions with 1–6 ppm Ni in the water, whereby, death of the plant did not occur despite the phytotoxic levels of Ni. The percentage entering into the plant from the contaminated media was 42–53 %. According to the authors, the highly efficient removal of Ni and the high accumulation capacity make *C. demersum* an excellent choice for phytoremediation of Ni.

Lead

There were no significant variations in the results for Pb during the research period (Tables S-III and S-IV). A slightly higher content of Pb was recorded in the leaves of *C. demersum*, 3.18–16.8 ppm (the mean annual value was 8.04 ppm) while in the stems, it was 2.74–12.7 ppm (the mean annual value was 6.92 ppm) (Table S-IV). The concentration of Pb in the stem decreased from April to the end of the vegetative cycle, while that of the leaf fell from April to August and then increases very slightly until October. Lead had the lowest ratio of leaf/ /stem of 1.02 (Table I) of the investigated metals, probably because of the limited translocation of toxic metals through the plant.

Keskinkan *et al*.[28] found 44.8 ppm in the tissues of *C. demersum*, grown under laboratory conditions in dilute solutions of Pb. Rai *et al*.[25] reported that more than 70 % of Pb was removed by *C. demersum* from industrial waste. Pourkhabbaz *et al*.[13] found a higher content of Pb (7.49–11.88 ppm) in the leaves of *C. demersum* compared to that in the stems.

Shaltout *et al*.[21] investigated the seasonal variation of Pb in the tissues of *C. demersum*. Their findings are to a certain degree different from the conclusions of this study. The content of Pb, similarly to Cu, increased from winter, when its concentration was lowest, during spring and summer, when it reached its maximum and then decreased until winter. Fawzy *et al*.[14] also monitored the spatial and temporal variation of metals in 6 macrophytes, of which *C. demersum* absorbed Pb the most. The maximum concentration of Pb, 31.55 ppm, was observed in the leaves in the winter. Therefore, the authors proposed *C. demersum* as ideal for phytoremediation of Pb.

Zinc

The concentration of Zn in the stem of *C. demersum* decreased from April, when it was the highest, and thereafter to the end of the growing season, it remained almost constant (Table S-III). The content of Zn in the leaves from increased April until the beginning of the growing season, fell until the end of the growing season and then grew to the end of the vegetative phase. The seasonal concentrations of Zn in the stems ranged from 16.7 to 75.6 ppm (the mean value was 38.7 ppm), and in the leaves from 25.6 to 114 ppm (the mean value was 69.2 ppm, Table S-IV). Out of the ten studied metals, after Mn, Zn had the highest potential for bioaccumulation and was the metal with the highest concentration in the tissues of *C. demersum* (Fig. 1). However, many other authors report the highest content of Zn being lower than the concentration of Mn.

Borišev *et al.*[10] found 20.6 ppm Zn in the tissues of *C. demersum* and Babovic *et al.*[12] found 106 ppm. Pourkhabbaz *et al.*[13] observed a higher content of Zn in the stem of *C. demersum*, in the range 19.89 to 40.01 ppm. Osmolovskaya and Kurylenko[20] reported a 5.3 times higher Zn concentration in the tissues of *C. demersum* from contaminated compared to uncontaminated areas.

Fawzy *et al.*[14] noticed no significant seasonal differences in the concentration of Zn in *C. demersum*. They found a higher content of Zn in the leaves of the plants, which was supported by El-Sarraf[19] who found that the Zn content of the leaves was much higher.

Vanadium

The concentration of V depended on both the season and the sampling location (Table S-III). The average seasonal value in the stems of *C. demersum* ranged from 0.34 to 6.87 ppm (the annual average concentration was 1.74 ppm) and it varied from 0.70 to 8.81 ppm (the mean annual concentration was 3.06 ppm) in the leaves (Table S-IV).

The content of V in the stems fell from April to October while its concentration in the leaves kept increasing until June, during the peak biomass production when it decreased until the end of the vegetative period of growth. After Cd, the stem of *C. demersum* and after Cd and Sr, the leaves of *C. demersum* showed the lowest bioaccumulation of V (Fig. 1).

The major anthropogenic sources of V are the products of oil and coal combustion. It is widely used as a catalyst in the production of plastics, although officially there is no such production in the area of Lake Skadar.

Correa *et al.*[29] registered the highest concentrations of V in *C. demersum*, from Ranco Bay, Lago Maggiore (Northern Italy), during the summer (19.5 ppm) with a reduced concentration in winter (6.1 ppm). Ravera *et al.*[30] found that in 8 macrophytes, the concentration of V ranged from 6 to 27 ppm and the content in *C. demersum* was 17 ppm. Zubcov *et al.*[31] recorded V contents in the range 0.5––4.4 ppm in *C. demersum* from the Dniester River ecosystem (Moldava). In 2008 and 2009, Fagbote and Olanipekun[32] found 0.29 and 0.36 ppm V in the Agbabu Bitumen Deposit Area (Nigeria) during the dry season, while in the rainy season of the same years, the values were slightly higher ranging from 0.36 to 0.48 ppm.

Strontium

Seasonal changes in the concentration of Sr in *C. demersum* from Lake Skadar were not observed, nor were they observed in the separate organs (stem and leaf, Table S-IV). Likewise, no spatial variation of the Sr content was noticed (Table S-III). A significantly lower content of Sr was observed only in the samples of stems taken from the Crnojevića River site, and a significantly higher content in the leaves taken from the left mouth of the Morača River (Table S-III). Strontium was, after Mn and Zn, the most abundant metal in the tissues of *C. demersum*. After Pb, Sr exhibited the lowest translocation ability from the stem to the leaf of *C. demersum* (Table I). Mean seasonal values in the stem are within the range from 10.8 to 35.1 ppm (mean value 22.3 ppm) and in the leaf from 12.1 to 37.4 ppm (mean value 23.5 ppm, Table S-IV).

At the same location, Stanković *et al.*[6] determined 141.7 ppm Sr in the tissues of *C. demersum* of the Lake Provala (Serbia) in 1996, and in 1998, they found 380.3 ppm Sr. These data indicate the reflection of changes in environmental conditions on aquatic plants. They also reported higher Sr contents in submerged as compared to emerged macrophytes.

Abdelmalik and El-Shinawy[33] asserted that *C. demersum*, of the Ismailia canal (Egypt), is a favorable biological indicator for radioisotopes of Sr in the concentration range from 0.5 to 10 μCi/L, while the contamination period lasted for 16 days. Strontium-89 uptake increased with increasing initial concentration of radionuclides in the water. The maximum intake was reached after 1–4 days.

CONCLUSIONS

Concentrations of metals in different parts of *C. demersum* were significantly different from their concentrations in water and sediment following the trend: sediment > leaf *C. demersum* > stem *C. demersum* > water.

Concentrations of metals in the stem and in the leaf followed the declining trend: Mn > Zn > Sr > Cu, Ni > Pb > Cr > Co > V > Cd. The bioaccumulation ability (*BCF*) decreased in the following order: Mn > Zn > Ni > Cr > Cu, Co > > Pb > Sr,V > Cd. Except for a few exceptions, there were difference in the sequence of the metal content in the plant compared to the sequences in their bioaccumulation capacity and their numerical relationships. These differences suggested a different capacity of macrophytes for different metals. Plants accumulate certain metals irrespective of the concentrations of the metals in water and sediment, which obviously are their characteristics determined by their capacity for individual elements. The ability of *C. demersum* to bioaccumulate Mn was, on average, several times higher annually than to bioaccumulate the other investigated metals.

The highest contents of Cd, Co, Cr, Pb, V and Sr were found in the tissues of *C. demersum* at the beginning of the growing season; the highest amounts of Ni and Zn were found during the growing season, while most Cu and Mn were accumulated at the end of the vegetative phase. Regarding the Sr content in the tissues of *C. demersum*, there is no statistically significant difference throughout the year, while Cr, Mn and V exhibited the highest temporal variation. The results did not show spatial variation for Co and Cr. Mn, Ni and Zn showed the greatest variation in relation to the sampling site. The content of Mn was higher in the organs of *C. demersum* from the following locations: the right estuary of the Morača, Raduš and Plavnica compared to the other three sites; Ni from the right and left estuary of the Morača and Raduš; Zn from the right estuary of the Morača, River Crnojevića and the left estuary of the Morača. In the waters of the River Morača flow into the wastewater of the capital Podgorica and the Aluminum Plant. Raduš is known as an area that is rich in fish. In recent years, the construction and renovation of old fishermen's houses had intensified. In River Crnojevića, there is a fish processing plant. In the last few years, Plavnica has been exposed to a large number of tourists and fishermen.

The highest translocation from the stem to the leaf was for Mn and Co and the lowest for Pb. Rootless submerged macrophytes absorb metals from water by the stem and leaf. Apart from the absorbed metals from water, the leaf contains a certain quantity of metals transported from the stem.

Due to its ability to accumulate metals, its large coverage of the lakes and the availability of *C. demersum* throughout the year, which makes it easily collectible, this plant is highly recommended for bio-monitoring studies within which trace metal contamination of the lake could be assessed.

SUPPLEMENTARY MATERIAL

Information about study area and collected data are available electronically from http://www.shd.org.rs/JSCS/, or from the corresponding author on request.

И З В О Д

БИОАКУМУЛАЦИЈА И ТРАНСЛОКАЦИЈА МЕТАЛА У ОРГАНИМА *Ceratophyllum demersum* ИЗ СКАДАРСКОГ ЈЕЗЕРА, ЦРНА ГОРА

ВЛАТКО КАСТРАТОВИЋ[1], СЛАЂАНА КРИВОКАПИЋ[1], МИЉАН БИГОВИЋ[1], ДИЈАНА ЂУРОВИЋ[2] и НАДА БЛАГОЈЕВИЋ[3]

[1]*Природно–математички-факултет, Универзитет Црне Горе, Џ. Вашингтона п. пр. 5455, 81000 Подгорица, Црна Гора,* [2]*Институт за јавно здравље Црне Горе, Љубљанска бб, 81000 Подгорица, Црна Гора и* [3]*Металуршко–технолошки факултет, Универзитет Црне Горе, Џ. Вашингтона п. пр. 5455, 81000 Подгорица, Црна Гора*

Језерски системи су врло сложени водени системи када је реч о транспорту и интеракцији тешких метала. Ткива макрофита, пре свега због високе варијабилности и тренутног карактера хемијских параметара су погоднији биоиндикатори степена оптерећења језерског еко-система металима од анализе воде или седимента. Као биоиндикаторска врста коришћена је макрофита *Ceratophyllum demersum*, узоркована из Скадарског језера, Црна Гора. Седименти, вода и биљка испитивани су на садржај десет метала у четири различита периода током 2011. године. Концентрације метала следе тренд: седимент > лист *C. demersum* > стабло *C. demersum* > вода. Постоји разлика у секвенци садржаја метала у биљци од секвенце њихове биоакумулационе способности (BCF). Та разлика указује на различит капацитет макрофите за поједине метале. BCF за Mn је неколико редова величине већи у односу на друге метале. Највећи нађени однос концентрација лист/стабло забиљежен је за Mn (2,19) а најмањи за Pb (1,02). Највећи садржаји

Cd, Co, Cr, Pb, V и Sr нађени су у ткивима *C. demersum* на почетку сезоне раста; Ni и Zn у току вегетативне фазе, а Cu и Mn на њеном крају.

(Примљено 9. априла, ревидирано 11. јула, прихваћено 14. јула 2014)

REFERENCES

1. M. Jović, A. Stanković, L. Slavković-Beskoski, I. Tomić, S. Degetto, S. Stanković, *J. Serb. Chem. Soc.* **76** (2011) 933
2. P. S. Rainbow, *Mar. Pollut. Bull.* **31** (1995) 183
3. J. Morillo, J. Usero, I. Gracia, *Chemosphere* **58** (2005) 1421
4. M. Roméo, C. Frasila, M. Gnassia-Barelli, G. Damiens, D. Micu, G. Mustata, *Water Res.* **39** (2005) 596
5. Q. Zhou, J. Zhang, J. Fu, J. Shi, G. Jiang, *Anal. Chim. Acta* **606** (2008) 135
6. Ž. Stanković, S. Pajević, M. Vučković, S. Stojanović, *Biol. Plantarum* **43** (2000) 583
7. O. Keskinkan, M. Z. L. Goksu, M. Basibuyuk, C.F. Forster, *Bioresource Technol.* **92** (2004) 197
8. V. Kastratović, S. Krivokapić, D. Đurović, N. Blagojević, *J. Serb. Chem. Soc.* **78** (2012) 1241
9. USEPA Method 3051a, *Microwave assisted acid digestion of sediments, sludges, soils and, Revision* 1, 2007
10. M. Borišev, S. Pajević, Ž. Stanković, B. Krstić, in 36th International Conference, Internat. Assoc. Danube Res. (IAD), Klosterneuburg & Vienna, Book of Abstracts, 2006, p. 21
11. W. M. Al-Ghanem, *J. Arab. Aquaculture Soc.* **5** (2010) 35
12. N. Babović, G. Dražić, A. Djordjević, N. Mihailović, in *Proceedings of 4th International Scientific Conference (Balwois 2010)*, Ohrid, Republic of Macedonia, 2010, Proceedings on CD ffp-1452, Balkan Institute for Water and Environment Ohrid, 2010
13. A. R. Pourkhabbaz, H. R. Pourkhabbaz, T. Khazaei, S. Behravesh, M. Ebrahimpour, *Afr. J. Aquat. Sci.* **36** (2011) 261
14. M. A. Fawzy, N. El-sayed Badr, A. El-Khatib, A. Abo-El-Kassem, *Environ. Monit. Assess* **184** (2012) 1753
15. T. I. Bilyk, K. S. Tsurkan, L. M. Koren, *Accumulation of heavy metals in biota of Vyrlytsa Lake*, Environmental Protection, Proceedings of National Aviation University, Kiev, Vol. 48, 2011, p. 158
16. A. A. El Falaky, S. A. Aboulroos, A. A. Saoud, M. A. Ali, in *Proceedings of Eighth International Water Technology Conference*, IWTC8, Alexandria, Egypt, 2004, p. 361
17. A. Samecka-Cymerman, A. J. Kempers, *Ecotox. Environ. Safe.* **35** (1996) 242
18. M. Foroughi, P. Najafi, S. Toghiani, *J. Appl. Sci. Environ. Manage.* **15** (2011) 197
19. W. M. El-Sarraf, *Alex. J. Agric. Res.* **40** (1995) 255
20. N. Osmolovskaya, V. Kurilenko, *Geophys. Res. Abstr.* **7** (2005) 10510
21. K. H. Shaltout, T. M. Galal, T. M. El-Komi, *J. Botany* (2009), Article ID 862565
22. P. Zuccarini, S. Kampus, *Plant Biosyst.* **145** (2011) 503
23. S. Pajević, M. Vučković, Ž. Kevrešan, M. Matavulj, S. Radulović, D. Radnović, in *Proceedings for Natural Sciences*, Matica Srpska, Novi Sad, 2003, Vol. 104, pp. 51–60
24. H. Y. Al-Rekabi, *J. Univ. Thi-Qar* **2** (2006) 8
25. U. N. Rai, S. Sinha, R. D. Tripathi, P. Chandra, *Ecol. Eng.* **5** (1995) 5
26. E. A. Al Sherif, *Agric. Biol.* **11** (2009) 425
27. M. Chorom, A. Parnian, N. Jaafarzadeh, *Int. J. Environ. Sci. Devel.* **3** (2012) 372
28. O. Keskinkan, M. Z. L. Goksu, A. Yuceer, M. Basibuyuk, *Eng. Life Sci.* **7** (2007) 192
29. M. R. Correa, E. D. Velini, D. P. Arruda, *Planta Daninha* **20** (2002) 45

30. O. Ravera, R. Cenci, G. M. Beone, M. Dantas, P. Lodigiani, *J. Limnol.* **62** (2003) 61
31. E. Zubcov, N. Zubcov, A. Ene, N. Bagrin, L. Biletchi, *J. Sci. Arts* **10** (2010) 281
32. O. E. Fagbote, E. O. Olanipekun, *Brit. J. Appl. Sci. Technol*. **3** (2013) 289
33. W. E. Y. Abdelmalik, R. M. K. El-Shinawy, *Hydrobiologia* **42** (1973) 3.

Journal of the Serbian Chemical Society

JSCS@tmf.bg.ac.rs • www.shd.org.rs/JSCS

J. Serb. Chem. Soc. 79 (11) S160–S165 (2014) *Supplementary material*

SUPPLEMENTARY MATERIAL TO

Bioaccumulation and translocation of heavy metals by *Ceratophyllum demersum* from the Skadar Lake, Montenegro

VLATKO KASTRATOVIĆ[1*#], SLAĐANA KRIVOKAPIĆ[1], MILJAN BIGOVIĆ[1#], DIJANA ĐUROVIĆ[2#] and NADA BLAGOJEVIĆ[3]

[1]Faculty of Natural Sciences and Mathematics, University of Montenegro, G. Washington Street, P. O. Box 5455, 81000 Podgorica, Montenegro, [2]Institute of Public Health of Montenegro, Ljubljana bb, 81000 Podgorica, Montenegro and [3]Faculty of Technology and Metallurgy, University of Montenegro, G. Washington Street, P. O. Box 5455, 81000 Podgorica, Montenegro

J. Serb. Chem. Soc. 79 (11) (2014) 1445–1460

Study area

Lake Skadar (42°03′–42°21′ N; 19°03′–19°30′ E), picturesque and in many ways unique within the surrounding environment, is one of the most interesting biotopes in the wider area. It is the largest lake on the Balkan Peninsula and is located on the border between Montenegro and Albania. Two-thirds of the lake is situated in Montenegro. During the summer, Lake Skadar has a surface of 370 km^2, while its surface is 540 km^2 in the winter. The lake is 44 km long with a width of 13 km. The average depth of the lake in its low water level is approximately 5 m, with the bottom part featuring cryptodepression. The maximum depth of the lake is about 60 m. The Skadar Lake exhibits a large change of the water level: on a rainy day, lake level can be raised to one meter. The size of the catchment area is 5500 km^2.

Skadar Lake is a flow type. The greatest amount of water along with a large amount of sediment enters *via* the River Morača and its tributaries the Zeta and Cijevna. The River Bojana is the primary outflow and can cause tumefaction of the Lake. The water in the Lake is completely exchanged two or more times a year.

Samples of sediment, water, and *C. demersum* plants from the Skadar Lake were collected from six locations (Fig. S-1): 1 – Raduš (42° 13′ 26.85″ N, 19° 09′ 54.44″ E); 2 – right estuary of the Morača River (42° 16′ 50.18″ N, 19° 07′ 38.92″ E); 3 – left estuary of the Morača River (42° 15′ 55.80″ N, 19° 08′ 31.49″ E); 4 – Plavnica (42° 16′ 17.48″ N, 19° 12′ 1.01″ E); 5 – Crni Žar (42° 17′ 49.30″ N, 19° 22′ 23.75″ E); 6 – Crnojevića River (42° 21′ 6.03″ N, 19° 02′ 23.05″ E).

Raduš is the deepest underwater source lake with a depth of 60 m. Plavnica is a tributary of the lake, a tourist complex with a large number of tourists and visitors, with an interflow of ground and surface waters gravitating towards it from the surrounding farming land. On the left and right banks of the mouth of the Morača into the Lake, its water quality is affected by numerous impurities in the river collected throughout its course. Probably the most noticeable

* Corresponding author. E-mail: vlatkok@ac.me

impact on the changing quality of the Skadar Lake ecosystem refers to the technological processes in the Aluminum Plant in Podgorica. Crni Žar with its lush waterway and wetland vegetation indicates to accelerated eutrophication, resulting in more water logging of the lake, which inevitably leads to changes in its ecosystem. Crnojevića River, a small town that lies on the eponymous river, possesses a number of factors that suggest caution when it comes to protecting that part of the lake: a fish processing plant, the development of a local fleet, and the waste water systems in the nearby villages and farms. All the above-mentioned measures of precaution are planned because of the large number of tourists to be taken into consideration.

Fig. S-1. Location of the sampling station in Lake Skadar.

TABLE S-I. Seasonal minimum and maximum concentrations (ppm) of the studied metals in the water of the Skadar Lake and the average concentrations ± standard deviation (*SD*); *LOD* – limit of detection. *LOD*(Cd) = 0.001 ppm; *LOD*(Cu) = 0.001 ppm; *LOD*(Co) = 0.001 ppm; *LOD*(Cr) = 0.002 ppm; *LOD*(Mn) = 0.001 ppm; *LOD*(Ni) = 0.001 ppm; *LOD*(Pb) = 0.005 ppm; *LOD*(Zn) = 0.001 ppm; *LOD*(V) = 0.001 ppm; *LOD*(Sr) = 0.001 ppm

Metal		Season			
		April	June	August	October
Cd	Min.–max.	< *LOD**	< *LOD*	< *LOD*	< *LOD*
	Average±*SD*				
Cu	Min.–max.	0.003–0.012	0.002–0.012	0.002–0.013	0.002–0.014
	Average±*SD*	0.007±0.004	0.007±0.004	0.007±0.004	0.007±0.004
Co	Min.–max.	< *LOD*	< *LOD*	< *LOD*	< *LOD*
	Average±*SD*				

TABLE S-I. Continued

Metal		Season			
		April	June	August	October
Cr	Min.–max.	0.002–0.003	0.002–0.003	< *LOQ*	< *LOQ*
	Average±*SD*	0.0022±0.0004	0.0023±0.0005		
Mn	Min.–max.	0.006–0.013	0.005–0.013	0.007–0.014	0.006–0.014
	Average±*SD*	0.009±0.003	0.010±0.003	0.011±0.003	0.010±0.003
Ni	Min.–max.	0.001–0.003	0.001–0.003	0.001–0.004	0.001–0.004
	Average±*SD*	0.0013±0.0008	0.0015±0.0008	0.0018±0.0012	0.0015±0.0012
Pb	Min.–max.	< *LOD*	< *LOD*	< *LOD*	< *LOD*
	Average±*SD*				
Zn	Min.–max.	0.002–0.008	0.002–0.007	0.003–0.008	0.003–0.008
	Average±*SD*	0.005±0.002	0.005±0.002	0.005±0.002	0.005±0.002
V	Min.–max.	0.002–0.007	0.002–0.007	0.002–0.006	0.002–0.005
	Average±*SD*	0.004±0.002	0.004±0.002	0.004±0.002	0.004±0.001
Sr	Min.–max.	0.023–0.047	0.019–0.046	0.020–0.052	0.020–0.051
	Average±*SD*	0.035±0.009	0.034±0.010	0.035±0.011	0.037±0.012

TABLE S-II. Seasonal minimum and maximum concentrations of metals in sediment (ppm) and average concentrations ± standard deviation (*SD*)

Metal		Season			
		April	June	August	October
Cd	Min.–max.	0.27–0.66	0.29–0.63	0.28–0.65	0.28–0.65
	Average±*SD*	0.40±0.15	0.41±0.14	0.41±0.14	0.40±0.15
Cu	Min.–max.	27.2–50.4	25.5–46.9	25.5–52.1	23.9–54.4
	Average±*SD*	34.5±8.84	33.1±7.81	33.3±10.2	34.0±11.1
Co	Min.–max.	6.31–10.1	5.73–12.9	5.28–13.2	5.12–12.6
	Average±*SD*	8.96±2.52	9.02±2.94	8.76±3.13	9.18±3.08
Cr	Min.–max.	42.4–127	42.3–117	39.8–122	35.6–126
	Average±*SD*	69.7±31.4	67.0±27.6	68.7±30.2	68.2±32.0
Mn	Min.–max.	99.0–424	120–357	118–379	95.4–419
	Average±*SD*	232±122	221±91.4	223±101	239±128
Ni	Min.–max.	29.3–131	34.8–110	30.1–113	34.6–125
	Average±*SD*	79.0±44.3	73.1±36.3	74.5±40.6	83.4±47.6
Pb	Min.–max.	19.1–43.2	16.6–37.6	19.4–43.5	17.6–46.2
	Average±*SD*	29.0±10.2	25.7±9.39	27.6±9.85	30.2±12.1
Zn	Min.–max.	47.6–117	56.1–135	59.1–128	53.2–108
	Average±*SD*	75.4±24.0	79.1±29.7	76.2±26.1	73.8±19.7
V	Min.–max.	20.4–46.7	20.1–45.3	18.8–49.5	18.1–45.5
	Average±*SD*	29.4±9.93	28.9±10.6	27.9±11.7	26.9±9.92
Sr	Min.–max.	17.7–101	20.4–101	18.2–113	16.8–105
	Average±*SD*	55.1±30.6	55.8±30.7	56.2±34.2	57.6±32.3

TABLE S-III. Temporal and spatial changes in metal concentrations (ppm d.w.) in parts of *C. demersum*

Location	Season	Specimen	Cd	Cu	Co	Cr	Mn	Ni	Pb	Zn	V	Sr
Raduš	April	Stem	0.20	15.2	3.57	6.15	606	11.1	8.75	48.4	3.36	34.4
		Leaf	0.30	13.5	7.60	7.65	1404	26.2	6.43	62.9	3.82	22.1
	June	Stem	0.15	9.58	1.28	1.49	491	5.75	9.95	29.4	1.12	15.4
		Leaf	0.35	15.3	3.86	4.55	1343	11.4	8.61	58.9	3.36	20.3
	August	Stem	0.05	8.92	2.48	2.86	468	7.31	4.38	24.1	0.69	31.8
		Leaf	0.22	14.7	4.90	3.36	1676	18.8	3.45	25.6	2.67	27.8
	October	Stem	0.03	15.6	1.79	0.89	391	5.87	4.48	16.7	0.84	15.9
		Leaf	0.19	15.7	5.24	2.88	1336	13.4	4.91	37.1	1.88	23.8
Right estuary of Morača	April	Stem	0.14	12.7	5.78	8.81	1189	12.6	12.7	61.5	3.49	27.5
		Leaf	0.15	14.7	7.63	13.6	1745	24.1	14.6	69.1	6.03	29.9
	June	Stem	0.11	12.0	2.75	4.43	1014	11.2	10.8	75.6	1.97	29.7
		Leaf	0.15	17.4	3.77	7.07	1632	14.5	16.8	104	2.48	23.1
	August	Stem	0.03	16.5	3.29	2.76	991	14.9	6.43	49.0	2.15	31.1
		Leaf	0.21	33.6	5.18	3.57	1709	21.8	8.02	85.4	2.98	24.2
	October	Stem	0.05	19.3	0.69	1.79	876	7.81	8.23	46.9	0.34	29.6
		Leaf	0.19	34.0	2.19	2.79	1984	11.7	10.8	88.5	0.70	23.2
Left estuary of Morača	April	Stem	0.12	24.5	3.05	5.74	733	10.7	10.6	38.7	2.25	35.1
		Leaf	0.28	29.4	6.18	4.27	539	11.7	8.97	47.1	7.32	25.3
	June	Stem	0.09	19.8	0.99	4.34	849	12.8	8.31	49.1	1.37	25.8
		Leaf	0.15	12.1	2.96	4.89	567	22.0	8.88	84.8	2.12	33.2
	August	Stem	0.06	22.6	1.38	2.38	357	10.3	7.57	26.9	1.28	25.1
		Leaf	0.08	34.5	3.28	5.62	659	26.1	3.18	62.8	2.69	37.4
	October	Stem	0.10	24.3	1.48	1.58	488	11.8	5.26	32.4	0.93	17.2
		Leaf	0.05	31.2	4.42	4.70	1655	28.5	7.76	107	2.36	29.2
Plavnica	April	Stem	0.16	13.1	1.78	7.91	584	5.04	11.4	61.3	4.05	24.3
		Leaf	0.20	9.85	5.24	18.6	1479	16.5	12.3	70.6	4.08	25.5
	June	Stem	0.14	7.93	1.47	2.86	382	3.95	9.59	43.6	0.69	18.3
		Leaf	0.12	13.2	4.20	6.06	809	10.1	4.75	72.1	1.71	30.1
	August	Stem	0.15	8.11	1.09	2.46	415	5.41	6.56	27.3	0.89	29.6
		Leaf	0.28	13.6	3.09	8.19	1149	16.8	3.99	45.1	1.48	22.4
	October	Stem	0.18	12.4	0.89	2.98	496	4.47	6.43	31.1	0.44	18.5
		Leaf	0.15	18.9	2.59	7.28	1770	18.8	3.96	70.4	0.85	24.8
Crni Žar	April	Stem	0.15	17.8	1.91	5.79	472	4.32	3.15	47.4	6.87	22.7
		Leaf	0.29	16.3	6.19	12.7	627	9.04	9.84	38.7	8.81	12.1
	June	Stem	0.09	13.8	0.69	4.26	427	5.91	3.94	38.3	2.28	14.9
		Leaf	0.17	10.7	1.48	9.00	722	16.9	6.46	61.3	3.95	20.4
	August	Stem	0.05	10.3	2.13	1.29	351	4.38	2.98	26.2	1.79	17.4
		Leaf	0.07	19.5	1.68	4.67	1291	8.73	4.57	48.7	4.95	17.6
	October	Stem	0.11	16.8	0.95	1.20	275	4.20	2.74	26.6	1.20	15.5
		Leaf	0.08	22.3	1.59	3.78	1525	9.35	4.54	52.2	2.29	15.0

TABLE S-III. Continued

Location	Season	Specimen	Cd	Cu	Co	Cr	Mn	Ni	Pb	Zn	V	Sr
Crnoje-vića River	April	Stem	0.35	10.1	2.09	3.55	356	3.68	8.92	48.2	1.89	19.8
		Leaf	0.42	17.5	2.06	11.7	722	9.21	11.9	103	2.49	23.4
	June	Stem	0.29	6.48	1.41	1.88	372	3.77	5.56	26.7	0.81	10.8
		Leaf	0.28	16.4	2.58	3.14	647	6.48	12.7	85.4	0.79	18.3
	August	Stem	0.20	8.64	1.68	1.00	424	4.08	4.56	21.1	0.70	12.9
		Leaf	0.30	21.2	3.76	2.29	1118	10.2	7.60	66.4	2.36	14.9
	October	Stem	0.17	15.4	1.32	1.23	356	4.97	2.87	31.4	0.45	11.0
		Leaf	0.32	21.7	1.48	2.08	1112	10.4	8.05	114	1.28	19.6

TABLE S-IV. Seasonal changes in the metal concentrations (ppm d.w.) in the parts of *C. demersum*; minimum and maximum concentrations and average concentrations ± standard deviation (*SD*); the values of individual metals with the same letter(s) are not significantly different at $p \leq 0.05$

Metal	Part	Season			
		April	June	August	October
Cd	Stem	0.12–0.35	0.09–0.29	0.03–0.20	0.03–0.18
		0.19±0.08 **ab**	0.14±0.07 **ab**	0.09±0.07 **b**	0.11±0.06 **b**
	Leaf	0.15–0.42	0.12–0.35	0.07–0.30	0.05–0.32
		0.27±0.09 **a**	0.20±0.09 **ab**	0.19±0.10 **ab**	0.16±0.10 **ab**
Cu	Stem	10.1–24.5	6.48–19.8	8.11–22.6	12.4–24.3
		15.6±5.08 **b**	11.6±4.82 **b**	12.5±5.83 **b**	17.3±4.09 **ab**
	Leaf	9.85–29.4	10.7–17.4	13.6–34.5	15.7–34.0
		16.9±6.68 **b**	14.2±2.60 **b**	22.8±9.13 **a**	24.0±7.14 **a**
Co	Stem	1.78–5.78	0.69–2.75	1.09–3.29	0.69–1.79
		3.03±1.52 **b**	1.43±0.71 **b**	2.01±0.80 **b**	1.19±0.41 **b**
	Leaf	2.06–7.63	1.48–3.86	1.68–5.18	1.48–5.24
		5.82±2.06 **a**	3.14±1.01 **b**	3.65±1.28 **ab**	2.92±1.56 **b**
Cr	Stem	3.55–8.81	1.49–4.43	1.00–2.86	0.89–2.98
		6.32±1.85 **b**	3.21±1.32 **bcd**	2.12±0.78 **cd**	1.61±0.74 **d**
	Leaf	4.27–18.6	3.14–9.00	2.29–8.19	2.08–7.28
		11.4±4.97 **a**	5.78±2.07 **bc**	4.62±2.09 **bcd**	3.92±1.88 **bcd**
Mn	Stem	356–1189	372–1014	351–991	275–876
		657±290 **cd**	589±273 **cd**	501±244 **cd**	480±211 **d**
	Leaf	539–1745	567–1632	659–1709	1112–1984
		1086±516 **abc**	953±431 **bcd**	1267±392 **ab**	1564±311 **a**
Ni	Stem	3.68–12.6	3.77–12.8	4.08–14.9	4.20–11.8
		7.91±3.97 **bc**	7.23±3.83 **bc**	7.73±4.20 **bc**	6.52±2.90 **c**
	Leaf	9.04–26.2	6.48–22.0	8.73–26.1	9.35–28.5
		16.1±7.52 **a**	13.6±5.48 **abc**	17.1±6.69 **a**	15.4±7.24 **ab**
Pb	Stem	3.15–12.7	3.94–10.8	2.98–7.57	2.74–8.23
		9.25±3.34 **a**	8.02±2.71 **ab**	5.41±1.72 **b**	5.00±2.12 **b**
	Leaf	6.43–14.6	4.75–16.8	3.18–8.02	4.54–10.8
		10.7±2.87 **a**	9.70±4.39 **a**	5.14±2.13 **b**	6.67±2.65 **ab**

TABLE S-IV. Continued

Metal	Part	Season			
		April	June	August	October
Zn	Stem	38.7–61.5	26.7–75.6	21.1–49.0	16.7–46.9
		50.9±8.89 **abc**	43.8±17.7 **bc**	29.1±10.0 **c**	30.8±9.78 **c**
	Leaf	38.7–103	58.9–104	25.6–85.4	37.1–114
		65.2±22.4 **ab**	77.8±17.1 **a**	55.7±20.6 **abc**	78.2±30.5 **a**
V	Stem	1.89–6.87	0.69–2.28	0.69–2.15	0.34–1.20
		3.65±1.77 **ab**	1.37±0.64 **cd**	1.25±0.61 **cd**	0.70±0.34 **d**
	Leaf	2.49–8.81	0.79–3.95	1.48–4.95	0.70–2.36
		5.42±2.38 **a**	2.40±1.14 **bcd**	2.86±1.15 **bc**	1.56±0.72 **cd**
Sr	Stem	19.8–35.1	10.8–29.4	12.9–31.8	11.0–29.4
		27.3±6.29 **a**	19.2±7.18 **a**	24.6±7.85 **a**	17.9±6.25 **a**
	Leaf	12.1–29.9	18.3–33.2	14.9–37.4	15.0–29.2
		23.0±5.98 **a**	24.2±6.02 **a**	24.0±8.00 **a**	22.6±4.84 **a**